Developing Carbon Paste Electrodes and Their Application to Electrochemical Immunoassays

Stuart Milne

Biomedical Engineering

University of Strathclyde

Thesis Submitted in partial fulfilment for the degree of Doctor of Philosophy

18/02/2026

This thesis is the result of the author's original research. It has been composed by the author and has not been previously submitted for examination which has led to the award of a degree.

Signed: Stuart Milne

18/02/2026

Abstract

Cancer is a major challenge faced by the NHS, accounting for up to 28% of annual deaths in England. Despite its high profile, diagnosis is still a lengthy process, due to its heterogeneity in presentation.

While screening is routinely performed to enable the detection of some of the most common cancers and can successfully reduce mortality, effective screening of other cancers is not yet possible due to the lack of effective detection tools. Liquid biopsy enabled via electrochemical detection may help provide these tools via the identification of cancer specific biomarkers from quickly and easily acquired body fluid samples. Although these electrochemical methods show great promise in literature, their commercial use is currently limited.

Work presented in this thesis shows the development of a cheap carbon paste electrode, its optimisation and its application in the detection of cancer related biomarkers through immunoassays.

A carbon paste electrode was initially developed in lab and suitable physical and chemical pretreatments ascertained to improve its performance. A chip format was then developed and used in the direct detection of dopamine where it produced limits of detection of 62.5 μM. It was also capable of detecting the key inflammatory biomarker, interleukin – 6, via measurement of ELISA products, producing a limit of detection of 150 pg/ml (in the clinically relevant range). Indirect detection of a more directly clinically relevant biomarker tested, PSA, was then performed. Although binding of this assay to the surface was possible, it could not improve performance significantly. Finally, an attempt was made to improve paste performance via further pretreatments and manufacturing changes. Improvements from chemical pretreatments were short lived and changes to manufacturing were unable to produce any significant improvement in paste performance.

Acknowledgements

Firstly, I would like to thank my supervisor, Damion Corrigan for the help and encouragement that he has provided throughout my PhD and the opportunities he has both made for me and encouraged me to make the most of.

I would also like to thank the rest of the Corrigan lab group, in particular Perrine, Sandy, Niamh and Rowan for both their technical and emotional support as well as all the other collaborators and co-authors that have helped me over all the various projects.

Finally, I would like to thank all my friends and family for their encouragement and assistance during the PhD process, in particular Geoff who was always keen for me to push myself.

Publications

Included in this thesis:

- Fabrication of a graphite-paraffin carbon paste electrode and demonstration of its use in electrochemical detection strategies. https://doi.org/10.1039/D4AN00392F

Contributed to during the PhD:

- A plug-and-play, easy-to-manufacture fluidic accessory to significantly enhance the sensitivity of electrochemical immunoassays. https://doi.org/10.1038/s41598-024-64852-5
- Cost-effective amperometric immunosensor for cardiac troponin I as a step towards affordable point-of-care diagnosis of acute myocardial infarction. https://doi.org/10.1016/j.sbsr.2024.100725

Conference Proceedings

Presentation: '*Producing Low-Cost Chips for Biomarker Detection using Carbon Pastes*', RSC Electrochem (2024).

Poster: '*Development of a carbon paste electrode for the detection of biomarkers via ELISA*', 8th International Conference on Bio-Sensing Technology (2024).

Poster: '*Low-cost carbon paste electrodes to enable high throughput screening for cancer*', 10th Analytical Biosciences Early Career Researcher Meeting (2023)

Poster: *'Development of low cost carbon electrodes for ELISA like measurements in point of care cancer diagnosis'*, RSC Electrochem (2022).

Abbreviations

BC	Before Christ
UK	United Kingdom
NHS	National health service
GP	General practitioner
CT	Computed tomography
MRI	Magnetic resonance imaging
PET	Positron Emission Tomography
HPV	Human papilloma virus
AJCC	American Joint Committee on Cancer
UICC	International Union for Cancer Control
DNA	Deoxyribonucleic acid
RNA	Ribonucleic Acid
Ig	Immunoglobulin
ELISA	Enzyme linked immunosorbent assay
WE	Working electrode
CE	Counter electrode
RE	Reference electrode
IHL	Inner Helmholtz layer
OHL	Outer Helmholtz layer
CV	Cyclic Voltammetry
V	Volts
A	Amperes
K^0	Heterogenous electron transport rate
SWV	Square Wave Voltammetry
EIS	Electrochemical Impedance Spectroscopy
LoD	Limit of Detection
LoB	Limit of the blank
LoQ	Limit of quantification

ELoD	Experimental limit of detection
Ruhex	Hexaammineruthenium(III) chloride
FF	Ferri-ferrocyanide
PBS	Phosphate Buffered Saline
OCP	Open Circuit Potential
s	Second
M	Meter
CPE	Carbon Paste Electrode
POC	Point of Care
Gox	Glucose Oxidase
HRP	Horseradish Peroxidase
ALP	Alkaline Phosphatase
IL-6	Interleukin 6
Hz	Hertz
L	Liter
PSA	Prostate Specific Antigen
CA	Chronoamperometry
DI	Deionised
rpm	rotations per minute
FDM	Fused deposition modelling
SLA	Stereolithography
UV	Ultraviolet

Contents

Figures

Tables

Equations

1 Introduction

1.1 Cancer

Cancer is the aberrant growth of previously healthy cells[1] and leads to the formation of tumours within the body. It is an ancient disease, being recorded from as early as 3000 bc[2] however despite this, still has a huge impact on health in the modern age, both in the UK and worldwide.

1.1.1 Incidence

Cancer is one of the major challenges the modern NHS faces, accounting for between 27-28% of deaths in England annualy[3]. It can occur anywhere in the body however there are common sites that are different for men and women. In men prostate, colorectal and lung cancers are the most diagnosed and common causes of cancer mortality. In women breast, colorectal and lung cancers are the most diagnosed and common causes of cancer mortality (stats for the UK)[4]. These trends are shared with the rest of Europe, where prostate (in men) and breast (in women) are the most common cancers and lung (in men) and breast (in women) the largest causes of cancer mortality[4].

These trends are global, with lung, breast, colorectum and prostate cancers being the most common. In general cancer is a larger issue in the developed world with its incidence being linked to the human development index. Interestingly these increases in incidence do not always lead to increases in mortality[5].

1.1.2 Causes

At a fundamental level, all cancers are caused by mutations in cells that stimulate their uncontrolled growth. These mutations occur in both proto-oncogenes that encourage cells to grow and divide and tumour suppressor genes which inhibit cell growth and division[6]. Mutations must occur and be preserved in multiple genes to allow a cell to become cancerous and can be inherited

(commonly tumour suppressor, oncogenes, DNA repair and angiogenesis genes[7]) or far more commonly (over 90% of cases) occur sporadically over an individual's life[1].

These sporadic mutations may occur due to exposure to environmental, occupational or lifestyle 'risk factors' that will increase the chance of mutation and therefore the chance of developing cancers (attribute for 37.7 % of cancers in the UK[8]). Many cancers however develop randomly or from currently unknown risk factors. Given the random nature of gene mutation and whether it is conserved in cells, exposure to risk factors will increase an individual's risk of developing cancer however will not guarantee it. On the other hand, this also means that an individual who has not been exposed to any risk factors may still develop the disease.

The most impactful known risk factors are the use of tobacco and obesity, followed by occupation, exposure to ultraviolet radiation, insufficient dietary fibre, alcohol use, infections, a diet high in processed meat, exposure to ionising radiation, air pollution and insufficient physical activity[8]. Family clustering of cancers is also common, due to shared genetic susceptibilities and exposure to environmental risk factors[7]. It should again be considered that both the severity of a risk factor and the amount of exposure to it both contribute towards likelihood of causing cancer.

1.1.3 Pathophysiology

1.1.3.1 Initial Growth

The initial growth of a tumour occurs in three stages (summarised in Figure 1.1). During initiation, mutations will occur and be preserved in a cell that allow its uncontrolled growth. If this cell survives, promotion will take place, and the initial mutated cell will divide and grow into a small cluster. This is followed by progression, where the cluster will further divide into a tumour that can spread to surrounding tissue[9].

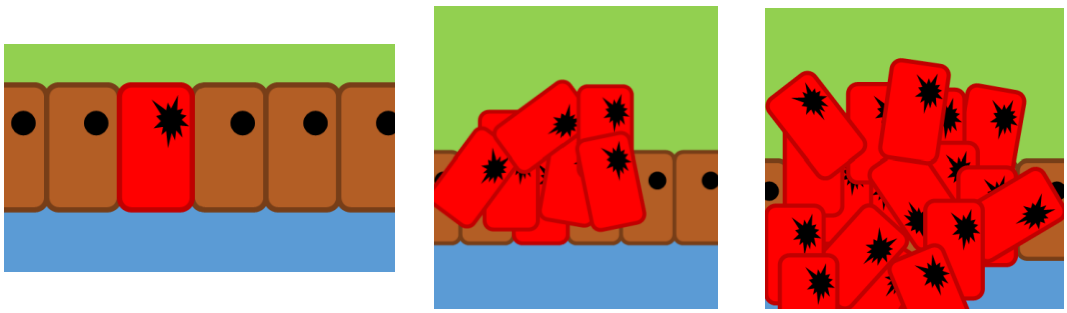

(a) **(b)** **(c)**

Figure 1.1: Initiation **(a)**, promotion **(b)** and progression **(c)** seen in the early stages of tumour growth.

1.1.3.2 Tumour composition

The resulting mature tumour will contain tumour, immune and stromal cells, along with non-cellular components:

- Tumour cells descend from the initial mutated cell and may be clones of this cell (homogenous tumours) or have acquired further mutations and become multiple cell lines (heterogenous tumours).
- Stromal cells are supporting cells such as liposomal or epithelial cells which are recruited to the tumour site to support its further growth.
- Immune cells are recruited to the tumour site due to inflammation and can be found either fighting the tumour or encouraging tumour growth via the dysregulation of the immune response.
- Extracellular matrix will be secreted by immune and stromal cells and acts as a scaffold for the tumour[10].

More specific roles of these components are shown below in Table 1.1:

Table 1.1: Components of a tumour and their role in the tumour microenvironment[10]

Component	Role
T cells	Can help or hinder depending on cell type, cytotoxic T cells will target cells for destruction whereas regulatory t cells will reduce the inflammatory response
B cells	Rare in the microenvironment however prognostically important, can produce both pro and anti-inflammatory signals
Natural killer cells	Effective at killing tumour cells and secrete inflammatory cytokines, good at preventing metastasis but less effective in the microenvironment
Macrophages	Tumour microenvironment promotes M2 macrophages that are immunosuppressive, can also secrete endothelial growth factor, inducing blood vessel formation in the tumour
Neutrophils	Early on in tumours help promote inflammation and tumour apoptosis, later they promote tumour growth
Dendritic cells	Cytokines in the tumour microenvironment trigger the dendritic cells to tolerate the tumour cells,
Endothelial cells	Important in larger tumours, allows angiogenesis or the production of blood vessels allowing tumours the nutrients to grow, this angiogenesis also allows metastasis through leaky blood vessels in the tumour
Cancer associated fibroblasts	Diverse in origin, allow crosstalk between cancer cells and the tumour microenvironment. produce most extracellular components
Adipocytes	In the body store excess energy as fat, in the TME they can secrete metabolites, enzymes, hormones, growth factors and cytokines, in some cancers they are stimulated to release fatty acids used in tumour growth

Stellate cells	Located in the liver and pancreas. Promote crosstalk within the tumour microenvironment and can promote migration and proliferation.
Extracellular matrix	Provides a physical scaffold for cell growth and can act as a store for cytokines and growth factors
Exosomes	Micro vesicles released from cells, whose contents reflects the cell of release, facilitate cross talk and promote inflammation, tumour progression, blood vessel growth and metastasis

1.1.3.3 The tumour microenvironment

The combination of the cells in a tumour and the extracellular components they produce form the tumour microenvironment. This microenvironment can affect immune cells where it inhibits activation[11], drives differentiation and induces cell death[12].

Oxygen saturation in the microenvironment has a substantial impact on both tumour cells and the immune response. Although a tumour will recruit epithelial cells and 'bud' vessels off nearby vasculature to create a blood supply, this supply is poor and often does not provide sufficient oxygenation within the tumour. Tumour cells in such an environment are found in three states, oxygenated (normal oxygen levels), hypoxic (lower oxygen levels) or necrotic (from a complete lack of oxygen) largely dependent on their proximity to the closest blood supply (Figure 1.2)[13]. Hypoxia has a range of effects on tumour tissue, stimulating angiogenesis, reprogramming metabolism and epigenetics and encouraging both immune evasion and tumour cell migration. This not only aids in the growth of a tumour but also encourages its migration and metastasis[13]. Hypoxic cells may also begin to respire anaerobically, reducing the pH of the microenvironment.

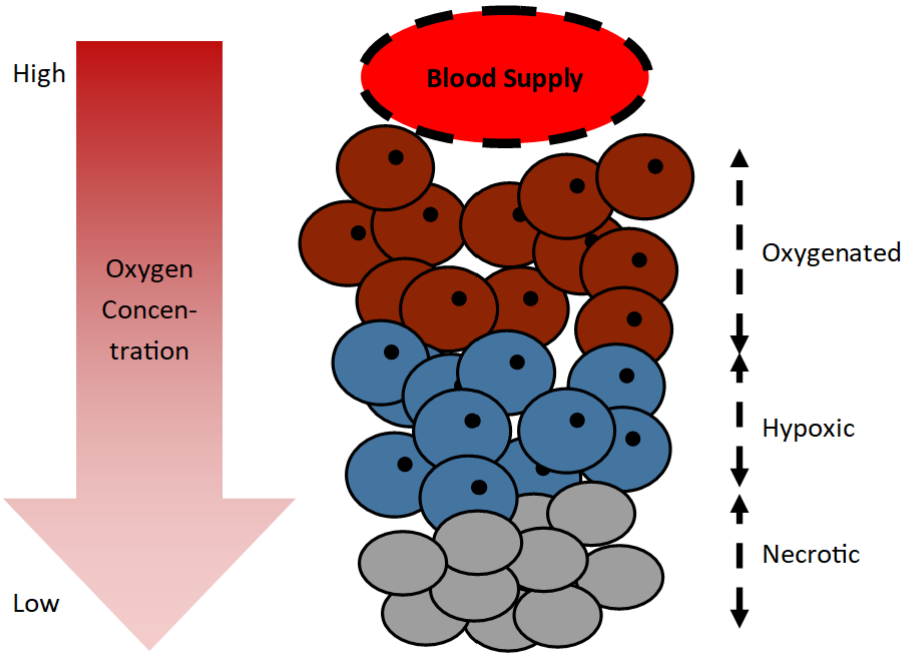

Figure 1.2: Oxygenation in the tumour microenvironment

1.1.4 Diagnosis

In the UK, cancer is often discovered only when it becomes symptomatic, and a patient presents to their GP[14]. The symptoms are often general and can include fatigue, insomnia, weight loss, muscle loss, delirium, fever, pain and itching although they will be persistent and worsen over time as a cancer progresses. Patients may also experience organ specific symptoms, especially if a cancer has progressed to the stage where it is able to affect its normal function, as well as paraneoplastic symptoms not caused directly by the tumour but the pressure it exerts on surrounding tissues[15]. General symptoms mean that often patients will require multiple general appointments before being referred to a specialist[14]. After this referral, specialist tests will be performed including CT, MRI, PET scans, blood tests and if a tumour is found, biopsy.

To help identify cancer cases at earlier asymptomatic stages, common cancers are routinely detected through screening, this is a process especially useful when combatting cancers that may not be symptomatic until advanced stages. Screening involves the examination of populations for specific diseases (in this

case cancers) and aims to catch the small number of asymptomatic patients in this population. Screening is either performed on a whole population or more commonly a smaller 'at risk' population identified via general risk factors such as age or gender. Currently screening is performed mostly for breast, bowel, cervical and prostate cancers[16] and in the UK is performed for breast, bowel and cervical cancers, although given their varied presentation equally varied approaches are required for their detection.

In England screening programmes are performed via invitation. Breast screening is performed every 3 years on women between 50-71 years old primarily using mammogram (Xray of the breast). Xray's are examined and further testing (such as biopsy) is performed as needed[17]. This screening programme has successfully reduced the risk of death and need for treatments such as mastectomy (surgical breast removal), chemotherapy and radiotherapy[18].

Bowel cancer screening is performed every 2 years on individuals between 54-75 years old and involves the collection of faecal samples which are tested via faecal immunochemical tests to detect the presence of blood. Tests can be followed up by colonoscopy if required[19]. Screened populations have a lower risk of bowel cancer death when compared to non-screened populations and have bowel cancers identified at earlier stages, allowing more cost-effective treatment (treatment of cancers at earlier stages is often lower cost)[20].

Cervical cancer screening is performed every 3 or 5 years on individuals between 25-49 years old using 'PAP smears' which test for the presence of the human papilloma virus (HPV), the most common cause of cervical cancer. If detected, cytology tests will be performed to identify abnormal cells in the cervix[21]. Despite the large success of this screening, with a single PAP smear being performed after the age of 35 being able to reduce the risk of death by 70%[22] (further screening is able to reduce risk even more), HPV vaccination during adolescence may supersede the need for screening at all, being able to prevent most cancers[23].

Although both prostate and lung cancers are common, they are not currently screened for in the UK. A programme is currently being developed for lung cancer screening aimed at high-risk individuals such as smokers[24]. Screening for prostate cancer on the other hand is not recommended due to the inaccurate tests available[25].

1.1.4.1 Cancer Grading

Once diagnosed, either through presentation to clinicians with symptoms or screening, cancers are graded to provide prognostic and treatment value[26]. The most common method for this grading is the Tumour-Node-Metastasis (TNM) scale (summarised in Table 1.2) which is maintained and updated jointly by the American Joint Committee on Cancer (AJCC) and the International Union for Cancer Control (UICC) and is updated every 6-8 years[27]. This scale contains information about the size or spread of the primary cancerous tumour (Tumour), the extent or absence of cancer in local lymph nodes and whether a large number or specific nodal groups are effected (Node) and the spread (metastasis) of cancerous cells either locally or through the body[27] where tumours can either be in situ (not crossing tissue boundaries) or malignant (crossing boundaries and shedding cells into blood)[6]. Patients are then further grouped by anatomic progression or prognosis into stages, classified from stage 1 to stage 4 in increasing severity.

Table 1.2: Elements of the TNM scale used in the grading of cancerous tumours

Tumour (T)		Node (N)		Metastasis (M)	
T0	No Evidence of Tumour	N0	No metastases in regional lymph nodes	M0	No distant metastases
Tis	In situ carcinoma	N1,N2,N3	Increasing Extent of regional lymph node metastasis	M1	Distant metastases
T1,T2,T3,T4	Increasing size/extension of tumour	NX	Cannot assess regional lymph nodes		
Tx	Tumour cannot be assessed				

1.1.5 Treatment

Once a cancer has been identified and graded it must then be treated. Given the heterogeneity of cancer location and presentation treatment approaches are highly variable however often involve surgery, radiotherapy or chemotherapy. These treatments can be used alone however are commonly combined[28].

1.1.5.1 Surgical Treatment

Surgery is the simplest form of treatment for a cancer and involves the direct removal of tumorous material via surgical procedures. If cancers are found at an early stage before metastasis has occurred, surgery can be sufficient to

completely remove a cancer. Most commonly it is used to partially remove a tumour before being followed by radiotherapy or chemotherapy which treat remaining cancerous tissue. Surgery can also be palliative and used to alleviate pain and obstructions or reconstructive and used to rebuild or recover the function of damaged organs[28].

1.1.5.2 Radiotherapy

Radiotherapy involves the use of radiation to kill or prevent the growth of tumour cells and although its use damages both healthy and cancerous cells, healthy cells can more easily recover from this damage. There are three types of radiotherapy:

- Teletherapy is performed with a distance between the radiation source and target area to be treated.
- Brachytherapy uses radiation sources that are placed directly in contact with target tissues using small radioactive seeds that are implanted into the tumour to avoid damaging surrounding healthy tissue.
- Radiosurgery uses high doses of radiation that are precisely targeted to kill a small area of tissue and is commonly used in intracranial applications[28]

1.1.5.3 Chemotherapy

Chemotherapy uses combinations of chemicals to treat cancerous tissue. These chemicals are non-discriminatory and so cause damage to both cancerous and normal tissue however given the rapid rate of proliferation seen in tumorous tissue this is affected the most and is particularly effective in the treatment of small, rapidly growing tumours. This non-specificity can (but does not always) lead to damaging of non-target cells and tissues, especially sensitive are organs that do not constantly renew such as bone marrow, hair and the digestive tract. This damage often causes severe side effects which must be predicted and treated preemptively[28].

There are many chemotherapy agents that can be used during treatment which may cause changes in cellular DNA (alkylating agents), mimic natural

metabolites but once incorporated block enzyme production (antimetabolites), block cell mitosis (Plant derived antineoplastics) or interrupt the prolongation of DNA (antitumour antibiotics)[28]

1.1.6 Liquid biopsy

Current cancer treatment is often based on the molecular characterisation of tumours; performed on a small tissue sample taken during a biopsy. This characterisation provides a 'snapshot' of the tumour's characteristics however, especially in large well-developed tumours that may contain several different cell lines, may not provide a full picture. This traditional approach also cannot capture genetic changes that may happen within the tumour over the course of treatment without repeated invasive procedures. This tumour heterogeneity and failure to track it is a major reason treatment may fail[29].

Liquid biopsy seeks to perform characterisation more conveniently through the measurement of tumour components in bodily fluids (blood, saliva, urine etc.) and is less invasive, more comfortable and more repeatable[30]. This repeatability allows more frequent testing to take place and therefore allows treatment responses to be tracked easily[29]. Its use of bodily fluids also allows systemic measurement which enables the measurement of both tumours and the patient's response to treatments. Liquid biopsy techniques are employed to measure levels of different biological markers or 'biomarkers', the term biomarker can apply to a huge range of markers however in the context of cancers refer to proteins, nucleic acids, antibodies, whole cells or cell products that are able to provide information that helps identify, characterise, monitor and provide prognostic information about a cancer[31].

There are many biomarkers targeted in the diagnosis of cancer. Circulating nucleic acids are released from cells during their lifetime and carry genetic information about their parent cell, most targeted are DNA and microRNA whose levels are raised in cancer patients, however nucleic acids of interest are present in low concentrations and so can be difficult to detect.

Whole cells are also released from tumour tissue and are the driving force behind metastasis of the tumour, these cells enter the bloodstream and if captured can yield both genetic and phenotypic information about the tumour[29].

Extracellular vesicles are also released by cells, these are produced either intracellularly or bud from the plasma membrane and contain a range of proteins, nucleic acids and metabolites from their parent cell both internally and presented on their surface.

An extremely large number of proteins are also released from cancer cells and can be found either free in body fluids or attached to the membranes of vesicles or circulating cells[32]

Despite its advantages, liquid biopsy still has drawbacks, it is unable to localise tumours, gives little histological data and approaches using it are still mainly literature based[33]. Its current inability to give specific histological data on tumours indicates that it should be used in addition to more traditional biopsy methods rather than replace them.

1.2 Immunoassay

Biomarkers in these biopsies are commonly detected via immunoassay. Immunoassay is a family of analytical techniques found commonly in biochemistry labs. These techniques rely on the strong binding between antibodies and specific areas (epitopes) on a target molecule (antigen) which is then measured either directly or using tags. Antibodies are ideal in liquid biopsy as they can be specific to a wide range of targets which they create strong bonds with[34]. Although the wide-ranging spectrum of applications has led to an equally large number of immunoassay protocols, they can be categorised by their competitiveness, homogeneity and if measurements are performed directly or via tags.

Competitiveness (summarised in Figure 1.3) refers to whether there are sufficient antibodies in an assay to allow unrestricted binding of antigens. In competitive (saturated) immunoassay, the amount of antibody used is limited and so antigens compete for binding sites. A known amount of tagged 'marker' antigen is used to compete with an unknown amount of untagged antigen and the remaining bound or unbound marker measured which then relates to the amount of untagged antigen. In non-competitive (unsaturated) assays, antibodies are provided in excess. An unknown amount of antigen is added to these antibodies and allowed to bind before a tag is either read or added, for example through the binding of a tagged secondary antibody[35].

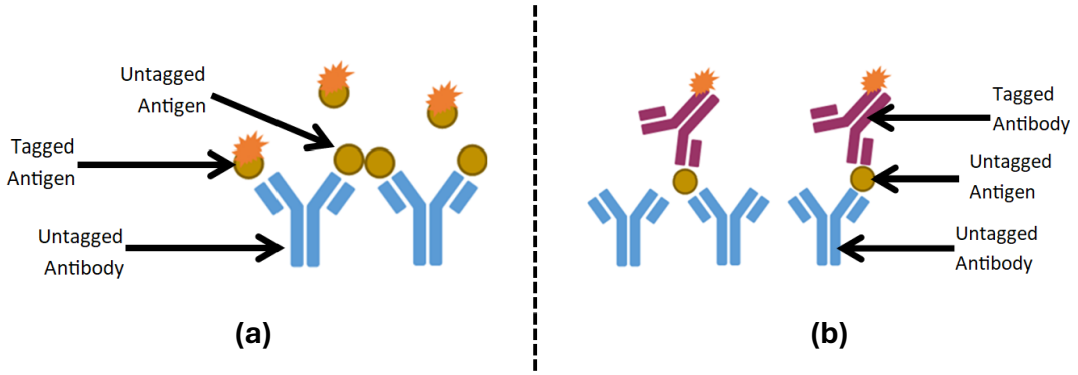

Figure 1.3: Competitive **(a)** and Non-Competitive **(b)** immunoassay

Homogeneity (summarised in Figure 1.4) refers to whether final antibody-antigen complexes require separation before measurement. In homogenous assays, bound antigens can be measured in the presence of unbound antigens. These assays commonly rely on the ability of binding to change the characteristics of an antigen or associated tag for example when the binding of an antigen inhibits an antibody tag. In heterogenous assays, separation of bound and unbound antigen is required before measurement can take place and is required when the binding of an antigen does not change it[35].

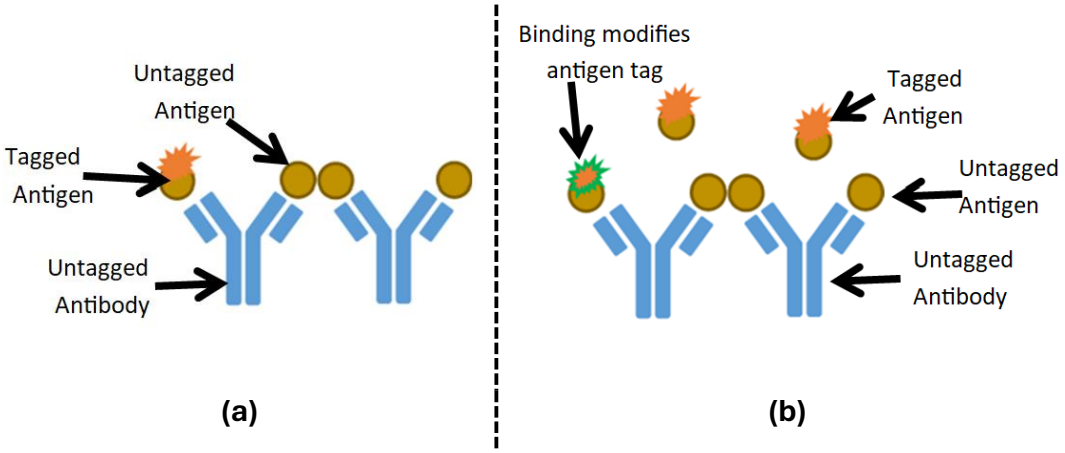

Figure 1.4: Heterogenous **(a)** and Homogenous **(b)** immunoassay

Assays can also be separated by whether tags are required for measurement. In untagged assays, the binding of an antibody to its antigen can produce a detectable signal in several ways:

- Agglutination (where binding causes agglutination of products)
- Precipitation (where binding causes a soluble antibody to become insoluble)
- Immunodiffusion (where precipitation assay is conducted on a gel-support and the diffusion of the precipitate measured)
- Immunoelectrophoresis (electrophoretic and immunological techniques combined)
- ELectroimmunoassay (combines electrophoretic and radial immunodiffusion)

- immunoturbidimetry (binding causes the formation of small aggregates, causing a solution to become more turbid/cloudy)[35].

Tagged methods are employed and required where binding itself cannot be readily detected. Tags are attached to either antigens or antibodies to couple binding events to a measurable signal. There are many tags used in immunoassays including radioisotopes, enzymes, fluorescent tags, luminescent tags, metals, electroactive species, bacteriophages and spin markers. These tags can be measured by an equally large range of techniques including colourimetry, fluorometry, luminometry, turbidity, radioisotope determination, Electron spin resonance, optically or electrochemically[35].

1.2.1 Antibodies

The functional unit of every immunoassay is the antibody. An antibody is an immunoglobulin which will bind to an antigen with high affinity[36]. Antigen refers to anything that is recognised by immune cells to be different from host tissue and can be exogenous (extracellular and found on pathogens or transplanted tissues), endogenous (intracellular and found in pathogens or expressed by cancerous cells) or an autoantigen (found on host cells)[37]. The binding between an antibody and antigen has both an affinity (how well the antibody binding site fits the antigen) and an avidity (how strong this bond is when made)[38].

1.2.1.1 Antibody Structure

Structurally an antibody consists of a pair of heavy chain polypeptides and a pair of light chain polypeptides held together by strong disulphide bonds and hydrophobic interactions[39]. This produces a Y shaped molecule (Figure 1.5) which consists of two large regions, a variable region (F_{ab}) responsible for antigen recognition and a constant (F_c) region that interacts with effector cells and molecules[40]. These regions are bound together via a hinge which allows movement of the F_{ab} arms, facilitating binding. The F_{ab} is tipped with a highly variable antigen binding fragment that is responsible for antigen binding[39].

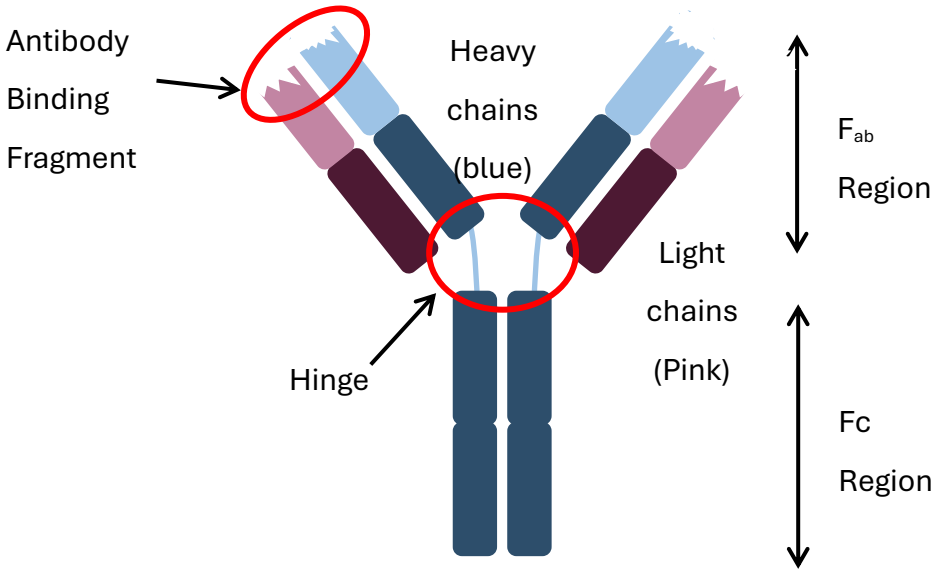

Figure 1.5: The general structure of an antibody

While the above structure is how antibodies are often presented, there are five subtypes (known as isotypes) of antibody, immunoglobulin G (IgG), immunoglobulin E (IgE), immunoglobulin D (IgD), immunoglobulin A (IgA) and immunoglobulin M (IgM). Each of these isotypes has a unique structure (shown in Figure 1.6) and function in immunity.

IgG is the most common isotype of antibody found in human serum (12 mg/ml) and has a molecular weight of 150 kDa[36].IgG can be split further into subclasses (IgG1-IgG4) which have a range of functions including foetal protection from infection, complement activation and the mediation of opsonisation (where pathogens are coated to aid phagocytosis).

IgE is an isotype of antibody that is schematically very similar to IgG, with differences arising through the addition of a heavy chain domain in the Fc region as well as the absence of a hinge between F_c and F_{ab} regions[41]. This produces the layout shown in Figure 1.6b, although it should be noted that in vivo the structure produced is compact due to bending, not an extended 'Y' shape as might be expected[42]. IgG has a weight of 200 kDa and is present in serum at very low concentrations (0.001 mg/ml)[36]. Despite this low abundance, allergy is caused by the over production of IgE through its activation of mast cells and basophils[43].

IgD is rare in the body, making up less than 1% of serum immunoglobulins[44]. It is an isotype that contains large structural differences between species, however in humans contains four heavy chains in its F_c region[45] to produce a molecule with a mass of 175 kDa[36]. It is found most on mature B cells, however, is also secreted[45] leading to low serum concentrations of 0.1 mg/ml[36]. Its exact function is unknown, although its presence in all vertebrae[46] indicates that it is crucial.

IgA consists of a 4 heavy chain Fc region and F_{ab} region containing 2 heavy and 2 light chains, connected via either a long or short hinge depending on IgA subtype, crucial to its function the Fc region terminates with an 18 amino acid sequence which allows polymerisation. IgA is therefore found in the body in monomeric, dimeric and polymeric forms[47], leading to the large range of masses seen between 180 – 500 kDa[36]. Although IgA is not the most prevalent antibody in serum, being found at concentrations of 3 mg/ml[36,] it is prominently found in mucosal secretions and surfaces which it helps to defend[47] through direct binding to pathogens, their products and the initiation of inflamation[48]

IgM is a large immunoglobulin that is found with a molecular weight of 950 kDa[36] in a pentameric shape produced through the binding of five antibody subunits however it can also be found in a monomeric form on the membrane of B cells. It is the first antibody produced by the body both after birth and in response to an antigen and provides the blood (where it has a serum concentration of 1 mg/ml[36]) with protection, with its pentameric shape being particularly effective at activating complement[44].

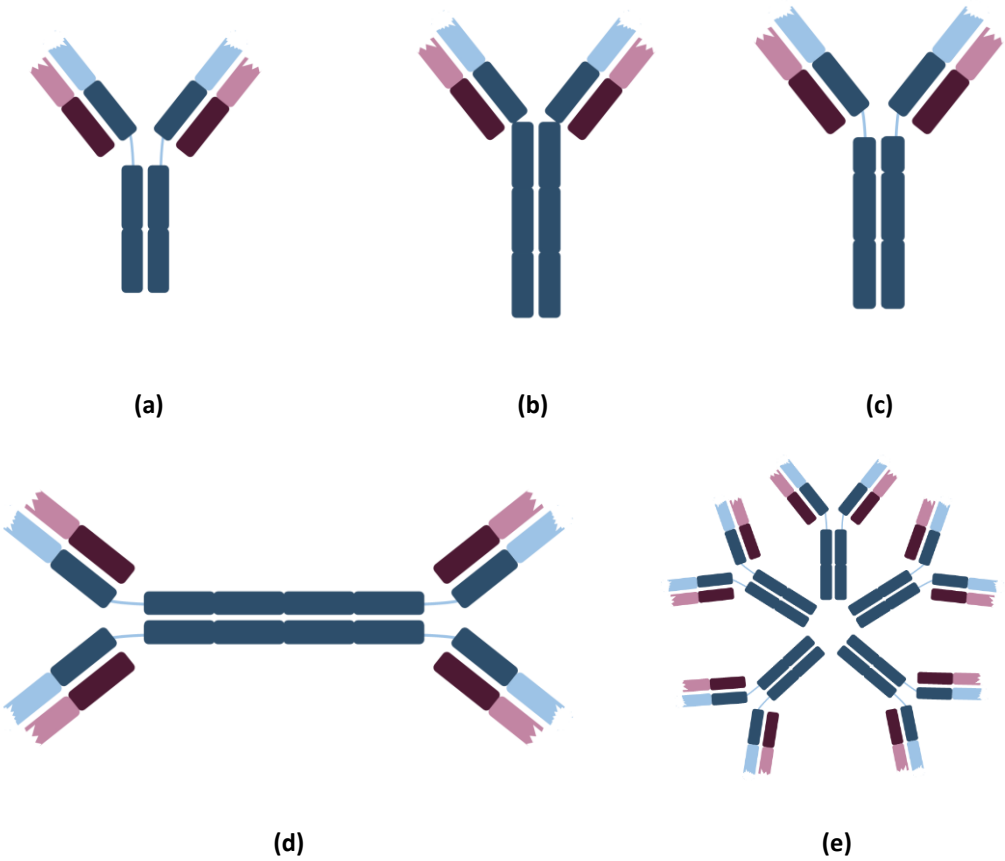

Figure 1.6: Illustrations of different immunoglobulins and the different structures they produce including IgG **(a)**, IgE **(b)**, IgD **(c)**, IgA **(d)** and IgM **(e)**.

1.2.1.2 Manufacture in and ex vivo

The most common immunoglobulin used in immunoassay is IgG[39]. In vivo IgG antibodies are secreted by activated B cells in response to a specific antigen. These B cells develop from hematopoietic stem cells in the bone marrow and during this development will pre-emptively commit to a particular antigen via the formation of specific cell-surface receptors before moving to peripheral lymphoid organs such as the lymph nodes or the spleen to wait for activation. While awaiting activation they are known as 'naïve' B cells and when they come into contact and bind to their specific target antigen they will be activated which will lead to their proliferation and differentiation (summarised in Figure 1.7).

This differentiation leads to the formation of two distinct cell types, effector B cells which actively secrete antibodies and memory B cells which act similarly to Naïve cells and await stimulation with antigen to proliferate into more memory and effector cells. Memory cells are the basis for immunological 'memory', with the stimulation of naïve or memory cells with antigen leading to an increase in the number of antigen specific B cells in the body which will accelerate future responses to the antigen[49].

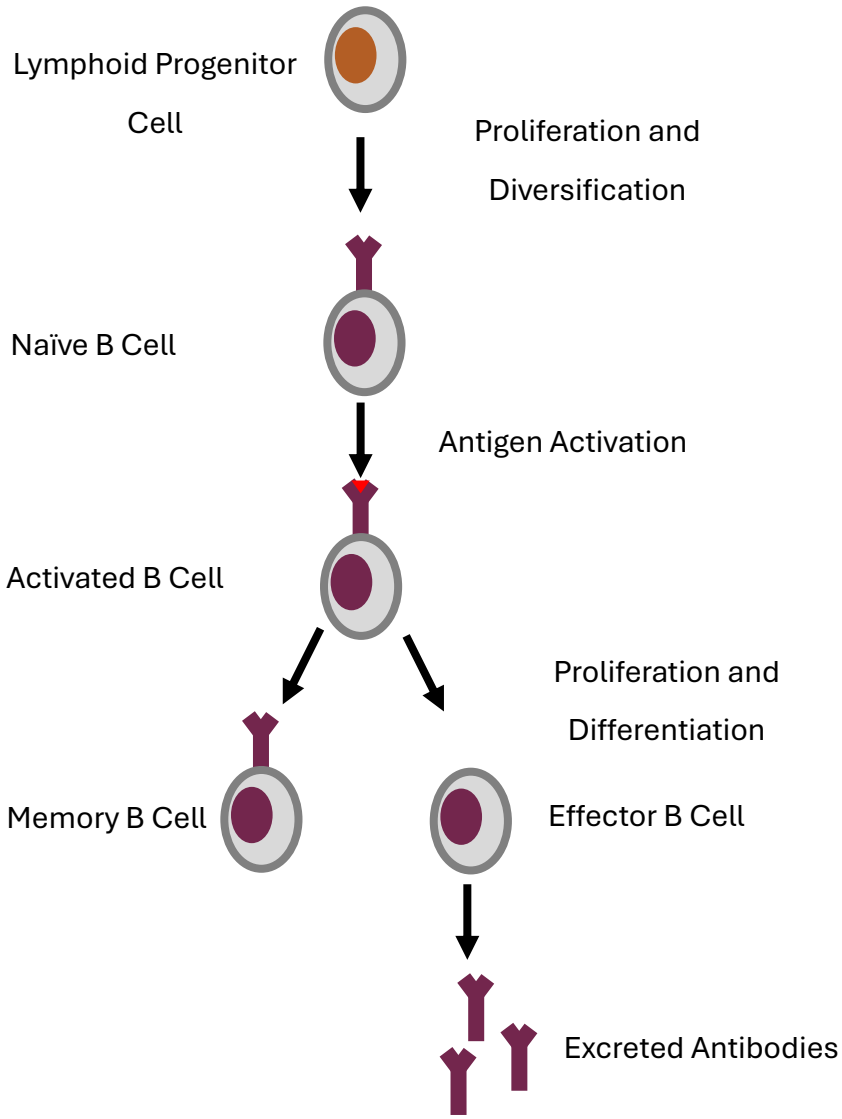

Figure 1.7: Activation and differentiation of B cells into memory and effector subtypes

The process of activation and differentiation will give rise to multiple clonal B cell populations which will target different locations (epitopes) of an antigen. The natural mix of antibodies found in blood after exposure will target a range of epitopes and so is known as a polyclonal mix[38]. Both polyclonal mixes and monoclonal mixes (that target a single antigen epitope) are used in industry and literature. Polyclonal mixes of antibody are less likely to be affected by changes in antigen shape however may cross-react with closely related antigens with similar epitopes. They are purified from the serum of donor animals (commonly

rabbits) which have been exposed to target antigens although the requirement for separate animal bleeds can lead to batch-to-batch variation[38].

Monoclonal antibodies that only target a single epitope on an antibody are highly specific and rarely cross react, although their specificity means that they lack flexibility in case of changes to the target antigen. Monoclonal antibodies are produced from tissue cultured cell lines of hybridomas (mixes of B cells and myelomas). Each cell line descends from a single B cell clone and so target a single epitope of an antigen[38].

1.3 Enzyme Linked Immunosorbent Assay

Enzyme linked immunosorbent assay (ELISA) is a technique where an immunoassay is tagged with an enzyme. Initially based on radioimmunoassay (where antigens tagged with Iodine-125 were bound to antibodies), ELISA replaces radioactive tags with enzymes which break down a substrate into a coloured or fluorescent product and can be used to measure antibodies or antigens qualitatively or quantitively as well as measure the affinity of a specific antibody-antigen pair[50]. There are four main ELISA formats: Indirect ELISA (Figure 1.8a), where an antigen is bound to a surface and an enzyme functionalised antibody is allowed to bind to the bound antigen. In indirect ELISA (Figure 1.8b) an antibody is bound to a surface immobilised antigen, and a secondary tagged antibody is bound to the primary antibody. In competitive ELISA (Figure 1.8c) a reference antigen that is tagged competes with untagged target antigen to be measured; the amount of unbound tagged antigen is then measured to indicate target concentrations. In sandwich ELISA (Figure 1.8d) a target antigen is bound between two antibodies, one of which is bound to a surface and one of which is tagged with an enzyme[51].

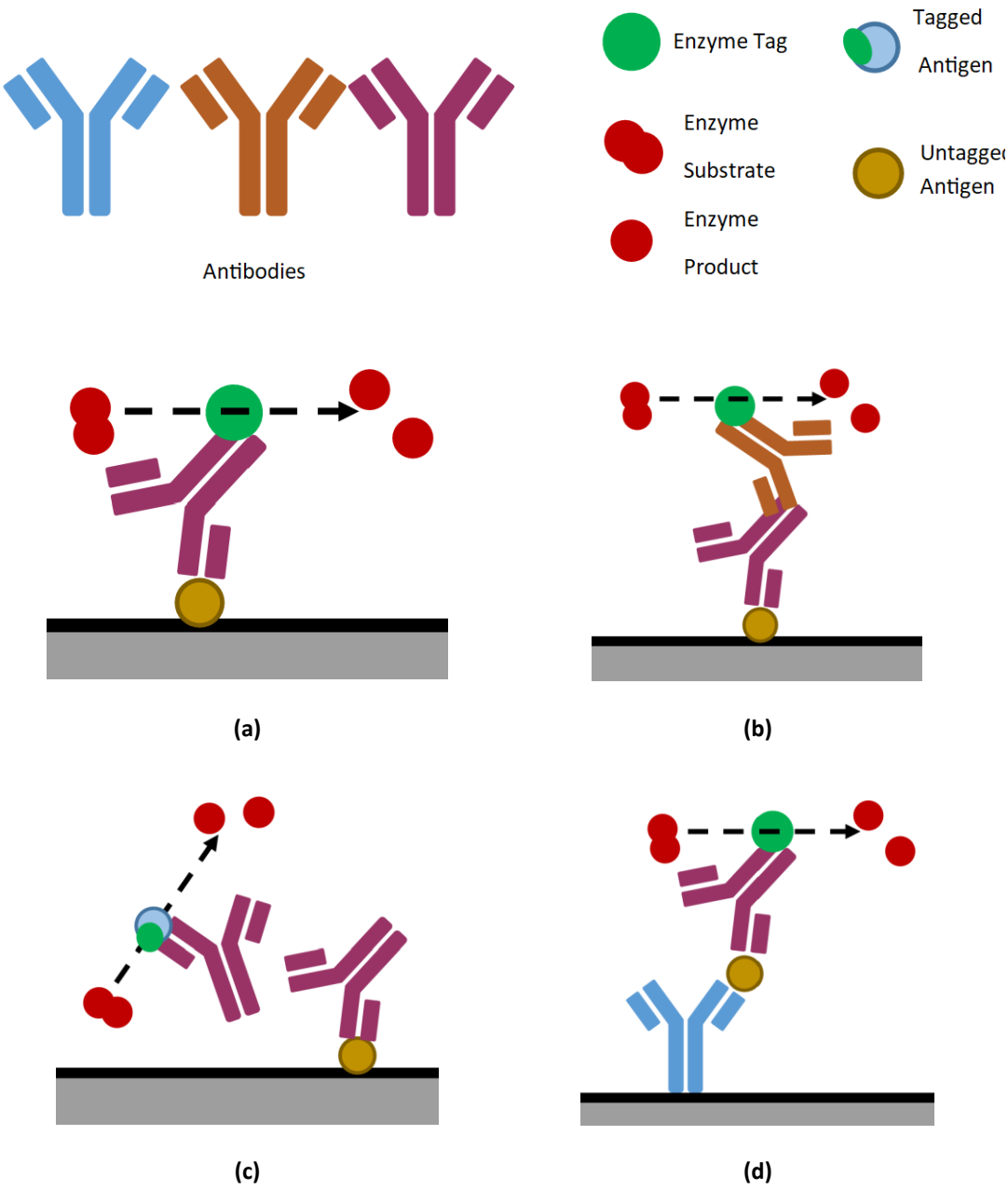

Figure 1.8: Schematics of some classical ELISA formats including direct ELISA **(a)**, Indirect ELISA **(b)**, Competitive ELISA **(c)** and sandwich ELISA **(d)**.

1.3.1 Common Enzymes in ELISA

A critical component of ELISA is the enzyme selected. An enzyme is a biological catalyst that acts on a stereospecific target, or substrate and can be purely protein based, or incorporate non-protein co factors[52]. Catalytic activity can be affected by a range of factors including temperature, pH, Enzyme and substrate concentration, enzyme specificity, the presence of inhibitors, activators or anti-enzymes[53]. There are many enzymes used in ELISA assays, chosen dependant on assay requirements, in particular the suitability and stability of the final product for measurement.

Alkaline Phosphatase (ALP) is a tag enzyme used in both electrochemical and optical immunoassays. It is a hydrolase enzyme used for the removal of phosphate groups from molecules and has a molecular weight of between 42 and 45 kDa[54]. A substrate commonly employed with the enzyme is p-nitrophenyl phosphate (PnPP) which is broken down into p – nitrophenyl, a product which has both a distinct yellow colour and an oxidative peak when tested electrochemically[55].

Horseradish peroxidase (HRP) is an enzyme made of a single polypeptide chain with a weight between 40 and 45 kDa[56] and is used in detection assays with a substrate containing hydrogen peroxide and 3,3',5,5'-tetramethylbenzidine (TMB). In these assays it decomposes peroxide, generating a reactive oxygen species which subsequently oxidises TMB into a blue product, which through further oxidation can form a yellow diimine that is stable at low pH[57] and is also electrochemically active.

Glucose Oxidase (GOx) is used both in the direct measurement of blood glucose levels and as a tag in assays. It is a glycoprotein consisting of two 80 kDa subunits each of which has a FAD co-enzyme. It catalyses the production of hydrogen peroxide and D-glucono-δ-lactone from β-D-glucose while removing oxygen from the local environment[58] which can be measured electrochemically.

Catalase is an important enzyme found in most aerobic cells with a weight of between 225 and 269 kDa depending on source[59]. It efficiently decomposes H_2O_2 into Oxygen and water, protecting cells from oxidative stress[60] and can be immobilised on electrode surfaces to determine H_2O_2 concentrations electrochemically[61] as well as being used as an electrochemical tag in ELISA[62].

1.4 Electrochemical Measurement

1.4.1 General concepts

Electrochemistry allows the measurement of chemical reactions via the use of electrodes. This measurement relies on the movement of electrons between a solution and an electrode, and so two types of reaction can be measured: oxidation reactions, in which a molecule loses an electron and becomes more positively charged (Equation 1.1) and reduction reactions, in which a molecule gains an electron and becomes more negatively charged (Equation 1.2). Often these reactions will be paired in a redox process in which a 'donator' will give an electron to an 'acceptor'. In electrochemistry, electrodes are employed to serve as an acceptor or donator to these reactions, and the movement of electrons at the electrode measured.

Equation 1.1: Example of an Oxidation Reaction

$$Na \rightarrow Na^{+} + e^{-}$$

Equation 1.2: Example of a Reduction Reaction

$$Cl + e^{-} \rightarrow Cl^{-}$$

Experimentally, a complete circuit is required for the measurement of this electron movement, this is produced by an electrochemical cell which is used to drive reactions via the application of voltage and measurement of resulting currents. Most commonly these cells consist of three electrodes connected to a driving potentiostat as shown in Figure 1.9.

These three electrodes have distinct roles in the system:

- The working electrode (WE) is where voltage is applied and therefore where reactions of interest take place. The current passed due to this voltage is measured and corresponds to interactions between analytes and the surface of the WE.

- The reference electrode (RE) holds a fixed potential which voltage at the working electrode is measured against.
- The counter electrode (CE) completes the electrical circuit along with the WE by passing current as required.

Although this is the most common arrangement for an electrochemical cell, two electrode systems are also used. These two-electrode systems consist of a working electrode and a combined counter/reference electrode.

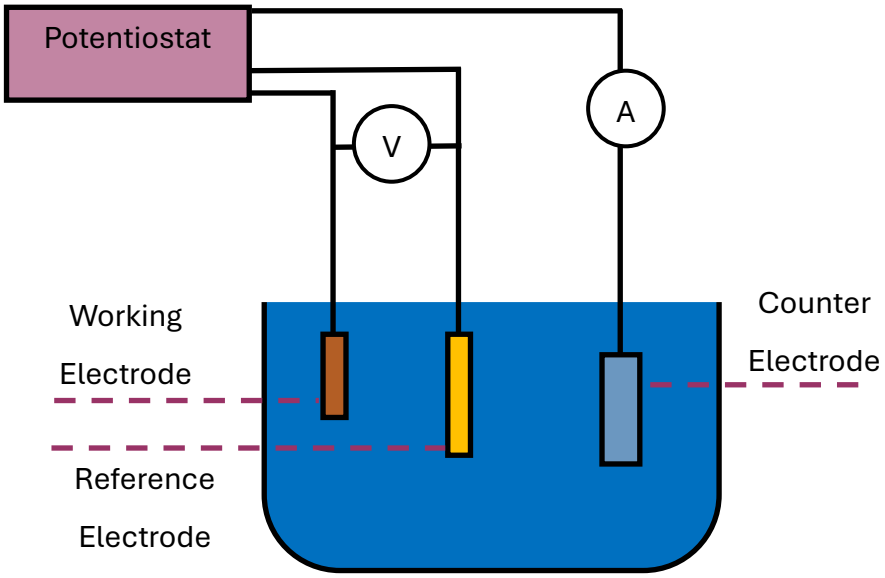

Figure 1.9: Schematic representation of a typical electrochemical cell showing where current and voltage are measured.

1.4.2 The Electric Double layer

During measurement, when a charged electrode meets a conductive solution, ions in the solution will be attracted or repelled to balance this charge. This produces a 'double layer' at the surface consisting of a bound Helmholtz layer of ions that are immobilized on the electrode surface, as well as a diffuse Gouy layer that extends towards the neutrally charged bulk electrolyte (shown in Figure 1.10)[63]. This Helmholtz layer contains ions in two states, some that have become unsolvated (are no longer surrounded by solvent molecules) and been allowed to adsorb to the electrode surface either through van der Waals or coulombic

interactions to form an inner Helmholtz layer (IHL) and those that have been attracted to the surface but cannot adsorb as they remain solvated in the outer Helmholtz layer (OHL)[64].

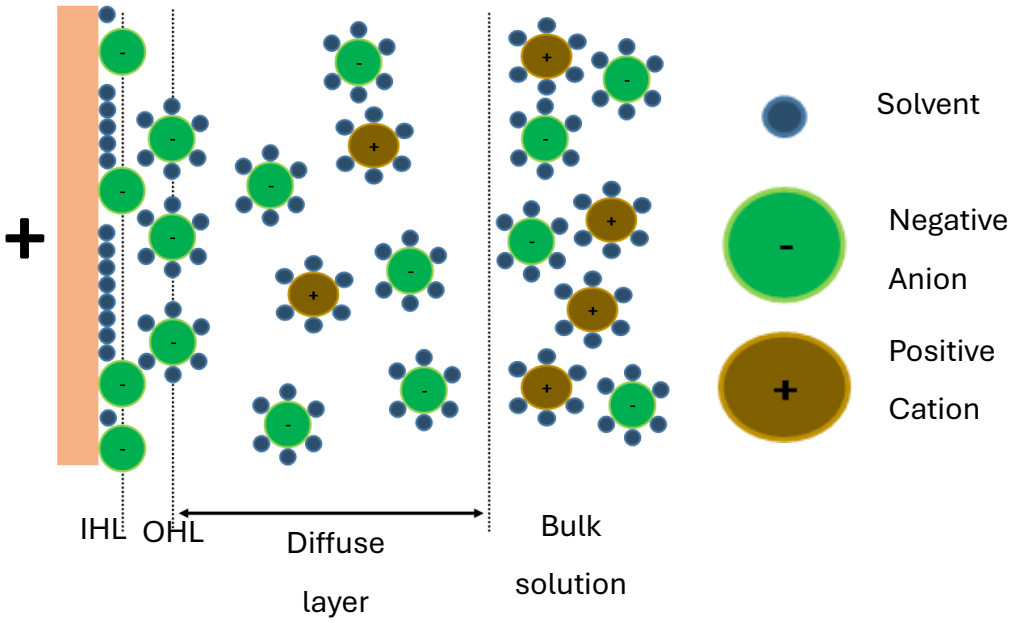

Figure 1.10: The electrical double layer seen at the surface of a charged electrode.

The double layer produced acts as a parallel plate capacitor, where there is a linear relationship between the charge on the plates and the potential difference between them related to the capacitance. The liquid nature of one side of this capacitor means that as potential is changed on the electrode surface, ions will rearrange and migrate to balance the new charge. This movement of ions will generate a charging/capacitive current that rapidly decays as this rearrangement stabilises[64].

1.4.3 Mass transport to the electrode

For electrochemical measurement to take place, species of interest must first move to the electrode surface, this process, known as mass transport, can happen via migration, convection or diffusion.

Migration refers to the movement of charged species along a potential gradient; in electrochemistry this gradient is produced from the electrochemical cell and

migration is the process in which charges balance across the cell. Its effect on species of interest is often minimised via the addition of a supporting electrolyte which responds to potential gradients rather than the species to be measured.

Convection refers to the movement of species due to mechanical forces and can be unintentionally introduced via bumps, knocks or vibrations in the experimental environment or intentionally introduced in a controlled way by flowing electrolyte solution over the electrode or using a moving surface.

Diffusion is the movement of species along concentration gradients from an area of their high concentration to an area of their low concentration and is often measured in electrochemical experiments. As substrates react on the electrode surface and generate products diffusion is relied on to replenish substrate at the surface and to remove excess product.

In laboratory experiments, two conditions of mass transport are used:

- Diffusion dominated, where solutions are unstirred and contain a large amount of supporting electrolyte (to diminish migration effects) and experiments are performed quickly (to reduce the impact of convection)
- Convection dominated, where solutions again contain a large amount of supporting electrolyte (to diminish migration) however the electrode surface and solution to be measured are moved past each other to diminish the impact of diffusion and maximise the effect of convection[65].

1.4.4 Electrochemical Measurement

Electrochemical measurement can be performed potentiostatically or galvanostatically. In Potentiostatic measurement, voltage is varied at the working electrode and current passing the counter electrode measured. In galvanostatic measurements the current is varied at the working electrode and resulting voltage at the counter electrode measured. Common potentiostatic methods used over the course of this thesis are outlined below.

1.4.4.1 Cyclic Voltammetry

Cyclic Voltammetry (CV) is a popular technique often used initially to allow the rapid observation of the redox behaviour of a system[66]. It is performed by sweeping the potential applied to a system between two values, or 'switching potentials' while measuring the resulting current. Results are plotted as a voltammogram of potential vs current (E vs i) with higher potentials either to the left or the right of the graph, in this thesis the latter layout will be used (high potentials will be seen to the right of graphs).

These voltammograms provide a large amount of information about an electrochemical system, in particular showing peaks in current response at potentials capable of eliciting redox reactions in the solution they are in, a classical response expected of a simple reversible redox couple is shown in Figure 1.11. Its behaviour is controlled by both mass transport and thermodynamics at different points on the plot.

As the potential is scanned between **A** and **D** in the positive direction, N at the surface of the electrode is steadily oxidised to N^+, between **A** and **C** this oxidation is thermodynamically controlled by the charge able to pass between the electrode and N and so as potential increases, so does current (also known as thermodynamic control). As the rate of oxidation on the electrode surface increases, more unoxidized N must diffuse to the surface from the bulk of the solution through a diffusion layer. At **C** this diffusion begins to limit the oxidation at the electrode surface and between **C** and **D** as the diffusion layer grows current response will drop (known as mass transport control). At **D** the direction of potential movement will reverse and the reduction of N^+ to N will begin. During both forward and backward scans there will be a point at which the concentration of N and N^+ at the surface of the electrode are equal (**B** and **E**), this point is known as the standard potential of N (E^0) and will lie midway between the peaks seen[67].

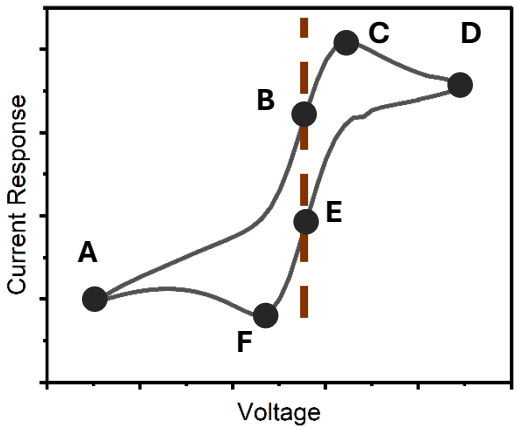

Figure 1.11: Classical response of a reversible system under CV measurement.

There are many equations that are used to describe these simple reversible systems and can either be used to predict the performance of a system or be used to calculate information about a system from its measured performance. Most of these equations are based around the peak currents seen in a system or the separation between oxidative (i_{po}) and reductive (i_{pr}) peaks, measured as shown in Figure 1.12.

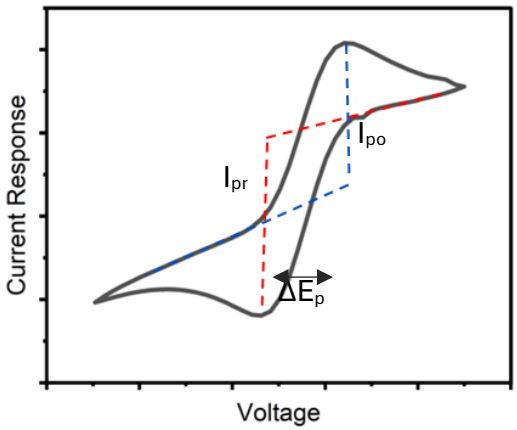

Figure 1.12: The measurement of peaks in a CV and their separation.

The Randles- Sevcik equation shown in Equation 1.3 can be used in the prediction of peak currents and is also often rearranged to calculate the concentration or diffusion coefficient of an analyte.

Equation 1.3: The Randles-Sevcik equation, used to calculate peak currents in a reversible system.

$$i_p = 0.466FAC(\frac{nF\vartheta D}{RT})^{1/2}$$

At 25 degrees, this can be simplified to:

Equation 1.4: Simplified Randles-Sevcik equation

$$i_p = 2.69 \times 10^5 n^{\frac{3}{2}} AC\sqrt{D\vartheta}$$

Where i_p is peak current **(a)**, n is the number of electrons transferred, F is the faraday constant (C mol^{-1}), A is the electrode area (cm^2), C is analyte concentration (mol cm^{-3}), D the diffusion coefficient of the analyte (cm^2 s^{-1}), R the universal gas constant (J K^{-1} mol^{-1}), T the temperature (K) and v is scan rate (V s^{-1}) [67].

Another common equation used to describe the CV response of a reversible system is the Nernst Equation (Equation 1.5). It describes the typical shape of a CV plot and allows calculation of the formal potential of a system, the expected potential of a system given the concentrations of reduced and oxidised species are known and the ideal peak separation of a system (59 mV if one electron is transferred). If the CV response of a system is characterised by two steep and opposite 'duck' shaped peaks separated by 59 mV it is known as a 'Nernstian' system.

Equation 1.5: Nernst Equation used to describe a reversible electrochemical system

$$E = E^0 - 2.3026\frac{RT}{nF}log_{10}\frac{[Red]}{[Ox]}$$

F is faraday constant, R is universal gas constant, n is number of electrons involved, T is temperature in kelvin, E is potential of the electrochemical cell, E0

is the standard potential of the species, Red and Ox are the concentrations of reduced and oxidated species [67].

The heterogenous electron transport rate (K^0) is also often calculated. It indicates the rate of electron transport between an electrode and species of interest and this thesis it is calculated using an approach shown by *Randviir*[68]. In this approach, CV measurement of a species is performed at a range of scan speeds (how fast potential is increased or decreased) and peak separation recorded.

At each scan speed ψ is first calculated via the use of Equation 1.7 before being plotted against $[\pi DnF\vartheta/RT]^{1/2}$ from Equation 1.6. After multiple measurements this plot is fitted with a straight line, whose gradient equals K^0.

Equation 1.6

$$\varphi = k^0[\pi DnF\vartheta/RT]^{1/2}$$

Equation 1.7

$$\varphi = (0.0021\Delta E_p - 0.6288)/(1 - 0.017\Delta E_p)$$

The calculated value of K^0 allows us to gauge the reversibility of a system as summarised in Table 1.3, with large values indicating reversible systems governed solely by mass transport and small values indicating irreversible systems governed solely by thermodynamics. Quasi reversible systems are also common, which are governed by both[69].

Table 1.3: How heterogenous electron transpot rates indicate system reversibility[69]

Rate constant (K^0)	**What it means**
$k^0 > 10^{-1}$ cm/s	System is reversible
$10^{-1} > k^0 > 10^{-5}$ cm/s	System is quasi reversible
$10^{-5} > k^0$ cm/s	System is irreversible

1.4.4.2 Square Wave Voltammetry (SWV)

Square waveforms have been used in the stimulation of electrochemical systems since as early as 1952[70], initially in square wave polarography. During square wave voltammetry an electrode is stimulated with a voltage composed of a symmetrical square wave superimposed upon a simple voltage staircase (Figure 1.13a).

This input is characterized by pulse height, the height of the underlying staircase, pulse time and cycle period. Current is measured at the end of forward and reverse peaks and the difference between these measurements displayed as a final current[71].

While providing similar current/voltage peaks as seen in cyclic voltammetry relating to redox events at the electrode surface, the measurement of both the peak (I_1) and the trough (I_2) of the applied wave (shown in Figure 1.13a) allows the effect of double layer capacitance charging, which will occur when the potential of an electrode is varied to be minimised. This minimisation is performed simply via the subtraction of I_2 from I_1, providing a 'capacitance free' graph which is either plotted with or without these two inputs (see Figure 1.13b)

Equation 1.8: Calculation of presented current in SWV.

$$I_{Net} = I_1 - I_2$$

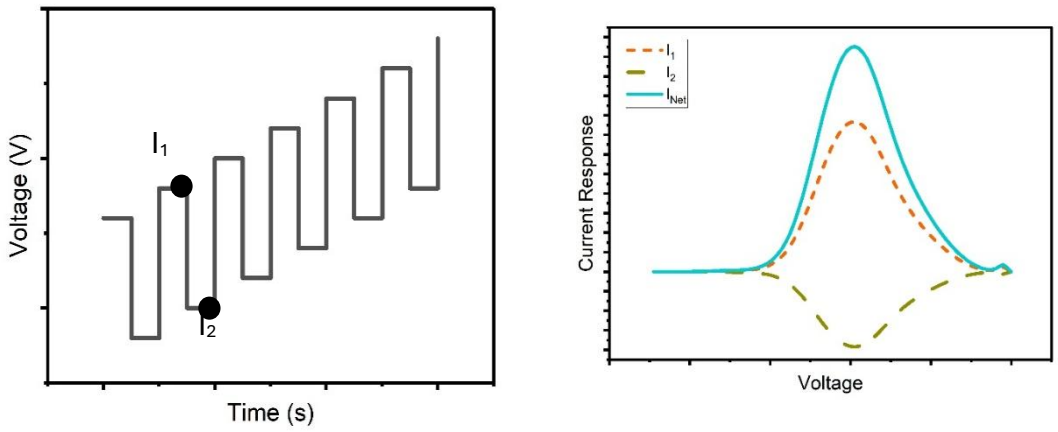

(a) **(b)**

Figure 1.13: Votage applied to a system during SWV measurement, showing where current measurements are made **(a)**. Resulting voltammagrams of this measurement, along with the 'combined' response produced and routinely presented **(b)**.

1.4.4.3 Chronoamperometry

Chronoamperometry is a technique where a single potential is applied to a system and held as shown in Figure 1.1a, and the resulting current response measured[72]. This response has three distinct regions, shown in Figure 1.14, controlled by the growth of a diffusion layer on the electrode surface:

- Before the potential step is applied, when t < 0, the concentration of the species to be measured will be in equilibrium between the electrode surface and the bulk of the solution.
- As the potential step is applied, when t = 0, a large spike in current response will be seen as the target species at the electrode surface reacts rapidly. As this species reacts, unreacted species will diffuse towards the electrode surface from the bulk of the solution through a diffusion layer.
- Long after the potential step is applied, when t >> 0, the current response will plateau. As the reaction continues, the diffusion layer between the electrode surface and bulk solution will grow and so unreacted species must move further to react at the electrode surface. The current able to pass at the electrode therefore becomes limited by the speed at which

species can diffuse from the bulk solution (which still has the original concentration) through this diffusion layer to the electrode surface.

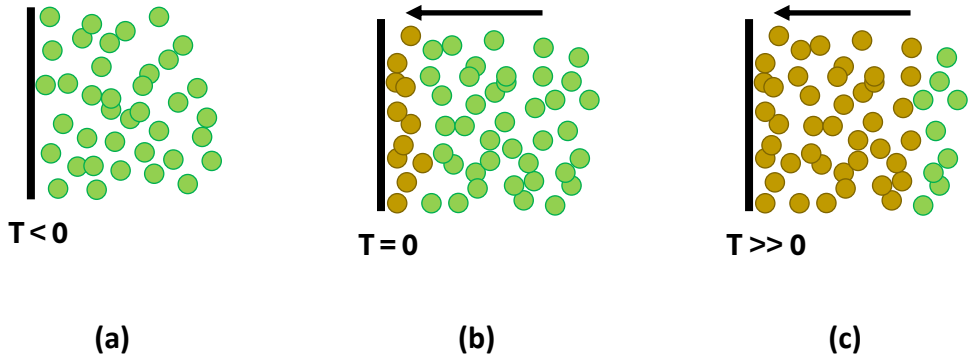

Figure 1.14: Concentrations of the target species by the electrode surface before **(a)**, just after **(b)** and long after **(c)** the application of a step potential

If a potential is applied that is in the diffusion limited area of a reaction and it is ensured that diffusion is the only mechanism of mass transport active (via the limitation of convection and migration), the resulting plateauing in current response over time can described by the Cottrell equation (Equation 1.9):

Equation 1.9: The Cottrell Equation

$$i = \frac{nFA\sqrt{D_0}C_0}{\sqrt{\pi t}}$$

Where C_0 is the initial concentration of the measured species, D_0 is its diffusion coefficient, n is the number of electrons transferred in its reaction, F is the faraday constant, A is the area of the electrode and t is the time passed since application of the potential step[73]. This models the current response shown in Figure 1.15b, however the Cottrell equation is often rearranged to calculate the concentration of a target or its diffusion coefficient.

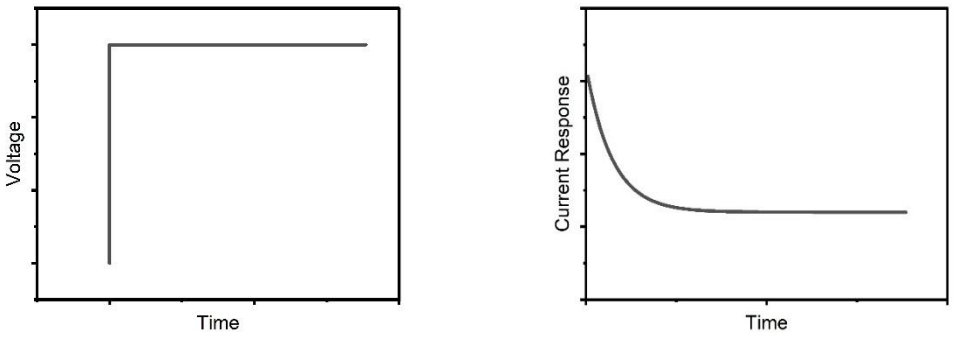

(a) **(b)**

Figure 1.15: The voltage applied to a system during chronoamperometry **(a)** and the standard time, current response produced **(b)**.

1.4.5 Electrochemistry on carbon materials

Regardless of the target and detection strategy of an electrochemical biosensor, the electrode that it is based on is critical. Guidance on this selection is available in literature and is often found in papers or books that focus on the manufacturing of whole biosensors[74,75] or other specialised systems[76]. More direct comparisons of electrodes are also available[77,78], although given the huge range of electrodes, they are better viewed as guides than definitive proof of the 'best' electrodes. This literature primarily focuses on two material families, gold and carbon.

Gold electrodes are commonly produced either through the patterning of a thin layer of gold or deposition through a stencil. As a material, gold immobilizes biological molecules well, enhances electron transfer between redox centres and electrodes, is highly stable, corrosion resistant, biocompatible, inert[79] and is readily functionalised via strong gold-sulphur bonds[80]. Despite these clear advantages, gold, as well as other noble metals, are often avoided in commercial applications due to their relatively high cost[81].

Carbon electrodes (introduced in the 1950s via the use of handmade graphite paste electrodes[82]) are commonly produced through the mixing of carbon powders with solid or liquid binders to produce electrodes or printable inks. They can consist of a large range of carbon materials and so their properties can vary drastically however in general they are low cost[83], highly conductive, chemically inert and have wide voltage ranges[84] although they often require overpotential which requires surface modification to negate[83].

Traditionally this positions gold and carbon electrodes as opposites. Where expensive gold-based electrodes can produce much better responses than their carbon counterparts which are preferred in high throughput applications (such as screening). Due to their lower costs carbon electrodes are also ubiquitous in literature (see Table 1.4).

Table 1.4: Examples of carbon-based electrochemical sensing seen in literature

Carbon Material	Material Class	Target Molecule	Measurement Type	Reference
Reduce Graphene Oxide	Solid	Escherichia coli.	Biologically Mediated Detection	[85]
Carbon Paste	Composite	Prostate Specific Antigen	Biologically Mediated Detection	[86]
Carbon /PLA mix	Composite	Serotonin	Direct Detection	[87]
Graphene /conductive polymer	Composite	Dopamine /cytokines	Biologically Mediated Detection	[88]
Glassy carbon	Solid	Prostate Specific Antigen	Biologically Mediated Detection	[89]
Glassy carbon	Solid	17β-estradiol	Biologically Mediated Detection	[90]

Until the 1980s, diamond and graphite were the only well-known structures of carbon[91] and while diamond is non-conductive, graphite (and the more recently discovered graphene) is highly conductive due to the presence of delocalised electrons in its structure.

This structure (shown in Figure 1.16) consists of a hexagonal pattern in which each carbon atom is covalently bound to three others (allowing the fourth valence electron to become delocalised) and forms sheets that may exist alone (in the case of graphene) or may stack upon one another (in the case of graphite).

They have two planes, a ‘basal’ plane that is perpendicular to the sheet and an ‘edge’ plane that runs parallel to a sheet[92].

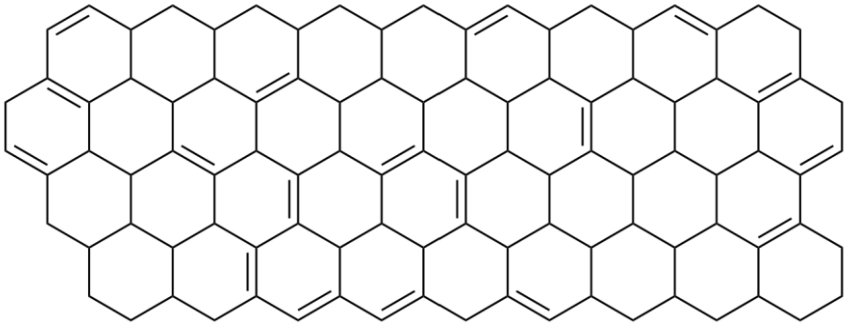

Figure 1.16: The general structure of graphite and graphene

Many other carbon materials are also used in the manufacturing of electrodes. Glassy carbon is one of the most well-known, having been applied in electrochemistry since 1964. It is a form of semi-amorphous carbon that although has no long-range crystal structure contains many sp^2 hybridised atoms which form planar 2D structural elements and contribute towards the presence of delocalised electrons in its structure[93].

Carbon black is a material that is similar to graphite and consists of individual graphene sheets that form a disordered structure with one another leading to the formation of nanoparticles. These nanoparticles then aggregate together to form clusters[94].

Carbon nanotubes are again a graphene-based material and consist of graphene sheets that are rolled into tubes of varying lengths in the nanometre to micron range. These tubes can be formed from a single graphene sheet (single walled nanotubes) or from multiple concentrically rolled sheets (multi walled nanotubes)[95].

Despite pure diamond being a good insulator, during the production of synthetic diamonds via chemical vapor deposition a diamond structure can be doped with a range of materials to affect its final properties. Of particular interest to

electrochemistry are diamond structures doped with boron (boron doped diamond) which produce conductive electrode material with a wide solvent window, is mechanically robust, has low capacitance and a high resistance to fouling[96].

Regardless of the material chosen for electrode construction, how its bulk structure meets the surrounding environment (known as its 'termination') is critical. Although this termination may take the form of a pure carbon edge, often a range of 'functional groups' containing other elements will be found. Most commonly functional groups containing oxygen (Figure 1.17) or nitrogen (Figure 1.18) are found.

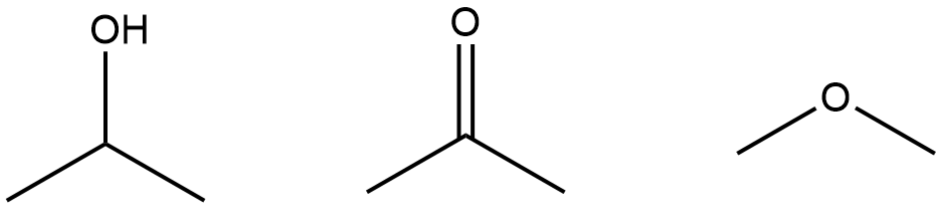

Hydroxyl Carbonyl Ether

Figure 1.17: Examples of oxygen termination seen in graphite and graphene materials.

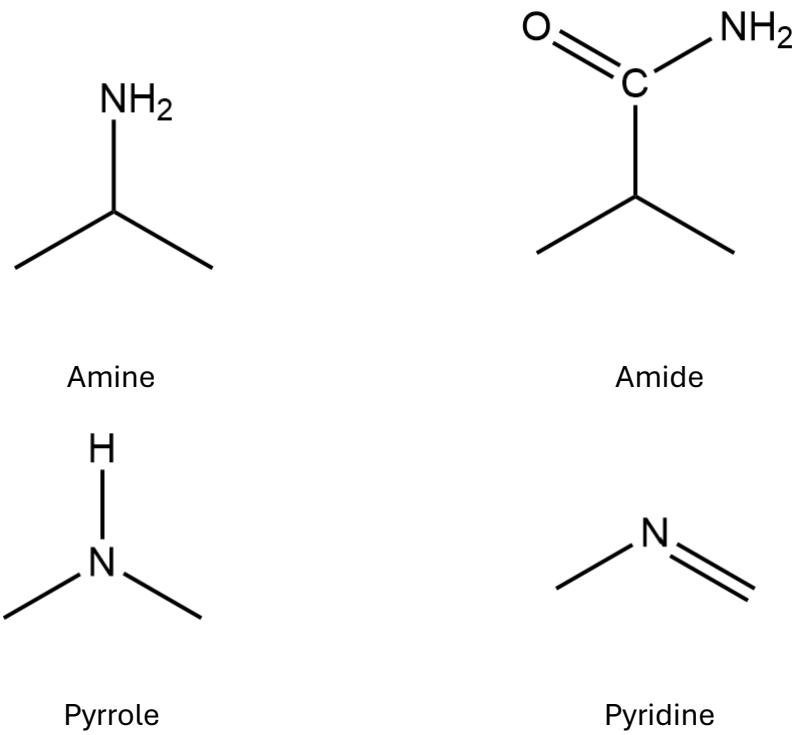

Figure 1.18: Examples of nitrogen termination seen in graphite and graphene materials[97].

These functional groups can have a large impact of the electrochemistry of a carbon material, however, often improve surface stability, hydrophobicity, electron transfer and enable specific chemical reactions. Many pretreatments of carbon in literature therefore aim to generate more functional groups on the surface of electrodes or to increase the number of edges or defects at the surface of a material at which termination can occur, although this is also commonly achieved or the use of nanoparticles (such as carbon black[94]).

1.4.6 Composite electrodes

These carbon materials are often used in the manufacturing of composite electrodes, produced through the mixing of conductive (providing electrochemical activity) and nonconductive (providing structure) materials. This creates electrodes with a mixed structure as shown in Figure 1.19, producing unique electrochemical activity through the combination of bulk and surface behaviour.

In the bulk of the electrode (Figure 1.19a), the random arrangement of conductive material leads to the random formation of conductive paths through it, leaving many dead ends and islands of unconnected material which will be prevented from passing charge. In general, the larger the proportion of conductive component within the compound material, the lower the resistance of the material as more full conductive paths can be formed through it. Conversely at very low proportions of conductive material the compound may act as an insulator. The minimum fraction of a compound material that must be conductive to allow overall conductivity is known as the percolation threshold (Glossary of terms relating to electronic, photonic and magnetic properties of polymers (IUPAC Recommendations 2021)). Given that charge must travel through an unbroken path from the electrode surface to a driving potentiostat, even above the percolation threshold the random arrangement of conductive pathways leads to unpredictable bulk performance even in materials with the exact same constituents.

On the surface of the electrode (Figure 1.19b), conductive material will again be randomly arranged and only areas connected to the potentiostat through the bulk will be active in electrochemical reactions. Each of these areas will act as independent electrodes and will each have independent fields of diffusion and charge surrounding themselves which may overlap and interfere with each other.

The combination of surface and bulk behaviour produces electrodes whose behaviour is variable and difficult to predict using standard electrochemical formulae which are developed around single material disk electrodes.

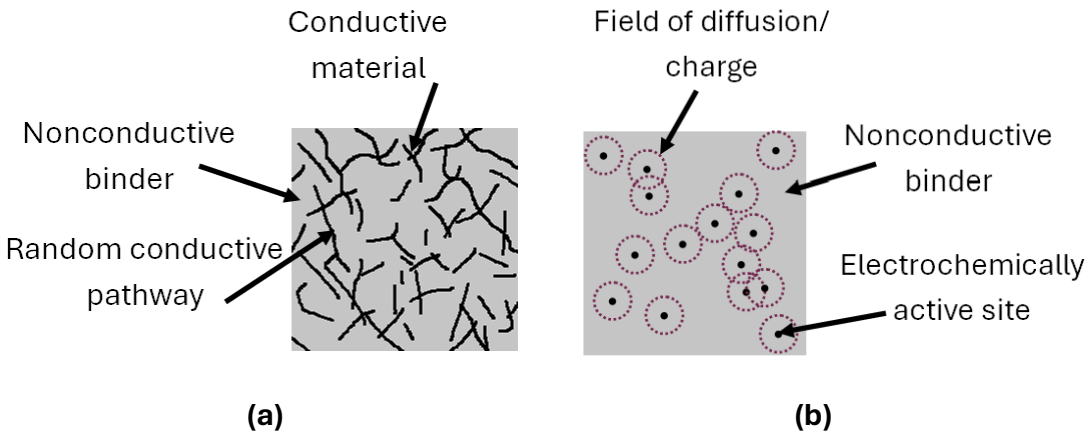

Figure 1.19: The general structure of a compound electrode within its bulk **(a)** and at its surface **(b)**.

1.5 Qualifying Sensor Performance

1.5.1 Limit of detection and limit of quantification

One of the most common methods for the defining of sensor performance, not only in biosensors but also more traditional sensors is the limit of detection of the system. Simply put, the limit of detection (LoD) of a system is the lowest concentration of target analyte that can be reliably measured. Limit of quantification (LoQ) is also used for the definition of performance, although this is usually found simply through the multiplication of LoD to produce a significant margin of error in industrial or medical use. In literature there are many ways that LoD can be calculated and, especially when left to individual investigators, practical performance of systems can often be vastly over or underestimated. It is therefore important to clearly define LoD calculation.

In this thesis limit of detection is calculated based on guidance from *Armbruster and Pry*[98] which itself is based upon the EP17 guideline produced by the Clinical and Laboratory Standards Institute. This approach breaks down calculations into LoD, LoQ and a third component, Limit of the blank (LoB).

Limit of the blank is the first quantity calculated and indicates the highest apparent concentration of analyte that is found from blank measurements, it is calculated using Equation 4.1 and requires only a blank measurement performed using medium without any analyte present to calculate.

Equation 1.10: Limit of the blank

$$LoB = Mean_{(Blank)} + 1.645(STD)_{(Blank)}$$

Limit of detection is calculated using both the limit of the blank and the standard deviation of a sample measurement (Equation 4.2), ideally this sample measurement should be taken at a low concentration near the expected LoD.

Equation 1.11: Calculating limit of detection

$$LoD = LoB + 1.645(STD)_{(Sample)}$$

Limit of quantification is not numerically defined in these guidelines. It is left up to individual investigators to define and so it will be omitted from reporting. An experimental LoD (ELoD) will be presented instead, defined as the concentration above the LoD that was measured in experimental work[98].

1.5.2 Other Factors

In addition to LoD and LoQ there are a range of other parameters that are used in the description of sensor performance:

- Sensitivity refers to how small a change in analyte a system can measure or at which statistical uncertainty will arise as to whether the results is zero or a measured value[99]
- Specificity refers to the ability of a sensor to distinguish between closely related targets[99].
- The accuracy of a sensor is its ability to produce readings that agree with other reference measurements[99].
- Precision is a system's ability to produce repeated results when measuring the same target[99].
- Linear range is commonly used in immunoassay measurement and refers to the range at which the relationship between target concentration and resulting signal is linear; this is often the range at which an immunoassay is used over[100]

1.6 Thesis Scope

Cancer is a major cause of both death and disability in the modern world and causes a large percentage of deaths in the UK. Despite its ubiquity, as a disease, its heterogeneity makes detection and treatment difficult and although many leading cancers are screened for, many are not due to inadequate methodologies existing. Liquid biopsy, where genotypic or phenotypic information about a cancer is extracted from bodily fluids, may enable expansion of screening programmes and allow the tracking of cancers and their treatments.

A common approach to the measurement of these liquid biopsies is immunoassay, performed through the strong, specific bonding that occurs between an antibody and its target antigen. This binding is primarily measured via labels and enzymes are commonly selected and used in 'enzyme linked' immunoassays. These enzyme tags can produce a large range of products, including those that are redox active.

Electrochemical approaches can easily read these redox active tags and have a large amount of potential in biosensing due to their ability to produce low cost, small and sensitive systems that can be used at the point of care. This is particularly true when using carbon-based sensors which are lower cost than many of their counterparts.

This thesis aimed to develop a carbon-based electrochemical immunoassay for the measurement of key cancer biomarkers in blood samples, this was performed via four chapters:

- In the first chapter a cheap, carbon-paste based electrode was produced and its function confirmed.
- The second chapter finalised this development and tested the ability of the electrode to detect analytes both directly as well as indirectly using ELISA protocols.

- The third chapter used this electrode in the detection of more specific cancer biomarkers.
- The fourth chapter further developed electrode manufacturing techniques and pretreatments to improve inter chip variability.

2 Development of a carbon paste electrode

2.1 Introduction

A material of particular interest in the low-cost development of electrodes is carbon paste. Carbon paste is a compound electrode material and was first described in 1958[82] and refers to mixtures of electrically conductive carbon materials and binders/solvents[101] that are used in the production of electrodes. This simple mixing approach allows manufacturing easily at a low cost on the bench. It also allows the facile inclusion of non-carbon materials such as metal nanoparticles, redox mediators and enzymes which can be thermally stabilised by paste incorporation[102].

The carbon components of paste materials often come in the form of powders that are mixed into a nonconductive support. Carbon particles in these powders can be 3D (graphite, boron doped diamond), 2D (graphene), 1D (nanotubes) or 0D (fullerenes)[103].

As carbon paste electrodes are formed of individual conductive particles, charge must pass from the electrode surface to a potentiostat by 'jumping' between particles as shown in Figure 2.1, the resistance to each of these jumps is known as the 'contact resistance'. The effect of this contact resistance between carbon particles and between carbon particles and the metal connector between an electrode and potentiostat often contribute a significant amount of resistance to a carbon paste system and however can be minimised through the incorporation of larger carbon particles which reduce the number of 'jumps' required between the electrode surface and potentiostat.

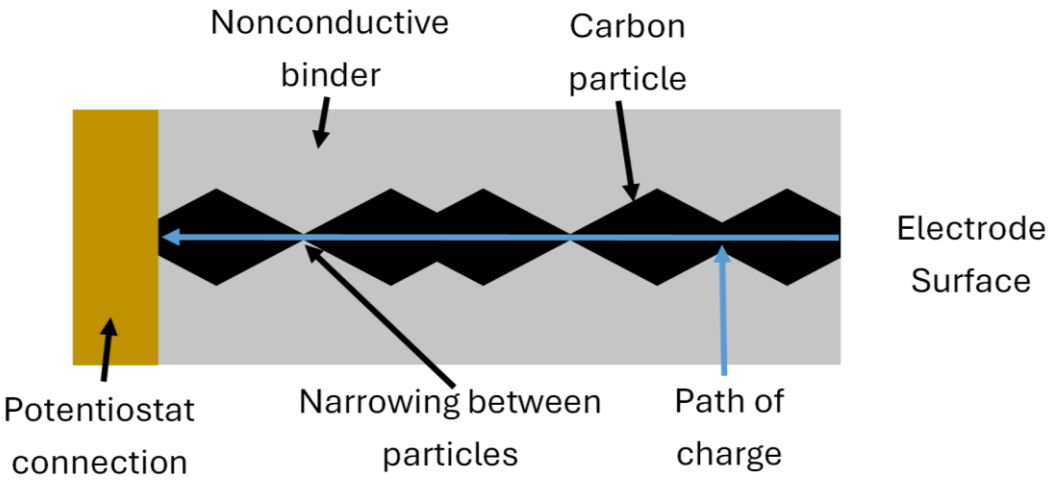

Figure 2.1: How contact resistance arises in carbon paste electrodes

The size of carbon particle incorporated within a paste material also has a large effect on its percolation threshold (how much conductive material must be incorporated to make a compound that is conductive). Where smaller particles can reduce this threshold through increasing the amount of particle contacts within the material, 'longer' particles such as nanotubes are also able to reduce the percolation threshold.[103]

The nonconductive component of a paste also has a huge impact on its overall performance. Traditionally, 70% of carbon pastes are made with oil binders[104], the properties of which dictate the physical characteristics of a resulting paste and can produce viscous pastes that are packed into moulds[82] or inks suitable for pritnting[88]. Pastes can also be manufactured from solid binders such as paraffin wax[105] as well as printable plastics such as PLA[106]. Although less common, these solid pastes can have several advantages over their liquid counterparts in particular improved robustness and reproducibility[107].

Whether carbon paste or otherwise, sensors are often pretreated before use. Physical pretreatment (Table 2.1) aims to homogenise the sensor surface.

Table 2.1: Examples of physical electrode cleaning seen in literature

Electrode	Cleaning method	Reference
Carbon paste	Smoothed on cardboard	[108]
Glassy carbon	Emery paper and sonication	[109]
Glassy carbon	Alumina slurries and polishing paper	[78]

Electrochemical pretreatments (Table 2.2) aim to either etch the surface of an electrode to reveal conductive material or produce active functional groups on the material surface that can facilitate electron transport.

Table 2.2: Examples of chemical or electrochemical electrode cleaning seen in literature

Electrode	Cleaning method	Reference
Screen printed carbon	CV in H_2O_2	[110]
Screen printed Carbon	CV in H_2SO_4	[78]
Screen printed carbon	CV in NaCl	[111]
Screen printed carbon	CV in KCl	[112]

2.2 Chapter Outline

This chapter aimed to produce a useable carbon paste electrode within the lab and answer three questions:

- Can a carbon paste electrode be produced in the lab?
- Can physically cleaning this electrode improve its reproducibility?
- Can chemical pretreatment of this electrode improve its reproducibility?

2.3 Materials and methods

2.3.1 Materials

Chemical	Supplier	Product Number
Paraffin wax	APC Pure	PW56-Y
Graphite powder	Inoxia	0029882791622
Polishing kit	IJ Cambria	011975
Sandpaper	RS components	188-3425
Hexaammineruthenium (III) chloride	Thermo Scientific	363340010
Deionised water	Scientific Laboratory Supplies	CHE3874
Phosphate Buffered Saline (PBS) Tablets	Merck	P4117
Sulphuric Acid	Merck	258105
Hydrogen Peroxide	Merck	1086001000
Potassium Chloride	Merck	529552
Sodium Chloride	Merck	S9888

2.3.2 Paste manufacturing

Carbon paste was produced by mixing solid paraffin wax with graphite powder in various weight ratios (wax: graphite mixes of 40:50, 50:50 and 60:50). Paraffin wax with a melting point of between 56-60 degrees Celsius was used. Synthetic graphite was used with particle sizes of below 53 μM. Both materials were weighed and added to a metal beaker before being heated using a heating mantle (Electrothermal).

During heating, mixing was performed using a metal spatula and once fully melted and combined (shown in Figure 2.2) the paste was either left to cool or

used in the manufacturing of electrodes. On reheating the paste was mixed for five minutes to ensure homogenisation.

Figure 2.2: Homogenised paste before use.

2.3.3 Electrode manufacturing

Paste based electrodes were produced via sandwiching of the heated carbon paste between two parts printed from blue polylactic acid (PLA). These parts contained holes of differing diameters which allowed the escape of paste during sandwiching, after cooling excess paste was removed. With the addition of a copper wire during the setting process this produced the electrode shown in Figure 2.3.

During use, the produced circular working electrode was covered in solution and a silver/silver chloride electrode (produced through the anodization of a silver wire by 10 % bleach solution) inserted and used as a combined counter and reference electrode.

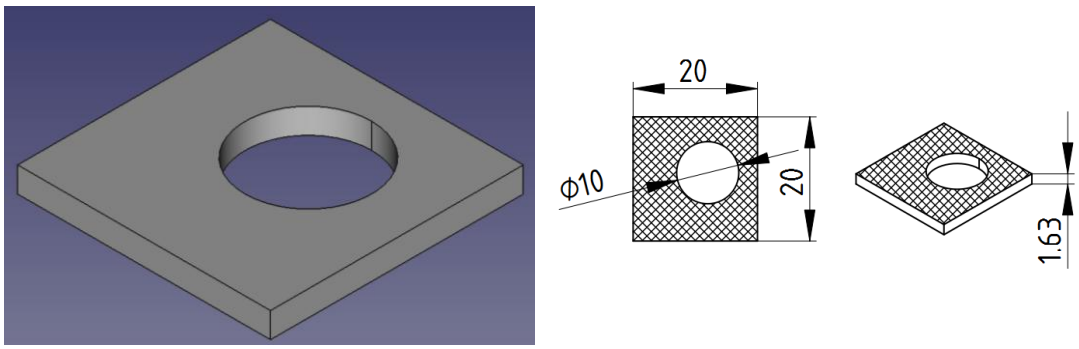

(a) **(b)**

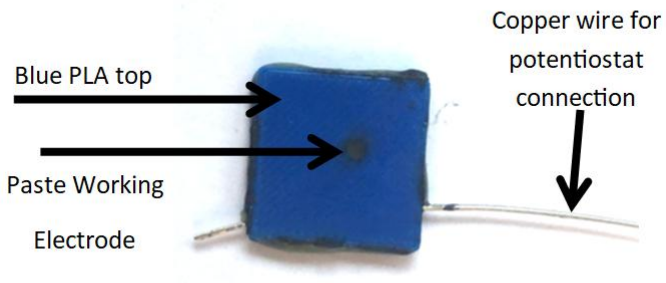

(c)

Figure 2.3: The carbon paste electrode used in this chapter. The initial CAD of the top, PLA component of the electrode **(a)**, drawing of the CAD with dimensions in mm **(b)** and resulting electrode **(c)** are shown. It should be noted that the hole in the middle of the PLA component was varied.

2.3.4 Electrode Pretreatment

Three physical pretreatments were performed, during each, electrodes were moved in a figure of 8 motion on a cleaning medium, 10 times clockwise then 8 times counterclockwise before being rinsed with DI water. This cleaning was performed on 80 gsm printer paper, 1000 grit sandpaper and using 1 μM Alumina polishing solution.

Electrochemical pretreatment was performed using Hydrogen peroxide, Sulphuric acid, Potassium chloride, sodium chloride and PBS.

Hydrogen peroxide pretreatment was taken from literature[110] and involved the CV cycling of electrodes in 10 mM H_2O_2 solution, 10 cycles were performed between corner potentials of -0.7 and 1.0 V at a speed of 10 mV/s.

Sulphuric acid pretreatment was based on literature[78] and involved a single linear scan of electrodes in 0.2 M H_2SO_4 between -1.2 and 1.5 V at a speed of 100 mV/s.

Potassium chloride pretreatment was based on literature[112] and involved the CV cycling of electrodes in 0.1 M KCl. 40 cycles were performed between potentials of -2 and 2 V at a speed of 100 mV/s.

Sodium chloride pretreatment was based on literature[111] and involved CV cycling of electrodes in 20 mM NaCl for 10 cycles between 0 and 1.4 V at a speed of 100 mV/s.

PBS pretreatment was developed independently and involved CV cycling of electrodes in 1 x PBS (0.01 M phosphate buffer, 0.0027 M potassium chloride and 0.137 M sodium chloride) for 10 cycles between -0.6 and 1.3 V at a speed of 100 mV/s.

2.3.5 Electrochemical Characterisation

Electrochemical characterisation was performed using 1 mM Ruhex in 1 x PBS. Square wave voltammetry was performed with a step of 10 mV, amplitude of 100 mV and frequency of 20 Hz.

2.3.6 Data Analysis

SWV results were baseline subtracted in PSTrace software using a moving average baseline. Statistical analysis and data plotting used Origin 2022 software (OriginLab, Massachusetts, USA). Mean and standard deviations were calculated using inbuilt origin functions. Anova was performed using the inbuilt origin one-

way Anova function with a significance level of 0.05. A Tukey post-hoc test was used to group results, again at a significance level of 0.05.

2.4 Results and discussion

2.4.1 Initial Paste optimisation

Initial work was performed to determine the ideal ratio of paraffin wax to graphite powder. Three pastes were made using varying ratios and moulded into 1-inch-long pucks using 1 ml pipette tips (Eppendorf). The end-to-end resistance of these pucks was measured and their ease of use qualitatively noted, three ratios of wax: graphite were tested, 40:60, 50:50 and 60:40.

40:60 paste could produce resistances between 50-100 Ω when measured, when heated paste softened however no amount of manual mixing was able to fully incorporate all the graphite powder into the mixture. 50:50 paste was highly viscous when heated, producing a fluid that flowed slowly and required a lot of mixing to fully incorporate graphite powder, producing pucks with a measured resistance of between 300 – 500 Ω. 60:40 paste, although being easy to mix and work with as it produced a freely flowing fluid when heated was non – conductive, producing resistance values of infinity.

From this initial testing it was decided that 50:50 paste would be the most suitable for the manufacturing of paste electrodes as it allowed full incorporation of the graphite powder while still providing adequate conductivity.

2.4.2 Electrode Size

A simple experiment was then performed to ascertain if varying paste electrode size could affect the sensitivity of electrodes. Electrodes of varying diameters were produced and cleaned using a method shown by *Hannah et al*. in which CV cycling is performed between 0.4 and 1.4 V at a speed of 100 mV/s for 10 cycles in 20 mM NaCl solution[111]. After this cleaning they were characterised via SWV (between -0.7 and 0 V) in 1 mM Ruhex solution, peak SWV currents found via automatic peak search function in PSTrace, and peak current densities (peak current/electrode area) were then calculated. Results of this measurement are shown below in Figure 2.4.

Both visually and statistically though Anova at 0.05 significance, changing the size of electrodes had no difference on the current density produced. This is surprising given higher current densities should be seen on larger surface areas due to their potential to produce more conductive pathways through the compound paste material.

Of note in this data was the large amounts of error seen which made it difficult to ascertain the impact of electrode size on final performance. The source of this error stemmed from the homemade nature of the electrodes which made three key aspects of the electrodes difficult to control:

1. The surface roughness of produced electrodes.
2. The thickness of paste material being sandwiched between PLA parts.
3. The positioning of the connection wire within the sandwiched paste material and how well surrounding paste was connected to this wire.

[113]Despite this large error, work was continued using 2 mm diameter electrodes as they were practically easier to manufacture.

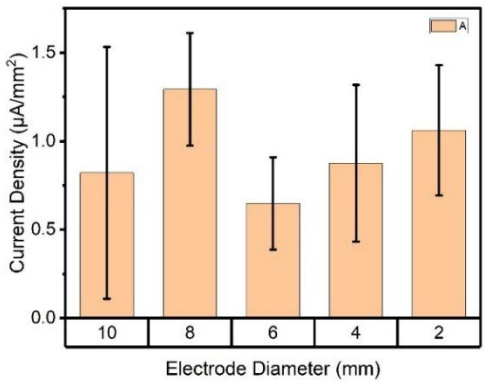

Figure 2.4: Current density of SWV peaks produced through the characterisation of different diameters of carbon paste electrode. Electrodes were cleaning via CV cycling in 20 mM NaCl before being characterised in 1 mM Ruhex solution. Resulting SWV plots were baseline subtracted, peak currents found, and current density calculated. Results were compared using One-way Anova with a 0.05 significance level with a Tukey grouping test at 0.05 significance level. Three electrodes of each size were characterised (n = 3), however during use a 10 mm electrode broke and so 10 mm results were calculated from the remaining two (n = 2).

2.4.3 Physical cleaning

After a suitable electrode geometry had been selected, an experiment was performed to gauge if physical cleaning taken from literature could improve consistency or performance of the electrodes

Electrodes were produced with a diameter of 2 mm and physically cleaned using sandpaper, alumina polish or printer paper and characterised using SWV (between -0.7 and 0 V) in 1 mM Ruhex and peak SWV currents were found via automatic peak search function. Results are shown in Figure 2.5.

While cleaning with sandpaper was able to significantly improve the magnitude of responses, potentially through its roughening of the electrode surface, consistency was improved through all cleaning methods, indicated by reduced standard deviations in comparison to control (uncleaned) electrodes. The greatest improvement was seen in by paper cleaning which was able to reduce

standard deviations from 6.89 μA (in control measurements) to 1.48 μA (in paper cleaned measurements).

Due to this reduction in standard deviation and therefore increased consistency it was decided that paper cleaning should be carried forward

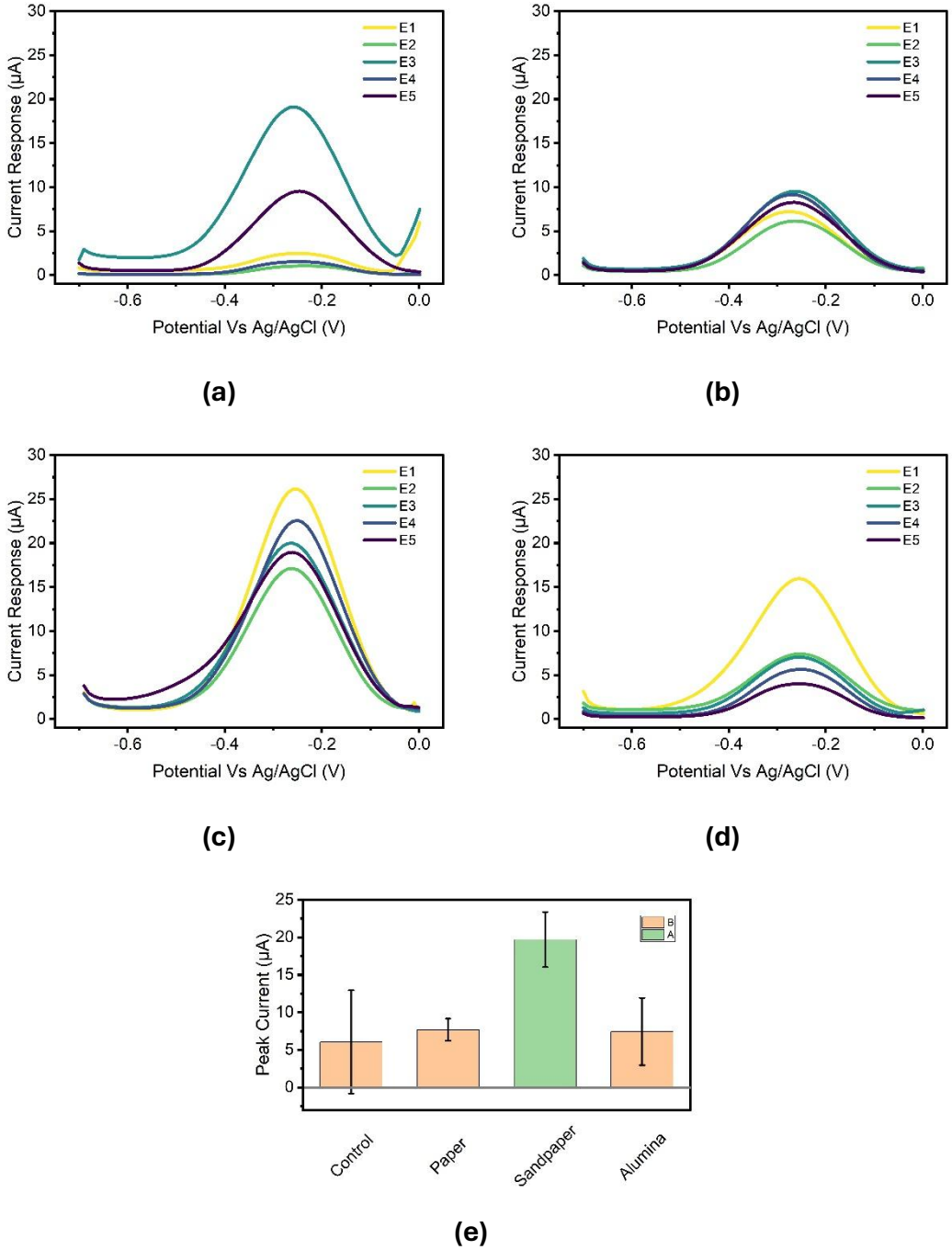

Figure 2.5: Peak SWV currents generated by electrodes cleaned using different physical approaches. Characterisation was performed using SWV in 1 mM Ruhex solution on five electrodes for each approach (n = 5). Resulting plots were baseline subtracted, and peak currents were found, averaged and compared using a one-way Anova with a Tukey grouping test both at 0.05 significance level. Raw plots of control **(a)**, paper **(b)**, sandpaper **(c)** and alumina **(d)** cleaning are shown as well as a summary of the peaks found **(e)**.

2.4.4 Electrochemical Pretreatment

To investigate the effect of electrochemical pretreatment on the performance of the paste electrodes they were physically cleaned using 80 gsm paper before being rinsed with DI water and electrochemically cleaned using PBS, Sulphuric acid, Hydrogen peroxide, potassium chloride or sodium chloride. Characterisation was then performed via SWV (between -0.7 and 0 V) in 1 mM Ruhex and peak currents of SWV results were found using inbuilt peak searching in PSTRACE.

Although results of this characterisation (shown in Figure 2.6) showed trends, with sodium chloride and hydrogen peroxide pretreatments seeming able to raise peak currents, through Anova testing no significant difference was seen between any cleaning methods performed and many seemed to visually raise standard deviations compared to uncleaned control electrodes. Two peaks were also apparent after potassium chloride pretreatment, perhaps through the deposition of potassium on the surface during cleaning.

A large amount of the variation seen in results seemed to be present in electrodes whether cleaned or not, this 'inherent' variation in results likely stemmed from two main sources.

Firstly, the compound nature of the carbon paste material makes variation unavoidable as its conductivity relies on the random arrangement of conductive carbon particles within its structure to conduct charge, this randomness in conductivity will subsequently lead to varying performance of electrodes.

Secondly, a large amount of variation also likely arose from the homemade nature of the electrodes, apart from a lack of fine control over their final geometric area, a lack of consistency was also unavoidable in both the thickness of the paste within the sandwich and how compressed paste was. This will have caused varying densities of carbon particles within the material and therefore effected both its surface and contact resistance. Contact resistance will have also been made variable through the inclusion of a copper wire within the paste

as a connection point. The impact of this varying contact resistance is apparent through the small changes in SWV peak position seen in characterisation.

Due to the variability of cleaning outcomes (rather than poor magnitudes of responses), further chemical pretreatment should focus on the homogenisation and functionalisation of already exposed carbon rather than the exposure of further carbon through the etching of paraffin wax. This could potentially be achieved using sodium hydroxide which has already been shown to improve the performance of screen-printed electrodes[114].

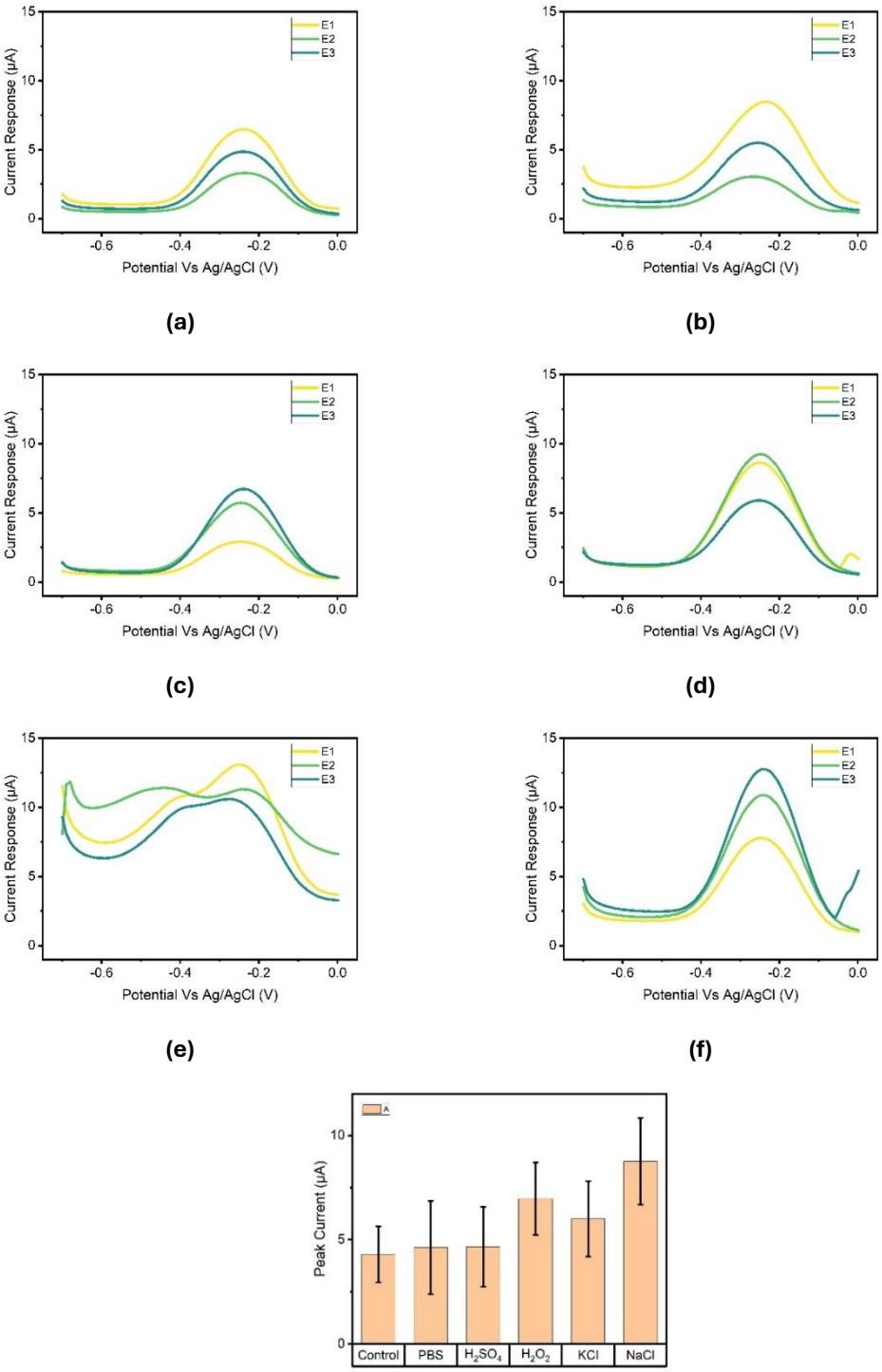

Figure 2.6: Peak SWV currents in 1 mM Ruhex solution on three electrodes for each cleaning approach (n = 3). Raw SWV plots of control **(a)**, PBS **(b)**, H_2SO_4 **(c)**, H_2O_2 **(d)**, KCl **(e)** and NaCl **(f)** are provided along with summarised results **(g)**.

Despite a lack of ability to produce improvements in measured performance, chemical pretreatment by PBS did show other utility (highlighted in Figure 2.7). PBS pretreatment could smooth the CV response of electrodes. Although this smoothing may not have an impact on the analytical response of the electrode, smoother, less noisy plots made analysis quicker and easier. For this reason, as well as its use of non-hazardous chemicals, PBS pretreatment was chosen as a suitable chemical pretreatment for the paste electrodes.

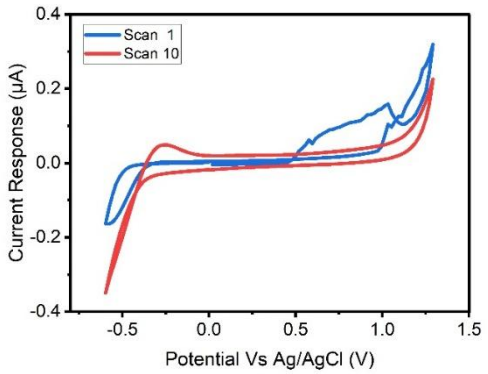

Figure 2.7: Change in CV plots seen during cleaning of electrodes in 1 x PBS, highlighting the reduction in noise seen.

2.5 Conclusions

Carbon paste is an attractive material for the manufacturing of electrochemical sensors due to its low cost, flexibility and ability to incorporate a range of particles through simple mechanical mixing. In this chapter a paste-based electrode was manufactured from a mix of graphite and paraffin wax. The physical dimensions and preparation of this electrode were then optimised.

A range of electrode sizes were tested however this did not have a significant effect on sensitivity, due to the smallest tried (2 mm diameter) not being capable of producing microelectrode effects. Physical pretreatment of the electrode surface was able to both improve consistency as well as overall performance, in particular cleaning using standard printing paper was able to reduce standard deviations in measured SWV results.

Chemical pretreatment of electrodes could not improve electrode performance or consistency significantly, however on further inspection cycling in 1 x PBS solution could remove noisy, unwanted peaks from plots. Despite improvements in electrode performance from these pretreatments, large inter chip variability was still present (due to the homemade nature of the pastes), future work should therefore focus on the reduction of this variability via investigation of more repeatable manufacturing techniques or further optimisation of pretreatments.

3 Fabrication of a graphite-paraffin carbon paste electrode and demonstration of its use in electrochemical detection strategies

3.1 Chapter Preface and Declaration

The following chapter consists entirely of a paper published during my PhD project in RSC Analyst (***Analyst***, 2024,**149**, 4736-4746). It has been reformatted to align with the rest of the thesis however is otherwise unchanged.

The paper included within this thesis is primarily the work of the first author (S Milne) who was responsible for the design, execution and analysis of experimental work included as well as the writing of the first draft of the paper. P Lasserre and D Corrigan provided experimental supervision, advice and aided in the writing of latter drafts of the paper.

Stuart Milne

18/02/2026

3.2 Introduction

A biosensor can be defined as 'a device that uses specific biochemical reactions mediated by isolated enzymes, immunosystems, tissues, organelles or whole cells to detect chemical compounds usually by electrical, thermal or optical signals'[115].

Biosensors can be used in either point of care (POC), or laboratory settings. While in laboratories optical methods dominate due to their simple, highly automated nature, they can struggle in POC settings. There are many reasons for this including interference from coloured samples, long analysis times, requirements for large/power intensive equipment and large sample volumes[116]. Although electrochemically active samples and especially those with changing pH can interfere with electrochemical sensors, their ability to provide fast, low-cost, specific responses[117] in the field[118] and general smaller size make them ideal for use in POC settings. The greatest illustration of their utility at the POC is the rise of continuous glucose monitors. Glucose biosensing testifies of evident success, being the focus of 90% of the global market for electrochemical biosensors[119]. Nevertheless, electrochemical sensing has not yet been fully exploited for wider commercial and medical applications[5].

One of the key factors that governs the performance of an electrochemical sensor is the electrode material on which it is based. To this end, a substantial range have been developed and tested in the literature, commonly based on either gold[120] or carbon[121]. Gold materials, although more expensive[122], are often chosen due to their chemical stability[123] and in the case of biosensors, their ability to be easily functionalized via strong gold-sulphur bonds[80]. Carbon on the other hand is inexpensive[83], highly conductive, chemically inert and has a wide voltage range[84]. Despite these advantages, carbon electrodes often require high overpotentials to reduce or oxidise molecules on their surface[83], an issue most often overcome via modification with suitable redox mediators[83] or catalytic nanomaterials[124].

Carbon paste electrodes (CPEs) are a popular subtype of carbon electrode with a long history, produced through the mixing of electrically conductive carbon materials with binders/solvents[101]. While the use of carbon paste itself is certainly not new, being described as early as 1958[82], its simple manufacturing process of mechanical mixing imparts several benefits, permitting the in-house manufacturing of electrodes at a low cost. Traditionally, 70% of carbon pastes are made with liquid binders[104]. In recent years, solid electrodes produced through the mixing of a solid binder such as paraffin wax with carbon materials have gained traction and are now commonly used, allowing the incorporation of current manufacturing methods such as additive manufacturing (3D printing). The versatility of carbon paste allows numerous modifications/enhancements to be made easily, such as the inclusion of redox mediators[125], recognition elements[84] such as enzymes[126,127] and binding molecules[128] being common choices.

Electrochemical sensors can function by direct detection, in which a molecule of interest is inherently electrochemically active, or by indirect detection, in which a molecule is coupled to a tag (e.g. an enzyme) which enables its detection. A molecule often targeted by direct electrochemical detection is dopamine, with 271 results being found from a search of 'Dopamine' AND 'Biosensor' in web of science since 2023. Dopamine is a neurotransmitter that plays a critical role in neuromodulation, being expressed, and detected in both the central and peripheral nervous systems[129], whose levels are raised in Parkinson's, Huntington's, and schizophrenia[130].

Direct electrochemical detection of dopamine and other neurotransmitters of interest has been reported on many electrode materials and morphologies[131], *in vivo* using carbon fibre electrodes[132] and through clinical depth electrodes[133]. Indirect electrochemical sensing of dopamine has been demonstrated extensively, for instance using a fluorescent artificial receptor[134] or electrochemiluminescence using copper nanoclusters[135]. However, many of these reports require complex multi-step functionalisation protocols due to well-

known interferents at similar oxidation potentials[136]. Given the large amount of literature showing both benchtop and *in vivo* detection, the ubiquity of measurement data and its challenging detection position dopamine as a good benchmark compound for electrode performance, especially because the mechanism of electron transfer and general oxidation mechanism is more complex than for the simple outer sphere ruthenium couple.

Enzyme-Linked Immunosorbent Assay (ELISA) is a commonly used method in laboratories worldwide and is reliable, sensitive, and specific, in part due to the amplification that is enabled by enzymes[137]. Enzymes are used to detect and often quantify immunological interactions, either the binding of an antigen of interest to an antibody or vice versa. Some common enzyme choices include alkaline phosphatase[138] and horseradish peroxidase (HRP)[139] which are both conveniently able to provide an optical and electrochemical signal. A common target of both optical and electrochemical ELISA is Interleukin-6 (IL-6)[140]. This pro-inflammatory cytokine is a key biomarker in sepsis[141] and many other diseases such as cancer, multiple sclerosis, Alzheimer's disease, rheumatoid arthritis, anaemia, inflammatory bowel disease, asthma, and inflammatory pulmonary diseases[142]. Both electrochemical[143,144] and optical[145] detections commonly test for the presence of IL-6. The popularity of ELISA and this specific cytokine position them both as a strong benchmark measurement for any potential detection platform.

This study demonstrates the facile manufacturing of a CPE chip aided with 3D printing. Considering the strengths of electrochemical systems as affordable solutions easily transferable to the point of need, the produced CPE performance will be assessed in both direct and indirect detection strategies of dopamine as an exemplar measurement of a redox active molecule and IL-6 as an exemplar immunoassay. Alongside a basic characterisation with ruthenium hexamine chloride, these measurements highlight the potential utility of the platform in a variety of useful analytical scenarios.

3.3 Materials and Methods

3.3.1 Chemicals

Phosphate-buffered saline tablets (P4117), dopamine hydrochloride (H8502), L-Ascorbic acid (A92902), Uric acid (U2625), Serotonin hydrochloride (H9523), human serum (H4522) and Hexaammineruthenium(III) chloride (262005) were purchased from Merck (UK). Streptavidin-tagged horseradish peroxidase, IL-6 capture and detection antibodies as well as IL-6 protein standard were taken from a Human IL-6 Duo Set enzyme linked immunosorbent assay (ELISA) kit (DY206, Bio-Techne, Abingdon, UK). Reagent diluent (DY995), wash buffer (WA126) and HRP substrate solution (DY999B) were also purchased from R&D Systems. Paraffin wax (56 - 60 degrees) was purchased from APC pure (Hyde, UK) and graphite powder from Inoxia Ltd (Cranleigh, UK).

3.3.2 3D-Printing of Electrode Base and Well

An electrode base and well to sit on top were printed using a RAISE3D E2 IDEX Dual 3D printer with a nozzle diameter of 0.4 mm. Computer-aided design (CAD) files were produced in FreeCAD 0.20.1 software and exported in .stl file formats to ideaMaker 4.2.3 (RAISE3D) for slicing.

Parts were printed using 1.75 mm white polyethylene terephthalate glycol (PETG) filament (ERYONE) and slicing was conducted using the slicers high quality template (0.1 mm layer height, 10% infill, 70 mm/s infill speed) with the 1.75 mm PETG filament option selected. Resulting .gcode and .data files were transferred to the printer via a flash drive for printing. CAD drawings of parts and final products are shown below (Figure 3.1).

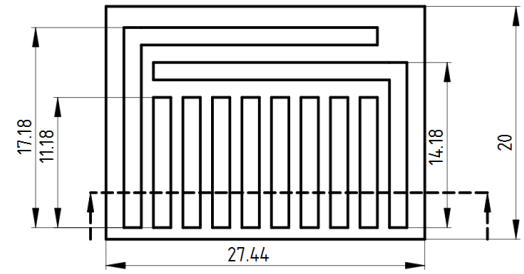

(a)

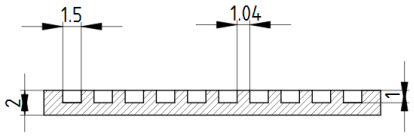

(b)

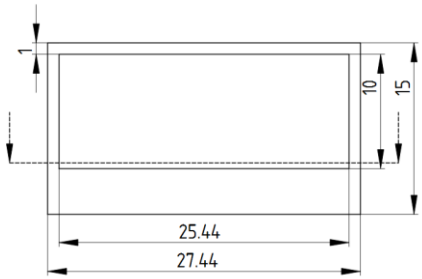

(c)

(d)

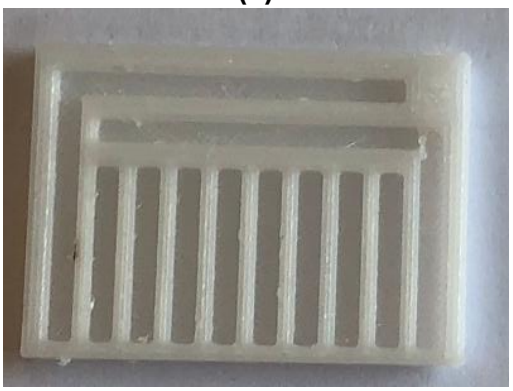

(e)

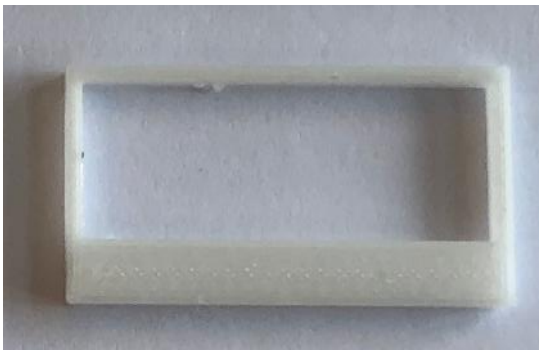

(f)

Figure 3.1: Dimensions required to duplicate the 3D printed parts (in mm) including a top down view of the base **(a)**, a section through the base **(b)**, a top down view of the well **(c)** and a section taken through the well **(d)** along with the printed base **(e)** and well **(f)**.

3.3.3 Ag/AgCl reference electrodes

During this investigation, Ag/AgCl reference electrodes were used. They were produced by the submersion of Ag wire in household bleach alike other methods seen in literature[146]. These electrodes produce a stable voltage through a reaction with chloride ions in the surrounding solution (*Equation 3.1*). It does however differ from a traditional reference electrode by being in direct contact with the analyte, not with a saturated chloride solution and so the voltage relies on the concentration of Cl^- ions in the solution. A few things were done to attempt to keep this constant:

- The only source of chloride ions was the phosphate buffered saline used.
- Measurements were performed quickly to reduce the effect of evaporation.

Equation 3.1: Half reaction of Ag/AgCl reference system

$$AgCl + e^- \leftrightarrow Ag + Cl^-$$

3.3.4 Carbon Paste Manufacturing

Graphite powder and paraffin wax binder were combined via heating and manual mixing in a mantle (Electrothermal). A 1:1 mix by weight was easy to work with while still providing suitable conductivity. This paste was used for the working and counter electrodes.

3.3.5 Chip Assembly

Electrode chips were assembled in a few simple steps. Firstly, carbon paste was heated until soft before being transferred to printed tracks via a spatula. It was then pushed into the tracks before excess was removed. While still warm, an Ag/AgCl quasi-reference electrode was added to the relevant track, producing a chip with 8 carbon paste working electrodes that share a single carbon paste counter electrode and Ag/AgCl quasi - reference electrode. A 3D printed well was then secured to the surface using nail polish. A flow diagram of this process is shown below (Figure 3.2).

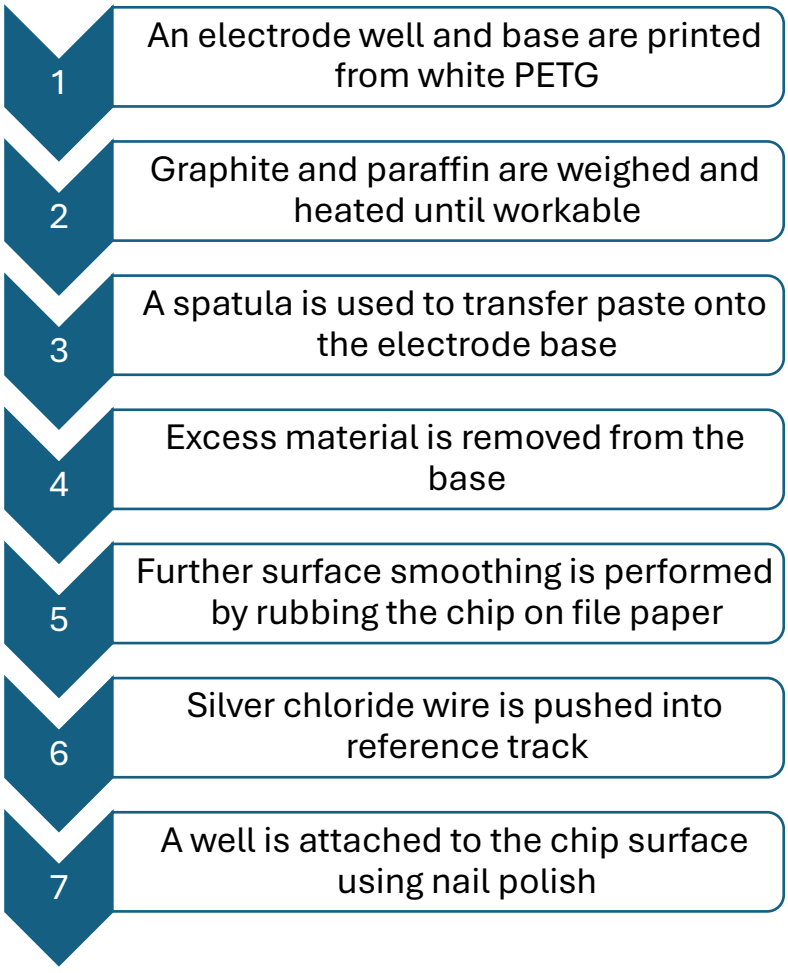

Figure 3.2: How carbon paste chips were manufactured

3.3.6 Use of Phosphate Buffered Saline (1 x PBS)

PBS used during this chapter was composed of 0.01 M phosphate buffer, 0.0027 M potassium chloride and 0.137 M sodium chloride, at a pH of 7.4. This was obtained by dissolving tablets in the volume of deionized water recommended by the supplier (200 ml per tablet).

3.3.7 Electrochemical Methods

Electrochemical procedures were performed using a PalmSens PS4 potentiostat driven by PSTrace 5.9 software (PalmSens, Houten, Netherlands). Data analysis was undertaken using Origin 2022 (OriginLab, Massachusetts, USA).

3.3.7.1 Surface Cleaning

Both physical and chemical cleaning methods were carried out on electrodes before use. Physical smoothing of the electrode surface was first performed by rubbing chips in a figure of eight motion on white printer paper until a glassy surface was obtained. Chemical cleaning was then performed by cyclic voltammetry (CV) cycling in PBS. 10 cycles were performed between potentials of -0.6 and 1.3 V at a speed of 100 mV/s and step of 0.02 V. Chips were then rinsed with deionised water, dried using compressed air and used.

3.3.7.2 Hexaammineruthenium(III) chloride Characterisation

CV, square wave voltammetry (SWV) and electrochemical impedance spectroscopy (EIS) in 1 mM Hexaammineruthenium(III) chloride (Ru-Hex) in PBS were carried out using the following parameters: CV voltage was scanned between 0.1 and -0.6 V at 100 mV/s with a step of 0.02 V. SWV voltage was scanned between 0.1 and -0.6 V with an amplitude of 0.1 V, step of 0.01 V and frequency of 20 Hz. EIS was performed at $E_{1/2}$ (calculated as -0.25 V after initial CV investigation) between 10000.0 and 5.0 Hz (10 steps per decade) with 10 mV sine wave stimulation.

3.3.7.3 Dopamine detection

CV measurement was carried out using 0.25 mM dopamine hydrochloride in PBS. Voltage was scanned between -1 and 1.5 V at increasing scan rates of 100, 300, 500, 700, 900, 1400 and 3000 mV/s with a step of 0.2 V. To gauge the oxidation voltage of dopamine SWV, measurements were then performed on a range of dopamine hydrochloride concentrations between -0.1 and 1.1 V with an amplitude of 0.1 V, step of 0.01 V and frequency of 20 Hz. A similar experiment was performed using chronoamperometric measurement at 1 V, measurements were taken at 0.1 s intervals for 60 s. The common interferents ascorbic acid, uric acid and serotonin hydrochloride was also tested via the SWV detailed above at a concentration of 0.5 mM.

3.3.8 ELISA Protocol

IL- 6 ELISA was performed as instructed by the duoset ELISA kit. In summary, 32 wells of a standard 96 well plate were successively incubated with 100 µL of capture antibody (2 µg/ml), 300 µL of reagent diluent (1 X diluted from kit stock), 100 µL of IL-6 standard added to 10% human serum in PBS (1200 - 9.38 pg/ml, 100 µL of biotinylated detection antibody (50 ng/ml) and 100 µL of streptavidin-tagged enzyme (40 fold dilution from kit standard). Between incubations, wells were washed via three successive washes consisting of filling and emptying wells with 300 µL of wash buffer (diluted from kit). This produced an antibody ‘sandwich’ as seen in Figure 3.3 tipped with HRP. 100 µL of HRP substrate was then added to these wells and incubated for 20 minutes before 50 µL of acidic stop solution was added. Absorbance and chronoamperometry were then measured to reflect the concentration of IL-6 added to each well.

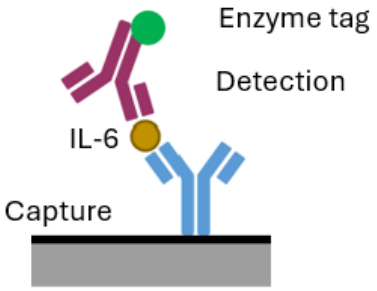

Figure 3.3: Schematic of a sandwich ELISA.

The reaction produced by this HRP tag and substrate are shown below (Figure 3.4). When the HRP enzyme tag encounters its substrate solution containing hydrogen peroxide and 3,3',5,5'-tetramethylbenzidine (TMB) it begins to break down the hydrogen peroxide to produce water which will also begin to oxidise the TMB in the solution producing a blue colour (from TMB^{+}). Through the lowering of this solutions pH (via the addition of acid) the reaction this reaction can be stopped and TMB^{+} in the solution is further oxidised to produce yellow TMB $^{2+}$ which can be measured optically and electrochemically.

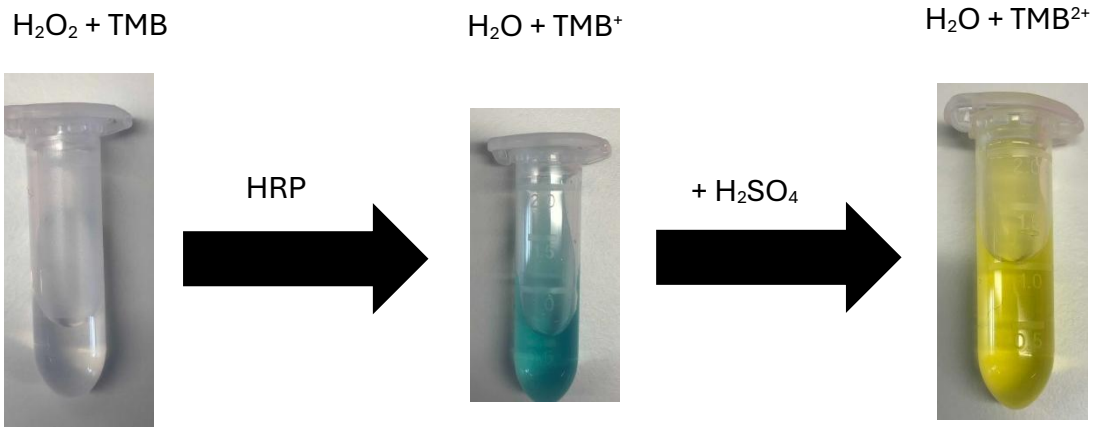

Figure 3.4: How HRP reacts with its substrate solution to produce coloured, measurable products.

3.3.9 Limit of Detection Calculation

Limit of detection (LoD) was calculated from concentration curves as shown in literature[98]. Firstly, the limit of the blank (LoB), the highest apparent concentration found from blank measurements, was calculated using Equation 4.1. Equation 4.2 was then used to calculate the LoD of the performed experiment.

Equation 3.2: Calculation of the limit of the blank

$$LoB = Mean_{(Blank)} + 1.645(STD)_{(Blank)}$$

Equation 3.3: Calculation of the limit of detection

$$LoD = LoB + 1.645(STD)_{(Sample)}$$

To relate this LoD to the real measurements taken, an experimental LoD (ELoD) will be taken as the closest measured concentration point above the LoD to represent the lowest analyte concentration able to be detected consistently.

3.3.10 K^0 Calculation

The heterogenous electron transport rate constant (K^0) is of great interest in the characterisation of electrochemical systems, indicating the rate of electron transfer between an electrode surface and electroactive substrate. In this chapter, it was calculated as shown by Lavagnini, Antiochia and Magno (2003)[147,41]. This approach is based on two equations, both centred around the dimensionless parameter, ψ.

Equation 3.4

$$\psi = (0.0021\Delta E_p - 0.6288)/(1 - 0.017\Delta E_p)$$

Equation 3.5

$$\psi = K^0[\pi DnFv/RT]^{-\frac{1}{2}}$$

where ΔE_p is the CV peak separation of an experiment, D is the diffusion coefficient of the electroactive species, n is the number of electrons transferred during its reaction, F is the Faraday constant, v is the scan speed of a measurement, R is the molar gas constant and T is the absolute temperature.

The measurement of a defined electroactive species was measured at several scan speeds using CV. Peak separation was extracted and Equation 3.4 used to obtain ψ. Based on Equation 3.5, the gradient obtained from fitting ψ plotted against $[\pi DnFv/RT]^{1/2}$ therefore represents K^0.

3.4 Results and discussion

3.4.1 Electrode Manufacturing

Electrodes chips were manufactured as shown. In general, this produced chips as shown in Figure 3.5. There were 8 linear working electrodes and two large L shaped electrodes, one of which operated as a carbon paste counter and one of which had an Ag/AgCl wire inserted into it to act as a reference. This produced chips with a geometric working electrode area of 4.77 mm^2 and a counter electrode with an area of 44.25 mm^2 with a similar layout to other designs utilised in literature[148]. The estimated cost of goods to produce one chip is £0.023 (excluding the reusable Ag wire that is regenerated between uses) and manufacturing including printing required around half an hour of work.

To characterise the CPEs performance with different redox mediators and enzymes, it was necessary to perform a series of investigations involving CV, amperometry and SWV while increasing the complexity of the species being a simple outer sphere redox mediator (Hexaammineruthenium(III) chloride), to the small biological molecule dopamine with it well known complex electrochemistry to the inflammatory biomarker IL-6 (23kDa). The following sections outline the results generated with the newly fabricated devices.

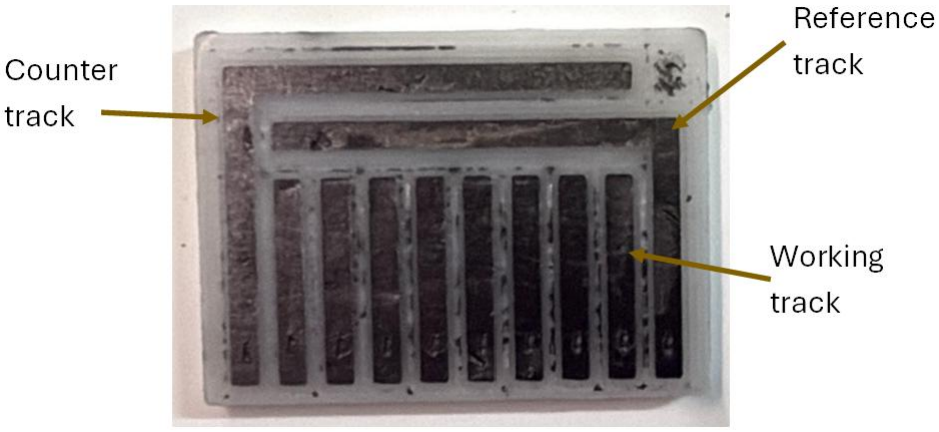

Figure 3.5: Carbon paste chip used during investigations with working, reference and counter electrode tracks highlighted (pre application of reference wire and well to improve picture clarity).

3.4.2 Hexaammineruthenium(III) chloride Measurement

Hexaammineruthenium(III) chloride (Ruhex) is a standard redox mediator often used to gauge the basic effectiveness of electrodes. Due to the outer sphere nature of this redox couple, it is often used with carbon materials. Outer sphere reactions occur when electrons are transferred from outer electron spheres easily via weak interactions. This can happen without the need of specific adsorption and so kinetics are less dependent on electrode surfaces[149]. A 1 mM Ruhex solution was made in PBS and used to investigate the consistency of electrode manufacturing.

Three freshly manufactured and cleaned chips were characterised in 1 mM Ruhex using SWV. Four electrodes on each chip where characterised and peak height averaged (Figure 3.6). Responses obtained were within a similar order of magnitude (82+/-12, 122+/-16, 104+/-25 µA). The produced CPEs would therefore be suitable for measurements which do not require 'high precision', since deviation both between individual electrodes on a chip and between chips was noticed, even after surface conditioning. This could be expected given their handmade nature and the potentially random generation of conductive paths in the bulk material of the electrode.

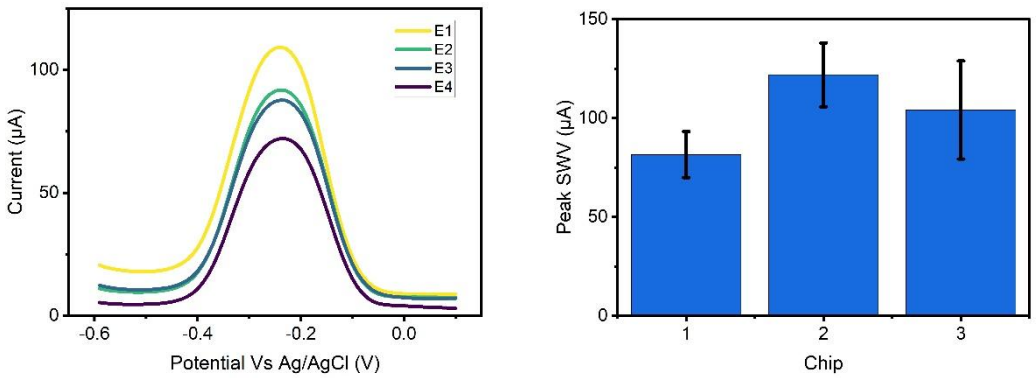

Figure 3.6:SWV peaks taken from measurements of three separate chips to highlight manufacturing consistency, four electrodes from each chip were measured in 1 mM Ruhex in PBS (n = 4). Raw SWV measurements of one chip **(a)** as well as summarised data of all three chips **(b)** are shown.

CV and EIS characterisation in 1 mM ruhex was also performed to estimate the basic electrochemical ability of CPEs. CV characterisation was performed on 4 channels of a single CPE chip. EIS characterisation was performed on 8 channels of a single CPE chip

On inspection of the CV response (Figure 3.7a), a few key points can be seen. The Randles-Ševčík equation (inputting the geometric area of the electrode surface) predicted a reduction current of 12.88 µA. The mean value of 8.70 µA ± a standard deviation of 4.38 µA was in reasonable agreement with the equation, with the discrepancy explained by electrode roughness and slight variations in area arising from the fabrication process.

A peak separation of 79 mV was recorded which was higher compared to the theoretical separation of 59 mV expected. In literature a breadth of performances has been reported, with paste electrodes from Fanjul-Bolado *et al.* (2008) capable of peak separation as low as 63 mV[150], while Wang *et al.* (2001) CPEs produced much more similar peak separations of 77 mV[151]. This range highlights both the variation in paste composition in literature and the effect of the paraffin binder on typical performance.

Differences in the oxidation and reduction peak amplitudes were also observed (10.56 (+/-0.83) µA vs 15.45 (+/-2.15) µA). This indicates a quasi-reversible behaviour of Ruhex on the electrodes as expected from reports of other untreated paste surfaces in literature[152]. To confirm this quasi-reversibility, CV measurements of 1 mM Ruhex in PBS were then taken at scan speeds of 100, 300, 500, 700 and 900 mV/s. Peak separations were recorded and K^0 calculated using a reported diffusion coefficient of $8.4*10^{-6}$ cm^2/s[153]. The obtained K^0 value of 0.055 cm/s was within the range of a quasi-reversible system (10^{-1} - 10^{-5} cm/s), where currents are constrained both by charge transfer and mass transport[69].

EIS measurements displayed in Figure 3.7b and c showed a highly resistive system. This was first evidenced in the Nyquist plot (Figure 3.7b), which although difficult to fit to standard circuits (Randles/simplified Randles equivalents) most closely resembled a single Warburg element, albeit at a much shallower angle than usual. This indicates a system under control of mass transport or 'semi-infinite' diffusion rather than any electrode effects. The Bode representation (Figure 3.7c) also showed a system dominated by resistance[154].

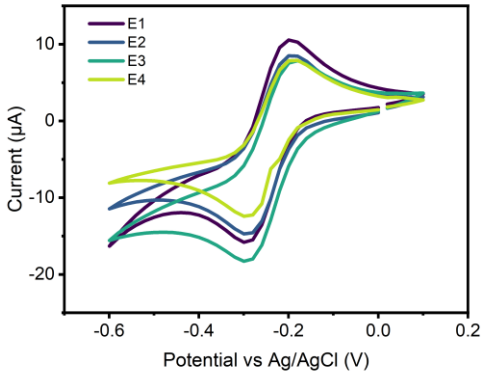

(a)

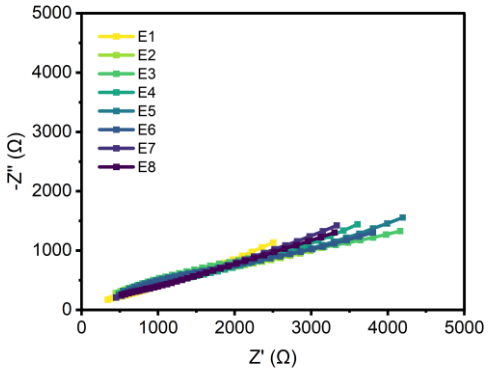

(b)

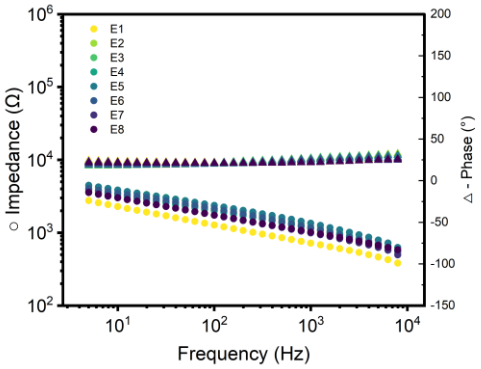

(c)

Figure 3.7: CV measurements of 1 mM Ruhex in PBS between -0.6 and 0.1 V at a scan speed of 100 mV/s performed on four channels of a single CPE chip **(a)**. Nyquist plot of EIS characterisation of electrodes in 1 mM Ruhex in PBS, performed at $E_{1/2}$ between frequencies of between 10000.0 and 5.0 Hz with 10 mV sine wave stimulation performed using eight channels of a single CPE chip **(b)**. Bode plot of the same EIS characterisation **(c)**.

Both SEM and FTIR measurements shown respectively in Figure 3.8 and Figure 3.9 may offer some explanations for this electrochemical activity. In particular, the 'solid dispersion'[155] structure of the paste shown both in this chapter and other pastes made in both solid[156] and liquid binders[157,158,159] where pastes consist of carbon particles coated in binder. This produced an uneven structure with a surface composed of high and low conductivity areas, shown by bright and dark patches in SEM images and through the presence of both hydrocarbon and pure carbon bonds in FTIR.

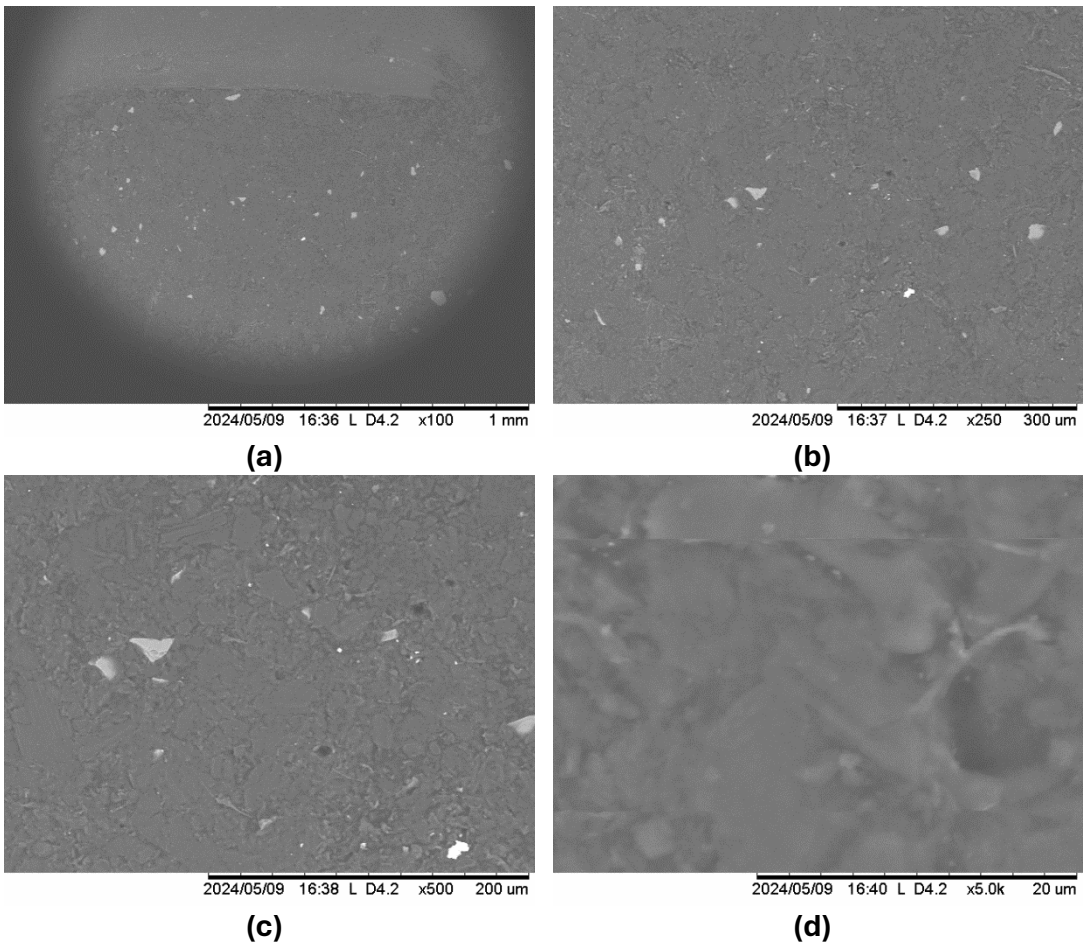

Figure 3.8 SEM measurement of the carbon surface of a produced chip, performed using a Hitachi TM – 1000 microscope. Taken at 100 **(a)**, 250 **(b)**, 500 **(c)** and 5000 **(d)** x magnification. The figure highlights the compound nature of the produced chips, showing an overall rough texture composed of areas of high and conductivity.

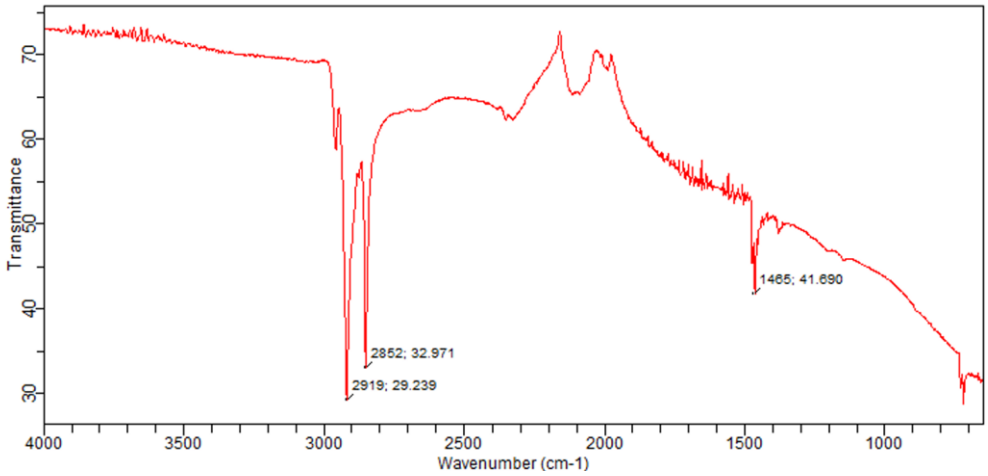

Figure 3.9: FT-IR measurements of carbon paste used in chip manufacturing, taken ,using an Agilent Technologies 5500 Series FTIR. When these peaks are compared to others seen in literature produced from similar carbon materials1,2 they indicate a structure primarily generated from C-H and C – H2 at 2919 cm-1 and 2852 cm-1 (expected in the hydrocarbon structure of paraffin wax) and C-C groups at 1465 cm-1 (expected in the pure carbon structure of graphite).

This dispersion produced conductive paths and therefore performed as an electrode. However, much of the bulk of the material can still be considered as 'inactive', either completely non-conducting paraffin or isolated graphite. This supports the behaviour observed in EIS measurements, governed by the ability of analytes to find conductive areas on the electrodes surface as well as in CV measurements, where high 'distributed resistance' has been shown to spread CV peaks[160].

3.4.3 Dopamine Measurement with CPEs

A 250 µM dopamine solution was made in PBS and measured by CV using several scan rates. Oxidation peaks showing the formation of dopamine-o-quinone (DOQ) were clear and although reduction peaks are not visible at slower rates due to the rapid desorption of this product from the electrode surface[161], faster scan rates record DOQ before desorption can take place.

Inspecting the CV responses, scan speed had minor impact on peak potentials, indicating a reversible system for the parameters tested. However, when plotting peak currents vs the square root of scan rate, a poor linear fit was seen (Figure 3.11b), especially at higher scan rates where currents deviated from the expected significantly, producing lower than anticipated peak currents. This highlights the complex nature of dopamine electrochemistry and may indicate the point at which diffusion became a limiting factor in the redox system, or potentially the point at which the oxidative production of polydopamine seen commonly in literature[162] began to interfere with measurement.

When different concentrations of dopamine were tested using SWV, concentration dependent differences were seen in peak currents down as low as 62.5 µM, however results also showed potential drift in measurements (Figure 3.11c), with higher concentrations of dopamine requiring higher potentials for full oxidation, one possible cause of this drift may have been due to the effect of *iR* drop within the chip. *iR* drop is the difference between the expected potential applied at the working electrode and the actual potential that is applied and is influenced by several factors including electrode and electrolyte conductivity, distance between working and reference electrodes, working electrode roughness and double layer thickness[163] and can lead to the shifting of electrochemical peaks on a plot. The increasing concentrations of dopamine measured may potentially have affected this drop in two major ways, firstly by

increasing the solution resistance and secondly through the altering of electrode conductivity through the binding of dopamine polymers to electrode surfaces.

These same dopamine solutions were then measured chronoamperometrically along with a PBS baseline to ascertain the electrode's ability to detect dopamine, producing the concentration curve seen in Figure 3.11d. When analysed, this data produced an ELoD of 62.5 µM of dopamine, although standard deviation error bars indicated that distinguishing between concentrations above this point may be difficult.

Although this LoD is much higher than those seen in literature (Table 3.1) and was not suitable for direct dopamine detection from any biological fluid, it showed the general utility of the produced chips for the direct measurement of biological molecules. In its current format, the chip may be useful for detecting biomarkers which have higher clinically relevant concentrations, or with modifications like those seen in literature may be capable of relevant dopamine detection.

SWV testing was also performed to gauge how well the chip may potentially fare in a more clinical setting with the potential impact from the common interferents ascorbic acid, uric acid[164] and serotonin hydrochloride which are often detected simultaneously[165]. SWV measurements of 0.5 mM solutions in PBS were performed both separately and with dopamine hydrochloride using the same electrode chip. Results of these tests are shown in Figure 3.10.

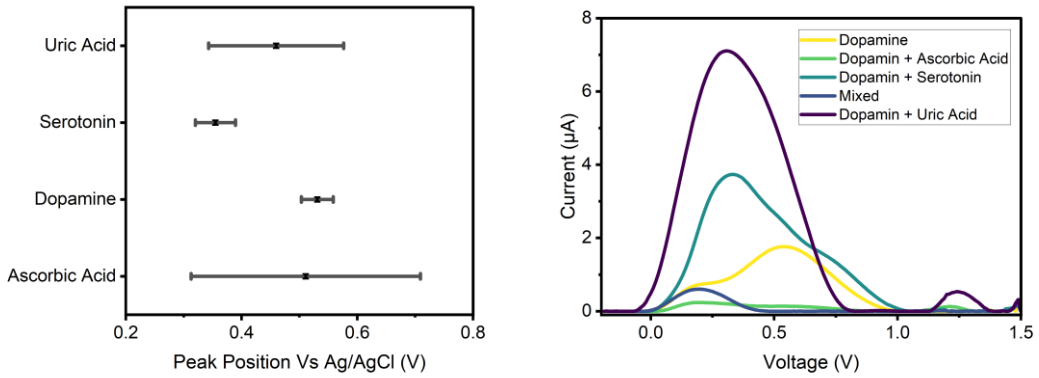

(a) **(b)**

Figure 3.10: Peak positions of the SWV measurement of both dopamine and some common interferents at concentrations of 0.5 mM diluted in PBS **(a)** and Example SWV scans of dopamine, alone and mixed with common interferents all at concentrations of 0.5 mM diluted in PBS **(b)**. Single electrode data plotted for simplicity.

The chip produced performed poorly in these mixed solutions, showing that use of the bare chip in real world samples will lead to interference from ascorbic and uric acid which both have overlapping SWV peak positions. Interestingly, combinations of these interferents and dopamine were able to produce large single peaks, and further work will be performed to ascertain if these are related to interferent or dopamine concentration. In the meantime, the detection of dopamine on these unmodified carbon sensors should be carried out with experimental removal of interferents before electrochemical testing, as suggested in literature[166].

Table 3.1: Different methods of dopamine detection seen in literature and the LoD they can produce.

Electrode Material	Method	LoD	Sensitivity	Linear range	Reference
Graphite Paste	Amperometry	62.5 µM	Na	Na	This Chapter
Carbon Fiber	Fast scan CV	11 nM	31 mA/M	0.025 – 1 µM	[167]
Ti_3C_2 Mxene + Multiwall carbon nanotubes + ZnO nanospheres	DPV	3.2 nM	16A/M	0.01 – 30 µM	[168]
Carbon quantum dots + copper oxide nanocomposite	SWV	25.40 µM	NA	1 – 180 µM	[169]
NA	Fluorescence	10 nM	Na	Na	[134]
Na	Electrochemiluminescence	1.9 fM	Na	Na	[135]
Graphene/Pedot	EIS	3.4 µM	Na	12.5 – 400 µM	[88]

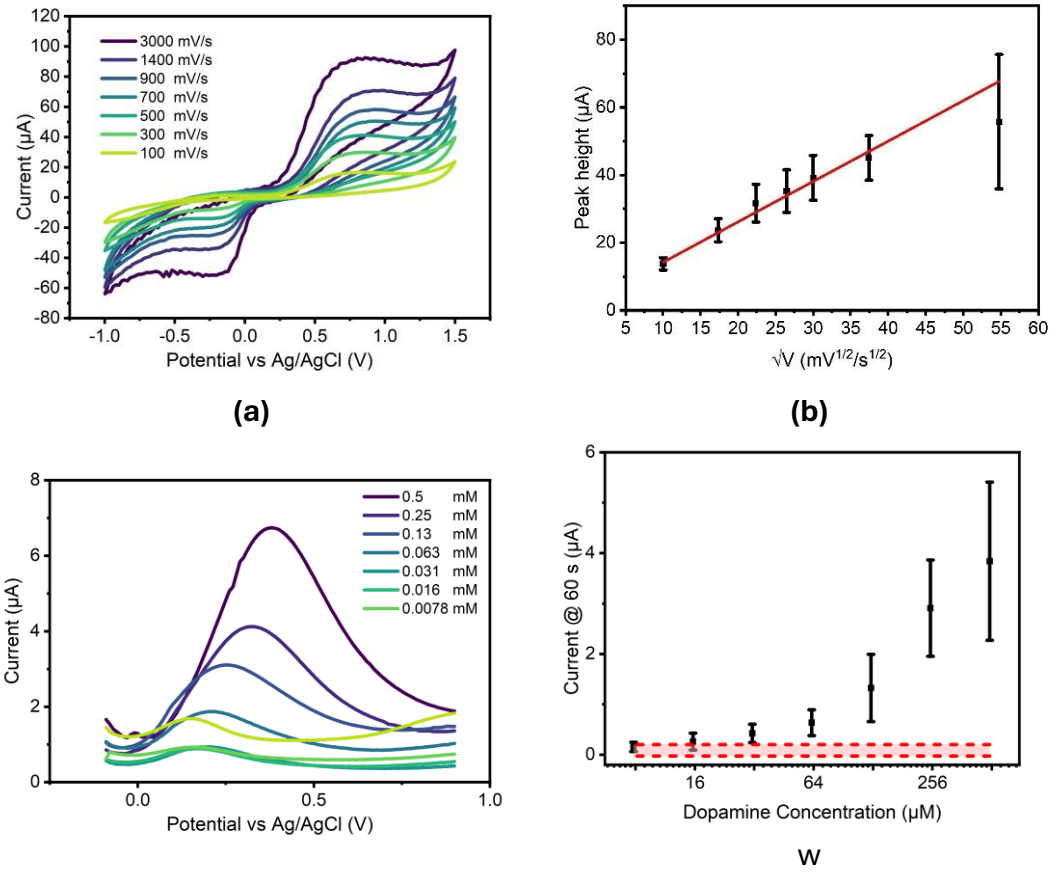

Figure 3.11: Measurements of 0.25 mM dopamine in PBS at increasing scan rates (mV/s) showing stability of the system **(a)**. Oxidative peak currents against the square root of the scan speed plotted (n = 8) (error bars plotted as +/- one sample standard deviation) **(b)**. SWV characterization of dopamine on the carbon paste sensor **(c)**. Chronoamperometric measurements of dopamine measured using all electrodes on a single chip, compared to PBS baseline measurements (red zone) (n = 8)(error bars plotted as +/- one sample standard deviation)**(d)**.

3.4.4 Detection of electrochemically active enzymatic products - Horseradish Peroxidase

Horseradish peroxidase (HRP) is an enzyme consisting of a single polypeptide chain with a molecular weight between 40 and 45 kDa[56] and is commonly used in detection assays with a substrate solution containing hydrogen peroxide and 3,3',5,5'-tetramethylbenzidine (TMB). In these assays, the enzyme decomposes peroxide, generating reactive oxygen species which subsequently oxidise TMB into blue TMB^{+}, which through further oxidation can form the yellow diimine TMB^{2+} that is stable at low pH[57] and is also electrochemically active.

A sandwich ELISA tagged with HRP (see Figure 3.3) was performed to gauge the ability of the electrode chip to detect the products of a more general measurement system. Interleukin 6 (IL-6) was chosen as a suitable biomarker for initial detection. It is diluted in 10% human serum, the liquid component of blood with both cells and clotting factors removed. This was chosen as a suitable medium for detection as it does not contain anti coagulants as plasma does, is stable and still contains many of the markers required for biosensing[170]. Importantly for the development of POC systems, it is routinely sampled from patients and so should indicate the chip's performance in a clinically relevant sample.

Results of this experiment are shown in Figure 3.12. Raw chronoamperometric plots (Figure 3.12a) contain some noise, potentially to be expected from a graphite-based sensor at low voltage[171]. While not able to seriously affect results, this noise should be watched closely and potentially dealt with using commonly employed data processing techniques such as 'spike removal' if deemed necessary for other applications.

Colourimetric measurement of the assay performed well (Figure 3.12b), with results showing a logarithmic trend that did not visually intersect the zero line in the y axis at all and a very low ELoD of 18.75 pg/ml. Clear visual difference between discrete concentration points also showed that colourimetric

measurement was not only able to detect the presence of IL- 6 but also able to discern small differences in concentration. Although a similar logarithmic trend was seen in chronoamperometric results (Figure 3.12c), a higher ELoD of 75 pg/ml was required to distinguish between control and IL-6 solutions. Large standard deviations prevent signal differentiation at low IL-6 concentrations. Even if the electrochemical LoD obtained was higher compared to optical ELISA results, this value proved much more comparable to literature (Table 3.2). Using the indirect detection strategy, CPEs performed at an equivalent level to literature reports and were in the useful and clinically relevant range for the biomarker tested (IL-6). This was achieved without further modification of these low-cost carbon paste electrodes indicating potential for use as a low-cost 'point of need' decision support tool. Advancing the system into an 'in the field' detection platform could provide a clinician an inflammatory response snapshot in terms of elevation and likelihood of associated illnesses, e.g. sepsis[172].

Table 3.2: Limit of detection for IL-6 seen in this system and via other techniques in literature.

Electrode Material	Method	LoD	Sensitivity	Linear range	Reference
Graphite Paste	Amperometry	75 pg/ml	Na	Na	This Chapter
Graphite Paste	Absorbance	18.75 pg/ml	Na	Na	This Chapter
Modified ITO	Amperometry	0.3 pg/ml	Na	1 – 40 pg/ml	[144]
Graphene/ PEDOT	EIS	9.55 pg/ml	Na	2 pg/ml – 200 ng/ml	[88]
Na	Surface-enhanced Raman scattering	0.1 fg/ml	Na	0.0001-100 pg/ml	[173]
Na	Fluorescence	0.37 pg/ml	Na	2 – 500 pg/ml	[174]

Further work will focus on the development of the CPE electrodes into an even more convenient and reproducible format through development of working electrode surface areas and reference electrode stability studies to give the improvement in precision necessary to push electrochemical ELISA sensitivity higher.

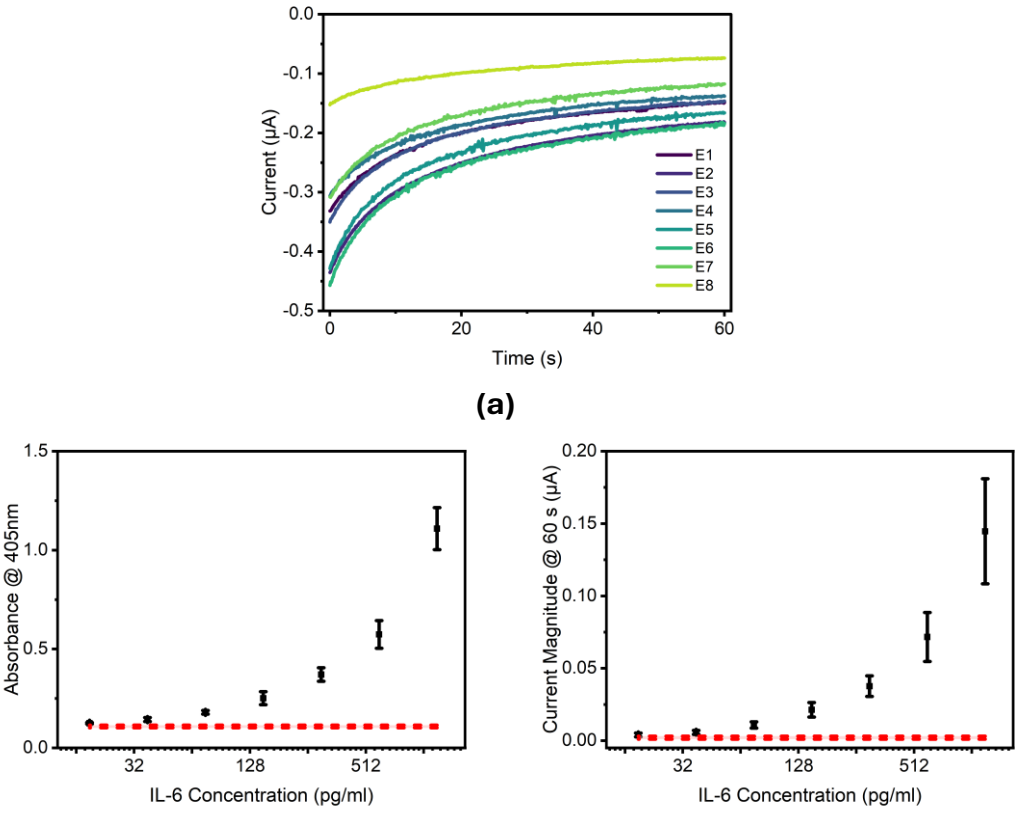

Figure 3.12: Example chronoamperometric data taken from one chipo during measurement of ELISA, measured at 0.2 V vs Ag/AgCl for 60 s **(a)**, Absorbance of IL-6 sandwich ELISA performed with 1200, 600, 300, 150, 75, 37.5 and 18.75 pg/ml standards of IL-6 diluted in 10% human serum, four wells of ELISA were performed for each concentration and plotted with zero line (error bars plotted as +/- one sample standard deviation) (n = 4)**(b)** and chronoamperometric measurement of well solutions pipetted onto a carbon paste chip, measured at 0.2 V over 60 s using all 8 electrodes of a single chip (n = 8), compared to PBS baseline measurements (red zone) (n = 8) (error bars plotted as +/- one sample standard deviation) **(c)**.

3.5 Conclusions

A low-cost carbon paste material was produced which is easy to deploy in various electrode formats. For an assay format, electrode chips were obtained in 0.5 hours, costing £0.023 each. This format focused on being produced using widely accessible equipment with little specific knowledge or expertise required by users in the field. Chips were capable of detection of biomarkers of interest

both directly (dopamine) and indirectly (IL-6) with an enzyme-tagged ELISA format. The system presently does not produce clear, quantitative data at the low abundance biomarker concentration (sub 100 pg/ml) but is able to detect clinically relevant elevations. In its current form, it may be more suitable for qualitative sensing or producing Yes/No diagnostic results at diagnostically useful thresholds.

4 Detection of Prostate Specific Antigen

4.1 Introduction

The prostate is critical to male sexual health through its function as an endocrine gland as well as its ability to produce prostatic fluid which makes up a large proportion of the seminal plasma[175]. In the UK, the most frequent location of cancer in men is the prostate[4], where it commonly manifests as an adenocarcinoma[176] in the glandular tissue. It is commonly diagnosed via digital rectal exams, measurement of prostate specific antigen (PSA), MRI scans and biopsy[177] and has many associated risk factors including age, race, family history, diet, body size, smoking and occupation[178]. PSA is a protease found in the seminal plasma in concentrations between 0.39 and 3 mg/mL[179] where it liquefies the gel constituent to allow sperm to move[180]. It is expressed in both normal and cancerous prostate tissue[181] and is present in the blood in the nanogram per mL range[182].

The commercial detection of PSA from serum samples is both widely available (a quick google search will bring up many 'at home' test kits) and routine. It is also a popular target molecule in literature where it has been detected via Traditional ELISA[183], fluorescent immunoassay[184], chemiluminescence[185]and surface enhanced Raman scattering[186] among other methods.

Its electrochemical detection is also common (some examples are shown in Table 4.1) and has been performed using a large range of electrode materials and detection techniques, although it should be noted that many techniques are immunoassay based.

Table 4.1: Examples of electrochemical PSA detection seen in literature and the limits of detection they are able to obtain

Electrode Material	Assay Format	Detection Method	LOD	Reference
Screen printed Gold	Antibody Sandwich Assay	SWV/CA	0.84 pg/mL	[187]
Carbon paste	Antibody Sandwich Assay	DPV	0.093 ng/mL	[86]
Gold	Antibody Sandwich Assay	DPV	2 pg/mL	[188]
Glassy carbon	Nanobody sandwich assay	DPV	0.08 ng/mL	[189]
Gold/Reduced graphene oxide	Direct Antibody Assay	DPV	0.003 ng/mL	[190]
Gold nanostructures	Direct assay with tagged aptamer	DPV	50 pg/mL	[191]
Reduced graphene oxide/Palladium	Direct Antibody Assay	CA	10 pg/mL	[192]
Screen printed Carbon	Antibody Sandwich Assay	LSV	0.46 pg/mL	[193]

The growing availability of PSA testing and development of more effective treatments have led to a drastic increase in 5-year survival rates. With earlier detection now possible, there is increasing interest in developing targeted, early treatments for prostate cancer before metastasis occurs[182]. Despite this success, the use of PSA testing in the screening of large populations is currently not recommended due to the large numbers of men required to be screened and treated to prevent a single death[194]. This lack of specificity is caused by the natural inter and intrapersonal variations in PSA seen between men[182] as well as

the potential for PSA to be raised in individuals without cancer[195]. The measurement of PSA is therefore better positioned to measure responses to treatments or therapies or perhaps be included with other promising biomarkers such as prostate cancer antigen 3 (PCA3), TMPRSS2-ERG RNA, a-Methylacyl–coenzyme A racemase (AMACR), circulating tumour cells or Exosomes[196] in a multiplexed sensor. Electrochemical methods are ideal for these sorts of multiplexed sensors, and are often shown in literature[197,188].

4.2 Chapter Aims

This chapter aimed to use the carbon paste electrode chips produced previously and determine their performance in the detection of PSA in a clinically relevant medium using enzyme linked immunosorbent assay (ELISA). This was performed by answering 4 research questions:

- Is the performance of a commercially available PSA ELISA kit replicable using carbon paste sensors?
- Can capture antibodies be bound to the carbon paste surface effectively?
- Does binding a commercial ELISA kit to the paste surface improve its performance?
- Can PSA be detected in a complex sample using the carbon paste chip?

4.3 Materials and methods

4.3.1 Materials

Table 4.2: Materials necessary for experimental work in this chapter

Material	Supplier	Product Code
Paraffin wax	APC Pure	PW56-Y
Graphite powder	Inoxia	0029882791622
PBS Tablets	Merck	P4117
Sulfuric Acid	Merck	258105
Deionised (DI) water	Scientific Laboratory Supplies	CHE3874
HRP substrate solution	R&D systems	DY999B
ELISA wash buffer	R&D systems	WA126
ELISA Reagent diluent	R&D systems	DY995
Mouse Anti-Human PSA Capture Antibody	R&D systems	DY1344 (part of Kit)
Biotinylated Goat Anti-Human PSA Detection Antibody	R&D systems	DY1344 (part of Kit)
Human PSA standards	R&D systems	DY1344 (part of Kit)
Strep – HRP (for use with R&D systems kit)	R&D systems	DY1344 (part of Kit)
Anti – HRP Capture antibody	Abcam	10183
HRP (for the above capture)	Sigma	P6782
Bovine Serum Albumin	Sigma	A7906
TWEEN20	Sigma	P1379
$NaNO_2$	Merck	8.22285
Recombinant protein A/G	Fischer	NBP2-34999

Aminobenzoic acid	Sigma	A9878
HCl	Fischer	H/1150/PB17
EDC	Merck	E7750
NHS	Sigma	130672
MES buffer	Thermofisher	J62081.AK
Chitosan	Merck	1003622237
glutaraldehyde	Merck	G6257

4.3.2 Chip manufacture

Carbon paste chips were manufactured as shown in Chapter 3. In summary, a 10-channel electrode base was printed out of white Polyethylene terephthalate glycol (PETG) material and filled with heated carbon paste (50:50 graphite powder : paraffin wax by weight) using a metal spatula. A silver chloride wire was then inserted into a track to function as a quasi-reference electrode.

4.3.3 Chip pretreatment

Electrochemical pretreatment was performed using a PS4 potentiostat and MUX8-R2 multiplexer, driven by PSTrace 5.9 software (PalmSens, Houten, Netherlands). This was connected to carbon paste chips via spring loaded pogo pins. Electrodes were pretreated via CV cycling in 1 x PBS for 10 cycles between corner voltages of 1.3 and -0.6 V vs Ag/AgCl at a speed of 100 mV/s with a step size of 0.02 V

4.3.4 ELISA format

PSA ELISA was performed in a sandwich format based on the R&D systems duoset PSA ELISA kit (DY1344) which antibodies and standards were obtained from. Incubation times and conditions were varied to optimise electrochemical performance of the assay; exact variations are provided along with datasets below (Section 4.4). These variations were based on the following basic protocol: 32 wells of a polystyrene 96 well plate were incubated successively with100 µL mouse anti-human PSA capture antibody (2 µg/mL), 300 µL backfill (1% BSA in 1

x PBS), 100 µL PSA standards (60 – 0.038 ng/mL), 100 µL biotinylated goat anti-human PSA detection antibody (12.5 ng/mL) and 100 µL streptavidin – HRP (200-fold dilution from provided stock) to produce the 'stack' shown in Figure 4.1. Between incubations wells were rinsed three times using a provided wash buffer (0.05 % TWEEN20 in 1 x PBS. Resulting antibody sandwiches were interrogated via the addition of 100 µL TMB substrate solution to wells which was followed by 50 µL of stop solution (0.1 M H_2SO_4) once colour had been given time to develop. Capture antibody was deposited in wells overnight at room temperature in the dark and subsequent incubations were conducted on a microplate shaker (SciQuip) in an incubator at 37 °C.

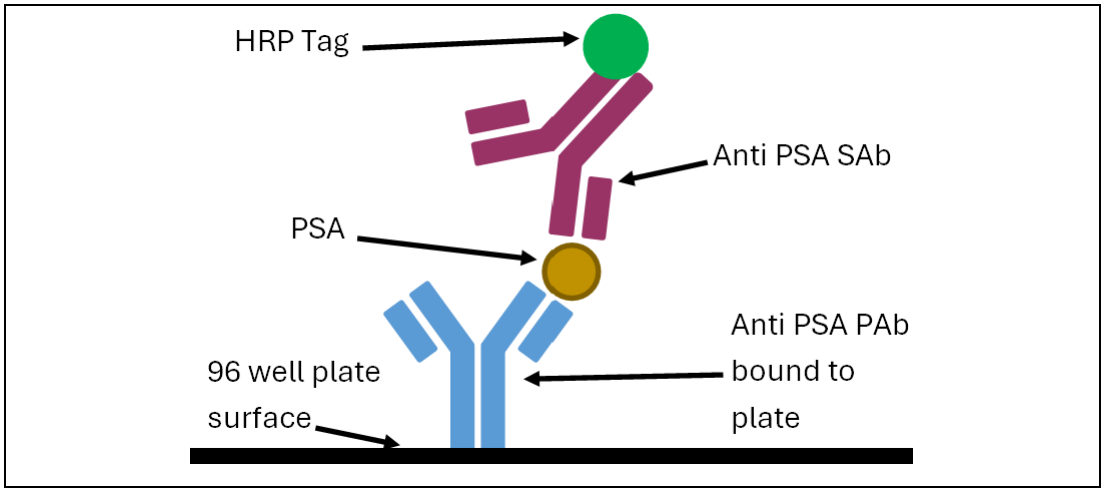

Figure 4.1: General scheme of the ELISA carried out in plate showing the 'stack' of antibodies and antigen that is interrogated with TMB substrate solution.

4.3.5 ELISA measurement

ELISA products were measured colourimetrically using a BioTex Elx800 absorbance microplate reader at 450 nm. Electrochemical measurement was performed using the same configuration as for pretreatment (Section 4.3.3) via chronoamperometry at a potential of 0.2 V vs Ag/AgCl for 60 s with a time interval of 0.1 s.

4.3.6 LoD calculation

The limit of detection (LoD) of performed ELISA (the lowest detectable target concentration) was calculated as shown by *Ambruster and Pry*[98]. Firstly Equation 4.1 is used to calculate the Limit of the blank (LoB), or the highest apparent concentration to be expected from blank measurements. This can then be used along with Equation 4.2, along with the standard deviation of the lowest concentration measured, to calculate LoD. To relate this LoD to the measurements taken, an experimental LoD (ELoD) is taken at the closest measured point above this calculated LoD as the lowest experimental response observed.

Equation 4.1: Calculating limit of the blank

$$LoB = Mean_{(Blank)} + 1.645(STD)_{(Blank)}$$

Equation 4.2: Calculating limit of detection

$$LoD = LoB + 1.645(STD)_{(Sample)}$$

4.3.7 Statistical Analysis

Statistical analysis was undertaken using Origin 2022 (OriginLab, Massachusetts, USA). Means and standard deviations of datasets were found using inbuilt mean and standard deviation calculators. Anova was performed in the comparison of binding methods, inbuilt one-way Anova was used with a significance level of 0.05 and a Tukey post-hoc test used to group results at a significance level of 0.05.

4.3.8 Antibody Binding

Assays were also bound to the surface of electrodes to potentially enable direct electron transfer between HRP tags and the electrode surface (possible when there is a short distance between them[198]). This was done to improve assay performance through the combination of signals from TMB^{2+} reduction and direct electron transfer between the HRP tags and electrode surface.

Testing of antibody attachment was performed based on work from *Sharafeldin, McCaffrey and Rusling*[199] in which the efficacy of anti-HRP immobilisation was quantified by the enzymatic activity of immobilised HRP target. In this investigation, mouse Anti – HRP monoclonal antibody (ab10183) was deposited on pretreated chip surfaces using a range protocols to produce the general structure shown in Figure 4.2. Regardless of protocol this deposition was interrogated through incubation with 500 µL of 0.1 µg/mL HRP solution for one hour and 400 µL of TMB ELISA substrate solution (H_2O_2 + TMB) for 20 minutes. The resulting solution (containing TMB^{+}) was stabilised through the addition of 200 µL of 0.1 M H_2SO_4 (to form TMB^{2+}) and 150 µL of this stabilised solution was transferred to a well of a 96 well plate for measurement via absorption at 450 nm. Incubations were performed at 37 °C on an orbital shaker at 100 rmp and between incubations chips were rinsed using a wash buffer (0.01 % TWEEN 20 in 1 x PBS) three times.

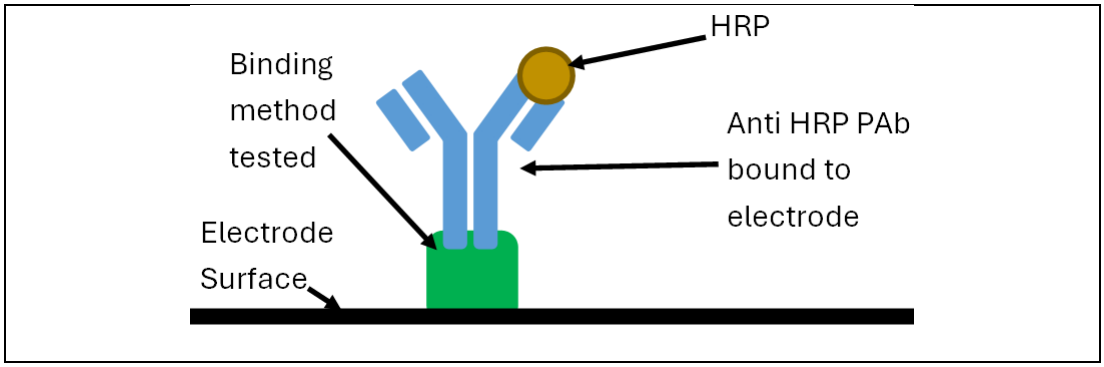

Figure 4.2: The general structure interrogated in binding experiments.

Antibodies were attached to the carbon paste surface via physisorption, chemical crosslinking and via an activated chitosan film. Physisorption is one of the simplest methods of antibody attachment and is used commonly in the attachment of antibodies to both gold[200] and carbon[201] surfaces. In this study it was performed via incubating 25 µg/mL of capture antibody solution diluted in 1 x PBS on the chips surface overnight at 4 °C.

Crosslinking to the carbon surface was performed via EDC/NHS coupling, shown in *Attoye et al.*[202]. A solution of 2 mM $NaNO_2$ and 2 mM aminobenzoic acid was made in 0.5 M HCl and stirred for 5 minutes at 25 °C to activate. This solution was then grafted to the chip surface via three CV scans between corner potentials of 0.4 and -0.1 V vs Ag/AgCl at a scan speed of 100 mV/s and step of 0.01 V. The solution was then rinsed off using DI water and a solution of 20 mM NHS, 100 mM EDC in 100 mM MES buffer incubated on the chips surface for an hour at 25 °C. This solution was then rinsed off using 100 mM MES buffer and 25 µg/mL of capture antibody solution diluted in 1 x PBS incubated on the chips surface overnight at 4 °C.

Binding via an activated chitosan film on the surface of chips was based on methods in *Sharafeldin, McCaffrey and Rusling*[199]. A film was created on the carbon chip surface via deposition of 0.25 mg/mL chitosan in 0.05 M HCl or one hour at 25 °C, chips were then air dried and Amine groups on the chitosan activated via incubation with 3% glutaraldehyde in 1 x PBS for 2 hours at 25 °C. After rinsing with DI water, 25 µg/mL capture antibody solution was incubated on the chip surface overnight at 25 °C.

Antibody binding to the chip surface was also attempted using a recombinant protein A/G intermediate. This is a chimeric protein that contains domains from protein A and protein G which targets the antibody F_c domain (common within antibody isotypes). In this case they were bound to the chip surface and used to anchor the anti – HRP antibodies via their Fc region (Figure 4.3) and improve their orientation. Addition of this intermediate was performed simply, the methods

above were repeated however in place of capture antibody, 2.5 µg/mL of protein A/G was instead incubated on the chip surface overnight at 4 °C, in the morning chips were then rinsed with wash buffer and capture antibody incubated on their surface at 37 °C for one hour while being agitated on an orbital shaker at 100 rpm.

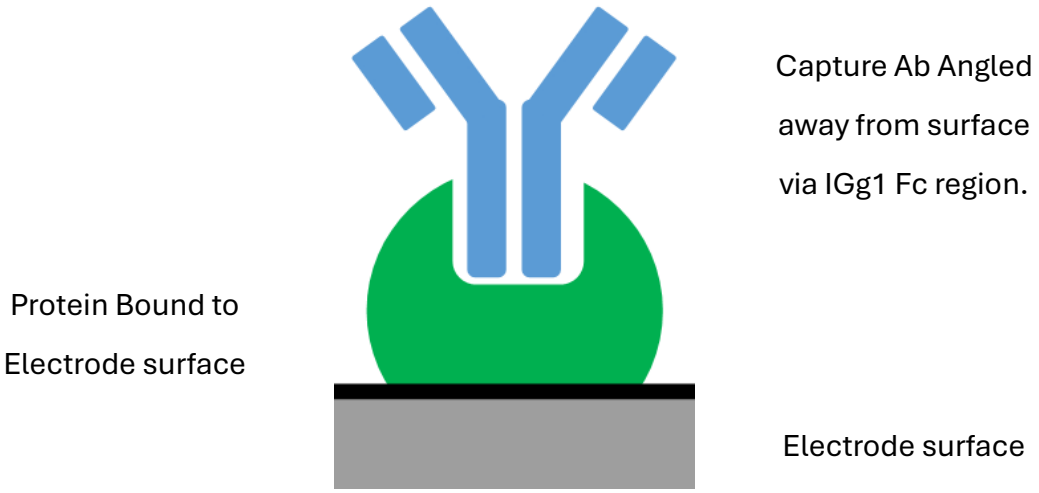

Figure 4.3: How Protein A/G is theoretically able to produce oriented antibodies

4.4 Results and discussion

4.4.1 Initial ELISA development

An initial ELISA was performed to gauge if a commercially available kit purchased from R&D systems would be electrochemically detectable via transferring of plate products to the carbon paste chips for measurement.

Absorbance data (Figure 4.4a) showed the bottom half of an expected sigmoidal dose response curve[51]. Higher concentrations produced higher standard deviations that began to visually overlap while at lower concentrations as well as in background measurements much lower standard deviations were seen leading to an LoD of 0.06 and ELoD of 3.75 ng/mL.

Sensitivity was lower than that seen for the IL-6 work (Chapter 3), where LoDs of 75 pg/mL (0.075 ng/mL) were possible. While 3.75 ng/mL is in the range that can be considered clinically relevant in the measurement of PSA from serum samples, poor resolution in measurements due to large standard deviations may prevent separation of low concentrations. This LoD however lay below the expected range of PSA in seminal fluid and so may be a much more suitable medium for measurement despite complications caused by sample collection[203].

Electrochemical data (Figure 4.4b) showed a sigmoidal curve with large intersecting error at high concentrations. As was also seen in absorbance measurement, low concentrations produced small error bars however large standard deviation and overall magnitude of the baseline results produced a large LoD of 8.76 nA which prevented the estimation of any ELoD.

Poor background consistency arose primarily due to a single channel of the carbon chip which produced large currents (highlighted in Figure 4.4c) and the fact that these erroneous currents were not seen in other measurements with the chip indicates that error here was likely caused by poor connection between that specific channel of the chip and the potentiostat. Without this error it is probable that an ELoD closer to that seen in absorbance measurement would be possible,

however it should be noted that even absorbance measurements produced poorer ELoDs than were seen in literature (Table 4.1).

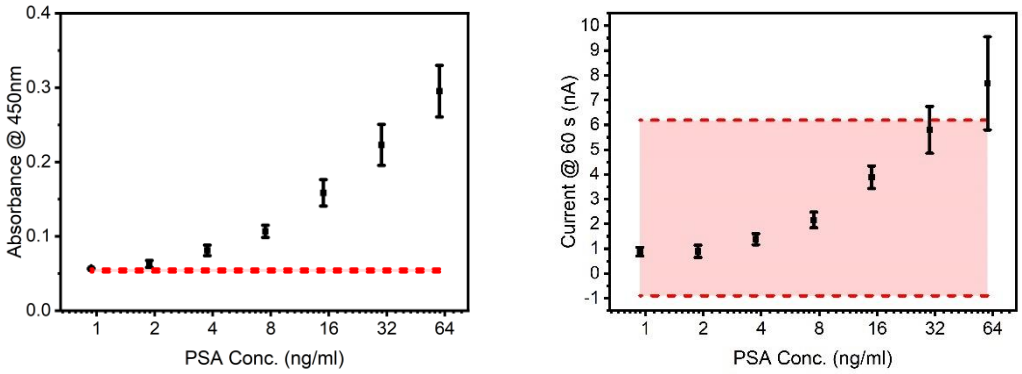

(a)

(b)

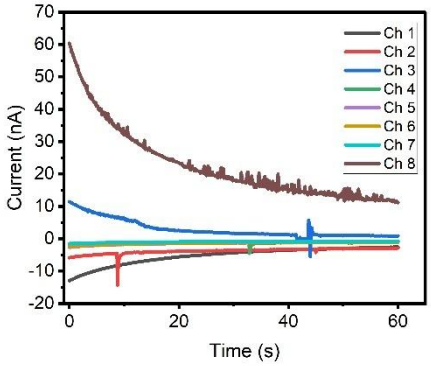

(c)

Figure 4.4: Absorbance of PSA sandwich ELISA performed with 60, 30, 15, 7.5, 3.75, 1.88 and 0.94 ng/mL PSA standards diluted in 1% BSA solution. Four wells of an ELISA plate were used for each concentration and resulting absorbance measured at 450 nm. Resulting data is plotted with a zero line (error bars plotted as +/- one sample standard deviation) (n = 4)**(a)**, chronoamperometric measurement of final ELISA products pipetted onto a chip, measured at 0.2 V vs Ag/AgCl over 50 s using all 8 electrodes of a single chip and compared to baseline measurements (red zone) (n = 8) (error bars plotted as +/- one sample standard deviation) **(b)** and raw chronoamperometric plots of zero-line measurements **(c)** to highlight the cause of poor ELoD.

The ELISA protocol was repeated with a longer TMB substrate solution incubation (50 mins vs. 20 mins). This longer incubation was an attempt to produce more measurable substrate and so decrease ELoD seen in both absorbance and electrochemical measurements. Results are shown in Figure 4.5

Both absorbance and electrochemical results showed similar 'S shaped' patterns as initial results seen in Figure 4.4, however lower ELoDs (1.875 ng/mL for absorbance, 3.75 ng/mL electrochemical) towards the lower limit of detection possible by the kit purchased were seen (0.938 ng/ml). Again, poor signal was observed on a single channel, due to poor connection and this channel was removed from analysis.

A major factor contributing to the lower ELoD was an increased magnitude in signals. At the highest concentrations measured, longer incubation times boosted the absorbance from 0.3 to 0.4 and increased the electrochemical response from 8 nA to 20 nA. The electrochemical method demonstrated greater sensitivity in comparison to earlier results (Figure 4.4b) largely due to stabilisation of background measurements. This stabilisation was produced by both increased magnitudes of results collected as well as removal of noisy channels from results, highlighting the need for data analysis, and particularly the automatic rejection of poor channel results.

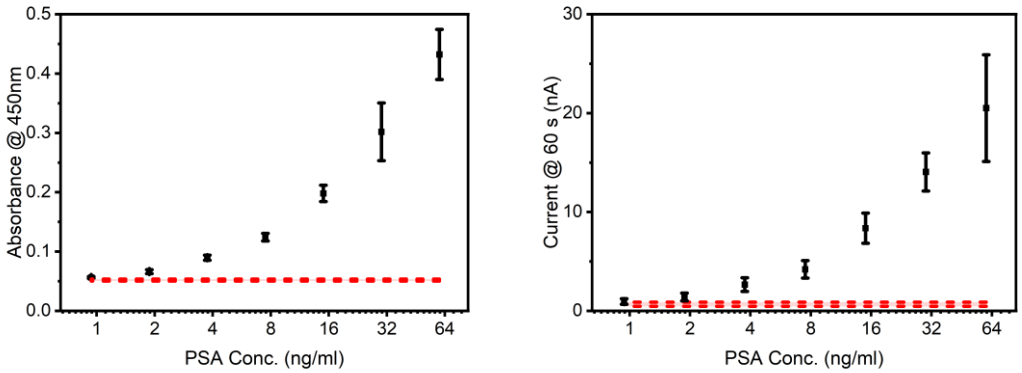

(a) **(b)**

Figure 4.5: Absorbance of PSA sandwich ELISA performed with 60, 30, 15, 7.5, 3.75, 1.88 and 0.94 ng/mL PSA standards diluted in 1% BSA solution and extended substrate incubation times. Four wells of an ELISA plate were used for each concentration and resulting absorbance measured at 450 nm. Data is plotted with a zero line (error bars plotted as +/- one sample standard deviation) (n = 4)**(a)** and chronoamperometric measurement of final ELISA products pipetted onto a chip, measured at 0.2 V vs Ag/AgCl over 50 s using 7 electrodes of a single chip (one failed during measurement) and compared to baseline measurements (red zone) (n = 7) (error bars plotted as +/- one sample standard deviation)**(b)**.

To summarise the initial optical and electrochemical ELISA development, results show that the PSA Duoset kit purchased from R&D systems was able to be measured both by absorbance and electrochemically via chronoamperometry, although absorbance measurements yielded lower ELoD and chronoamperometric data required removal of outliers to be suitable.

4.4.2 Binding work

After demonstrating the commercial ELISA kit could be used to measure PSA in both an optical and electrochemical format, investigation was performed to gauge if antibodies could be effectively attached to the carbon paste surface. This work was performed with a protocol based on *Sharafeldin, McCaffrey and Rusling*[199] where a direct ELISA is performed between an anti-HRP capture antibody bound to a surface and HRP. In this case anti HRP was bound via physisorption, EDC/NHS coupling and an activated chitosan layer both directly and through a protein A/G mediator. The completed ELISA was interrogated via a TMB substrate solution and resulting products transferred to 96 well plates for measurement via absorbance. Results shown in Figure 4.4 compare sample chips which were functionalised with anti-HRP antibody and control chips to which no antibody was added (antibody buffer containing no antibody was added at the relevant step of each functionalisation method). Both sets of chips were then interrogated with HRP and substrate solution.

Results from binding without the protein mediator are shown in Figure 4.6a. Visually, physisorbtion and EDC/NHS coupling were able to maintain low magnitudes of control response which led to good visual distinction between sample and control measurements despite large standard deviations of physisorbed measurements. Control measurements of chitosan binding were of a much higher magnitude which led to poor visual distinction between them and sample measurements.

Results from protein mediator binding are shown in Figure 4.6b. Chips where the protein mediator was physisorbed to the surface were able to maintain low magnitudes of control response while also shrinking in the deviation of sample measurements (± 0.67 in simple binding vs ± 0.12 In protein mediated binding). This produced a clearer difference between sample and control measurements and indicated that the antibody layer being formed was more consistent.

Protein deposition via EDC/NHS produced large magnitudes in control measurements while increasing variability in sample measurements (seen through increases in standard deviations) and while protein deposition via chitosan was able of both reducing variability in sample measurements and shrinking the magnitude of control measurements, overlap was still seen.

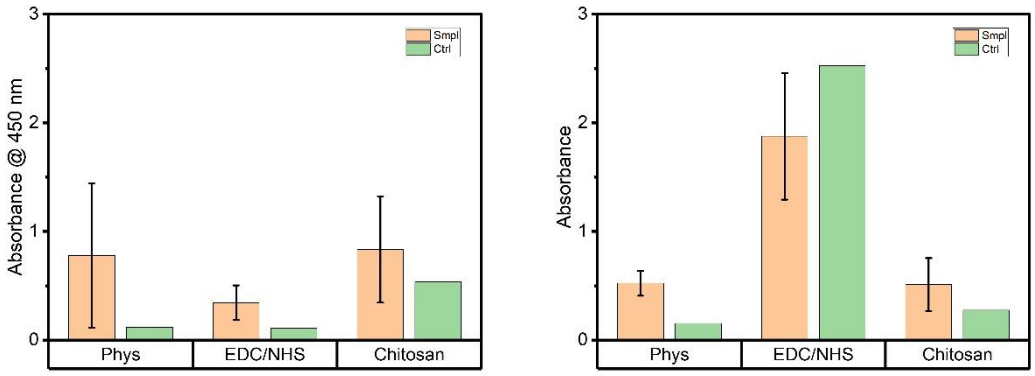

(a) **(b)**

Figure 4.6: Absorbance measurements of final well solutions after binding carried out without **(a)** and with a protein A/G intermediate **(b)**. Each dataset contains three sample chips to which antibody solution was bound and one control chip to which no antibody was bound. Both sets of chips were then interrogated through the addition of HRP and substrate solution and resulting products measured at 450 nm on a plate reader.

Poor results from chitosan-based binding potentially arose from the non-specific nature of the chitosan activation by glutaraldehyde. Glutaraldehyde is bifunctional and can react with two primary amine ($R\text{-}NH_2$) groups[204] which will crosslink them together, this binding is however non-specific and so crosslinking may occur between amines on the chitosan surface, amines on the attachment target or even amines on unwanted molecules. Chitosan-chitosan crosslinking has been well reported in literature, where its 'self-crosslinking' can lead to polymerisation and eventually, via internal rearrangement, a chemically inert material[205]. The potential for nonspecific crosslinking or 'self-crosslinking' may account for the variability and high background observed in the direct antibody deposition experiments using complex mediums, for high background measurements seen in directly deposited antibody experiments in which

antibody was deposited in a complex medium which contained many amine containing molecules that could also bind to the chitosan surface.

Surface functionalisation via EDC/NHS coupling may have also suffered from the non-specific nature of its binding reaction, in which carboxylate (COO^-) on the carbon surface was bound to a primary amine (NH_2) on the antibody surface[206]. Again, especially when measurements were performed in biological matrices this potentially caused a large amount of noise in measurement.

This non-specific binding did not however explain differences seen between binding performed with and without a protein mediator where protein binding suffered from large background signals. This difference highlighted the ability of serum (which antibodies were diluted in) to act as a blocking buffer able to passivate the active carboxylate surface via binding of serum proteins (e.g. albumin) and prevent further non-specific binding, whereas when protein (in a PBS buffer) was deposited, no blocking took place and so high backgrounds were seen in resulting chips

Both approaches using physisorbtion produced low baseline results due to the weak, non-specific bonds formed between unwanted proteins in solutions and the paste surface enabling their facile removal through rinsing. Although this rinsing was also able to remove wanted proteins and antibodies from the carbon surface (as seen in reduced magnitude of response compared to other methods) their high concentration ensured their presence post rinse. Much higher consistency was seen in surfaces functionalised via the protein intermediate, due to the successful orientation of bound antibodies.

Results showed that binding was possible although significant inter chip stability and separation between control and sample measurements was only achievable using a physisorbed protein intermediate either due to its ability to orient antibodies or simply due to the additional rinses used in its application.

4.4.3 Bound ELISA

An experiment was then performed to investigate if binding of a capture antibody to the carbon paste surface was able to produce comparable results to ELISA conducted in a 96 well plate. From results shown in Figure 4.6 it was concluded that this binding should be performed using a recombinant protein A/G intermediate physiosorbed to the chip surface due to its simplicity and ability to maintain a low baseline, ELISA was performed using 5 carbon paste chips and interrogated using PSA concentrations between 15 and 1.875 pg/mL (diluted in 1% BSA).

Results of this ELISA are shown in Figure 4.7. Compared to traditional in plate ELISA (Figure 4.5) bound ELISA produced both higher magnitudes of current response (82 nA vs 8 nA at a PSA concentration of 15 ng/mL) and standard deviations (68 nA vs 2 nA at a PSA concentration of 15 ng/mL). Visually, bound ELISA could maintain a low baseline and the bottom portion of the expected sigmoidal shape was visible. Despite this, large standard deviations contributed towards high LoD of 52 nA, which prevented the estimation of any ELoD.

This trend, particularly the large increase in baseline current seen, indicated that antibody sandwiches were being formed on the electrode surface and that these sandwiches were able to produce concentration dependant signals when exposed to target analytes. These signals were higher in magnitude than those seen in the measurement of ELISA products alone which indicates that they were contributed to by both the reduction of ELISA products as well as by direct electron transfer between HRP tags and the electrode surface. Despite this amplification, binding the sandwich to the surface also amplified errors leading to poor ELoDs when compared to ELISA.

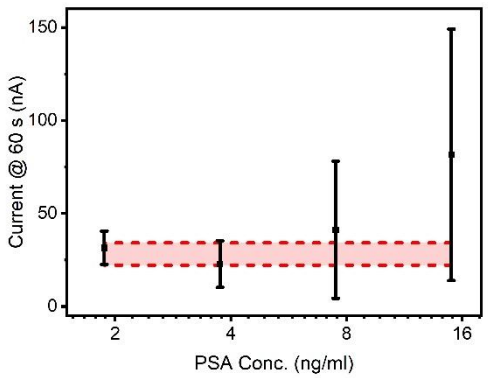

Figure 4.7: PSA ELISA performed attached to electrode chips via a recombinant protein A/G intermediate. Completed antibody sandwiches were incubated with substrate solution for 40 minutes before being stopped via addition of 0.1 M H_2SO_4. Resulting product was measured using chronoamperometry at 0.2 V vs Ag/AgCl for 60 seconds using all 8 electrodes on chips (n = 8) although it should be noted that control measurements (performed by addition of 1% BSA solution instead of a PSA concentration) are only taken using 4 electrodes due to product escaping the chip well after these measurements (n = 4).

4.4.4 ELISA in a clinically relevant medium

A final experiment was performed to assess the performance of the superior off-electrode PSA carbon paste system to detect PSA in a more complex clinically relevant medium. For this purpose, PSA standards were diluted in 100% human serum measured using an in-plate ELISA, this serum was filter sterilised and so still contained many potential interferents seen in clinical PSA testing.

When measured via absorbance (Figure 4.8a) results formed the same general sigmoidal pattern seen throughout this chapter, large differences were however seen in between the magnitudes of response seen here and in the measurement of samples diluted in 1% BSA (Figure 4.5). Again, using the highest concentration points measured to compare, serum ELISA increased absorbance results from 0.4 to 2.2 and electrochemical results from 20 nA to 49 nA. This increase in magnitude lead to a lowered optical ELoD of 0.94 ng/mL and electrochemical ELoD of 1.88 ng/mL.

Part of this increase in signal could be attributed to the addition of PSA already in the serum used in standard dilutions and its creation of a 'standard addition' effect commonly used in biosensors[207], however given the low magnitude of increase seen in baselines (0.052 to 0.061 in absorbance measurements) this alone cannot explain all the increases seen. It is more likely that the complex nature of the serum used is improving signal magnitudes via 'macromolecular crowding,' where large molecules occupy a large amount of volume in a fluid and therefore concentrate other molecules as they were forced into the remaining volume. This effect is well documented, and crowding agents can often be added to lateral flow formats to increase their sensisitvity[208].

The results showed that it was possible to measure clinically relevant concentrations of PSA in a clinically relevant medium both through colourimetric absorbance measurement and through electrochemical chronoamperometry measurement.

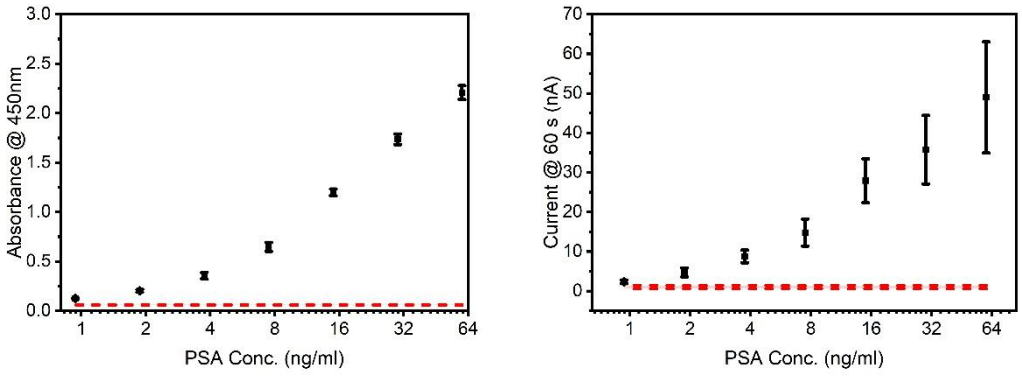

(a) **(b)**

Figure 4.8: Absorbance of PSA sandwich ELISA performed with 60, 30, 15, 7.5, 3.75, 1.88 and 0.94 ng/mL PSA standards diluted in 100% human serum and extended substrate incubation times. Four wells of an ELISA plate were used for each concentration and resulting absorbance measured at 450 nm. Resulting data is plotted with a zero line (error bars plotted as +/- one sample standard deviation) (n = 4)**(a)** and chronoamperometric measurement of final ELISA products pipetted onto a chip, measured at 0.2 V vs Ag/AgCl over 50 s using all 8 electrodes of a single chip and compared to baseline measurements (red zone) (n = 8) (error bars plotted as +/- one sample standard deviation)**(b)**.

4.5 Conclusions

In this chapter the ability of a carbon paste chip to detect a key indicator of prostate cancer, prostate specific antigen, has been investigated.

A commercial ELISA kit was used to detect PSA through colourimetric and electrochemical measurements, although resulting ELoDs (1.875 ng/mL from absorbance, 3.75 ng.ml from chronoamperometry) were in theory suitable for clinical detection from serum, substantial error above these LoDs may make the resolution of measurement unsuitable for clinical detection, at least in blood serum.

Anti-HRP antibodies were bound to the carbon paste surface by physisorbtion, chemical grafting and via an activated chitosan layer both with and without a protein intermediate. Although binding was feasible through all three methods,

only physisorbtion with a protein intermediate was able to reject non-specific binding while still maintaining consistency between chips.

Physisorbtion via a protein mediator was then used to bind a commercial ELISA kit to the carbon paste surface. Although this bound sandwich could produce higher magnitudes of measurements in comparison to unbound, in plate counterparts, large error seen in both background and sample measurements made the calculation of any ELoD impossible.

A final measurement of PSA spiked into 100% serum was performed in a plate and measured via colourimetry and chronoamperometry. Presence of PSA in the serum used and crowding increased magnitudes of measurements while lowering LoDs although again error reduces the resolution of measurements.

In future, the carbon chip and commercial ELISA used during this chapter should be used in the detection of PSA concentrations required for potential measurement in seminal plasma (in the low mg/mL concentration range) and further measurements performed in seminal plasma to gauge its effect on measurement efficacy. This should be performed with further literature review to gauge the sensitivity of PSA levels in seminal plasma to cancer in the prostate.

5 Improving carbon paste performance

5.1 Introduction

Throughout this thesis, a carbon paste chip was produced capable of the detection of surface insensitive molecules and ELISA products. Despite this, these chips still faced issues due to inter and intra chip variability which necessitates comparative measurements to be made on a single chip while also producing large standard deviations in results. Chips also struggled with the detection of surface sensitive mediators such as Ferri -Ferrocyanide (FF).

One of the principal methods used in literature to improve the sensitivity and reduce the variability of electrodes is chemical pretreatment. Which pretreatment is chosen, and how it will affect an electrode depends on its material (summary of common pretreatments provided in Table 5.1). As a material, carbon paste has characteristics that can be attributed to two different areas, the bulk of the paste which is responsible for conductivity and hardness and the surface, which is responsible for termination[209].

Table 5.1: Summary of common electrochemical pretreatments used with carbon materials

Electrochemical Pretreatment	Carbon Material	Reference
Multi Step Amperometry in NaOH	Carbon black + polylactic acid	[87]
Chronoamperometry in acetate buffer	Screen printed carbon	[202]
Chronoamperometry in Na_2CO_3	Screen Printed Carbon	[210]
Cyclic voltammetry in H_2SO_4	Carbon black + polylactic acid	[211]
Cyclic voltammetry in H_2O_2	Screen printed Carbon	[110]
Cyclic voltammetry in H_2SO_4	Screen printed carbon	[78]
Cyclic voltammetry in NaCl	Screen printed carbon	[111]
Cyclic voltammetry in KCl	Screen Printed Carbon	[112]

Termination describes the chemical structure seen at the surface of a crystal where the repeating structure meets the outside. When the structure of carbon is interrupted at a surface, reactions occur with oxygen and water to produce oxygen containing functional groups referred to as oxides or surface oxides[209], this is also known as 'oxygen termination' (shown in Figure 5.1). Oxygen termination is the end goal of many pretreatments and has been shown to improve electrochemical performance[212]. This termination can be achieved by binding oxide particles to the electrode surface, commonly either metal oxides[213] or graphite oxides[212] or through the direct generation of surface oxides, commonly achieved using sodium hydroxide. Direct surface pretreatment with sodium

hydroxide has been shown to improve both screen-printed electrode performance[114] as well as an ability to produce oxide groups (shown in Figure 5.1) on carbon black material[87].

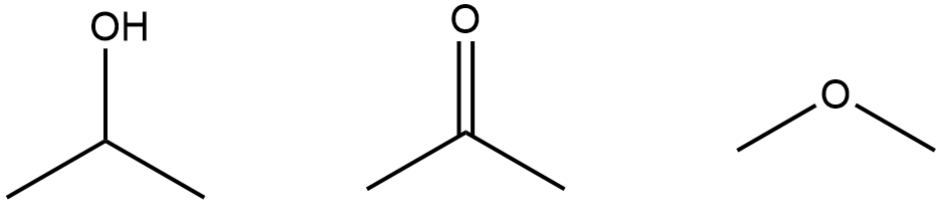

Hydroxyl Carbonyl Ether

Figure 5.1: Examples of oxygen termination seen in graphite/graphene materials

Hydrogen peroxide is another common chemical used in the pretreatment of carbon electrodes. It can enter the hexagonal carbon structure by a process known as intercalation, where molecules insert themselves between graphite layers, affecting the bulk electrode material. Although it is unlikely this intercalation occurs with OH^- as its intercalation requires high ionic solutions[214], being unfavourable at low molarities[215], solvated sodium ions readily intercalate in graphite structures, despite not being able to when unsolvated[216]. The intercalation of these solvent molecules can produce edge planes in the graphite, where electrochemical reactions can take place on the surface[217]. This explains the success and popularity of sodium-based solutions such as sodium hydrogen carbonate, sodium carbonate[152], sodium nitrate[114], phosphate buffered saline and sodium hydroxide in the pretreatment and modification of carbon electrodes.

The bulk of the electrode can also be modified to improve performance, though given its position in a finished chip this is done through modification of paste materials rather than pretreatment through the modification of the carbon component of pastes. Although the graphite powder used up to this point in manufacturing is ubiquitous in the manufacturing of paste electrodes[104], a range of alternatives are available. Of particular interest is carbon black, a form of carbon consisting of many small individual graphene-based nanoparticles that

aggregate to form larger three-dimensional structures[94]. When incorporated into carbon pastes, it offers cost effective[218] electroanalysis with higher signal to noise ratios than pastes produced from graphite or carbon nanotubes and under SEM analysis shows uniform surface topology when compared to graphite-based material[219].

Electrode manufacturing is undoubtedly one of the most important stages in the development of a sensor. It can affect everything about the final product and has an especially large impact on reliability and reproducibility. Additive manufacturing (commonly known as 3D printing) is a process where a physical object is fabricated directly from a digital model[220]. Although there are superior methods for large scale manufacturing, 3D printing allows flexibility in electrode design and compliments the ability of the paste to fill moulds. Up until this point, fused deposition modelling (FDM) had been used in the manufacturing of chips, primarily due to its ease of use and cleanliness[221] which makes it both fast and convenient to set up. This general ease of use means that FDM is now seen commonly in literature, both to produce full sensors[106, 222] and their individual components[87,223].

Stereolithography (SLA) is another common method used for the prototyping and production of sensors. During SLA manufacturing, light is used to cure a liquid photopolymer into solid parts[224], most commonly taking the form of a resin 'bath' that an object is slowly lifted from. SLA is an accessible method and its use of light rather than a physical nozzle makes high resolution parts much more achievable. However, the requirement for resin management (unused resin must be filtered and returned to storage)after use does make it more inconvenient to use. Despite these issues, it is also used in the generation of full sensors[225] and their parts[226].

Treatment of electrodes with ultraviolet (UV) light is also possible and in the case of parts produced via SLA can improve mechanical properties[227]. In the context of biosensors, this treatment is primarily used for sterilisation[228],

however has also been shown to increase the number of oxide groups on sensor surfaces[229].

5.2 Chapter objectives

This chapter aimed to address issues caused by variability and lack of sensitivity in the electrode chips manufactured previously through the answering of three questions:

- Does pretreatment of carbon chips with a hydroxide-based solution lead to improved chip performance, both in standard redox mediators and in the measurement of HRP-TMB system
- Can the use of stereolithography, press filling of chip bases with paste or UV curing of final chips reduce both inter and intra chip variability in standard redox mediators?
- Can chip performance be improved through the replacement of graphite powder with a lower particle size alternative, carbon black, in the carbon paste?

5.3 Materials and methods

5.3.1 Materials

Table 5.2: Materials used during this chapter

Material	Supplier	Product Code
Paraffin wax	APC Pure	PW56-Y
Graphite powder	Inoxia	0029882791622
Carbon Black/Lamp black	Inoxia	0029882790717
PBS tabs	Merck	P4117
Sulfuric Acid	Merck	258105
Potassium Ferricyanide	Thermo Scientific	223115000
Potassium Ferrocyanide	Thermo Scientific	211059000
Hexaammineruthenium (III) chloride	Thermo Scientific	363340010
Deionised water	Scientific Laboratory Supplies	CHE3874
HRP substrate solution	R&D systems	DY999B
ELISA wash buffer	R&D systems	WA126
ELISA Reagent diluent	R&D systems	DY995
Mouse Anti-Human PSA Capture Antibody	R&D systems	DY1344
Biotinylated Goat Anti-Human PSA Detection Antibody	R&D systems	DY1344
PSA standards	R&D systems	DY1344
Streptavidin-HRP	R&D systems	DY1344

5.3.2 Chip Manufacturing

Different manufacturing methods were used to gauge if improvements could be made to the manufacturing of chip bases. Chip bases were produced via FDM and SLA manufacturing. Initial computer-aided design (CAD) files for a base and well were produced in FreeCAD 0.20.1 and exported in .stl formats. FDM printing was performed using a RAISE3D E2 IDEX Dual 3D printer with a nozzle diameter of 0.4 mm and 1.75 mm white polyethylene tere phthalate glycol (PETG) filament (ERYONE). Files were sliced using ideaMaker 4.2.3 (RAISE3D) using the inbuilt high quality PETG template (0.1 mm layer height, 10% infill, 70 mm/s infill speed). SLA printing was performed using a creatily UV printer with elegoo grey UV curing resin. Files were printed with 5 initial layers exposed for 80 seconds and the rest for 10 seconds. Once printed, parts were rinsed in a bath of IPA to remove excess resin before being cured at 50 °C for two hours.

How paste was added to these bases was varied to gauge if it could be packed more densely into the produced bases. Manual manufacturing was performed as shown in earlier chapters. A graphite paste consisting of a 1:1 weight ratio of graphite powder to paraffin wax and a carbon black paste consisting of a 1:2 ratio of carbon black powder to paraffin wax were produced. Press manufacturing was carried out similarly, with molten paste being transferred to printed chips via a spatula. However, once the paste was positioned on the chip, it was then heated with a heat gun and compressed into tracks using a (VEVOR) press before excess was removed and an Ag/AgCl quasi-reference electrode added.

UV treatment was performed on manually produced FDM and SLA based chips. Chips were placed 0.5 M away from a UV lamp (rated as 2 8-watt bulbs) for 10 minutes before being pretreated as normal and characterised.

In summary, 6 approaches to electrode manufacturing were tested:

1. Chips produced through FDM printing and manually filled with paste (Manual FDM chips)
2. Chips produced through SLA printing and manually filled with paste (Manual SLA chips)
3. Chips produced through FDM printing and filled with paste via pressing (Pressed FDM chips)
4. Chips produced through SLA printing and filled with paste via pressing (Pressed SLA chips)
5. Chips produced through FDM printing and manually filled with paste before being exposed to UV light (UV treated manual FDM chips)
6. Chips produced through SLA printing and manually filled with paste before being exposed to UV light (UV treated manual SLA chips)

5.3.3 Electrochemical Pretreatment

Electrochemical methods were performed using a PalmSens4 potentiostat driven by PSTrace 5.10 software (PalmSens, Houten, Netherlands) connected to electrode chips via a jig (Figure 5.2). Before use, chips were pretreated in either PBS or sodium hydroxide.

Phosphate buffered saline pretreatment of chips was performed via CV cycling in a 1 x PBS solution (0.01 M phosphate buffer, 0.0027 M potassium chloride and 0.137 M sodium chloride, pH 7.4) between corner potentials of -0.6 and 1.3 V vs Ag/AgCl at a scan speed of 100 mV/s and step of 0.02 V.

Sodium hydroxide pretreatment was based on a method by *Xue et al.*[87]. Two chronoamperometric steps of equal length (initially 10 s) in sodium hydroxide were performed with a time interval of 0.1 s. The first step applied was 1.4 V and the second -0.1 V, both vs an Ag/AgCl reference.

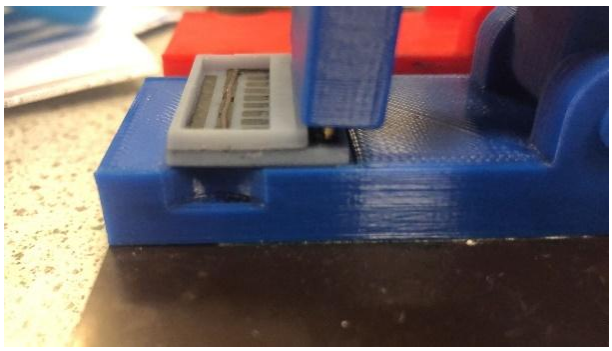

Figure 5.2: Jig used to connect paste chips to potentiostat. a 10 pogo pin array is soldered directly to wires which connect to potentiostat. The spring loaded hinge and internal pin springs are used to provide consistent pressure

5.3.4 Electrochemical Characterisation

Chip characterisation was performed using 2 mM Ferri/Ferrocyanide (FF) and 1 mM Ruthenium hexamine (Ruhex) solutions diluted in 1 x PBS. CV was performed between corner voltages determined independently for each experiment and scanned at a rate of 100 mV/s with a step of 0.01 V. SWV was performed between the same corner voltages with a step of 0.01 V, amplitude of 0.1 V and frequency of 20 Hz. CV peaks were identified manually from a manually drawn baseline in PSTrace 3 software. SWV results were moving average baseline subtracted and peak currents found automatically using inbuilt PSTrace software functions.

5.3.5 ELISA format

Prostate specific antigen (PSA) ELISA was performed based on instructions from the RnD systems PSA duoset ELISA kit (DY1344). In summary, 32 wells of a clear, polystyrene 96 well plate were incubated successively with 100 µL of capture antibody (2 µg/ml), 300 µL of backfill (1% BSA in PBS), 100 µL of PSA standards (60-0.038 ng/ml), 100 µL of biotinylated detection antibody (12.5 ng/ml) and 100 µL of streptavidin-HRP (200-fold dilution). 100 µL TMB substrate solution (used neat) was then added to wells and stopped using 50 µL stop solution (0.1 M H_2SO_4). Capture antibody was deposited in wells overnight at room temperature in the dark and subsequent incubations were carried out on a microplate shaker (SciQuip) in an incubator at 37 °C. Between steps, wells were rinsed three times

using a wash buffer (0.05 % TWEEN 20 in 1 x PBS). Resulting solutions were measured using a BioTex Elx800 absorbance microplate reader at 450 nm.

5.3.6 Electrochemical Measurement of ELISA products

Chronoamperometry of ELISA products were performed by pipetting well contents onto an electrode chip (4 completed wells fill a single chip) and performing chronoamperometry at a potential of 0.2 V vs Ag/AgCl for 60 s with a time interval of 0.1 s.

5.3.7 Statistical methods

Statistical analysis was performed with Origin 2022 software (OriginLab, Massachusetts, USA). Mean and standard deviations were calculated using inbuilt origin functions. Anova was performed to help the comparison of cleaning methods, the inbuilt origin one-way Anova function was used with a significance level of 0.05 and a Tukey post-hoc test used to group results, again at a significance level of 0.05.

5.4 Results and Discussion

5.4.1 Pretreatment

Before sodium hydroxide pretreatment was tested, the 'standard' PBS pretreatment used throughout this thesis was performed as a reference. A single chip was pretreated via CV cycling in a 1 x PBS solution between corner potentials of -0.6 and 1.3 V vs Ag/AgCl at a scan speed of 100 mV/s and step of 0.02 V and characterised using 2 mM FF in 1 x PBS. Looking at the first and last PBS pretreatment cycles (Figure 5.3a) PBS cycling was able to 'smooth' the CV response of the chip via removal of sharp, noisy peaks at 0.9, 0.1 and -0.5 V vs Ag/AgCl that were attributable to impurities in the graphite material, most likely sulphur, a common impurity in carbon materials that is electrochemically active and used in battery development[230].

Despite this improvement, FF characterisation (Figure 5.3b) showed little difference between chips pretreated via PBS cycling vs those which were not. Reduction peaks in both pretreated and 'stock' chips showed irreversible behaviour via their imbalanced, highly separated peaks[69] indicating that although PBS cycling was able remove impurities from the chip surface, it could not improve overall performance

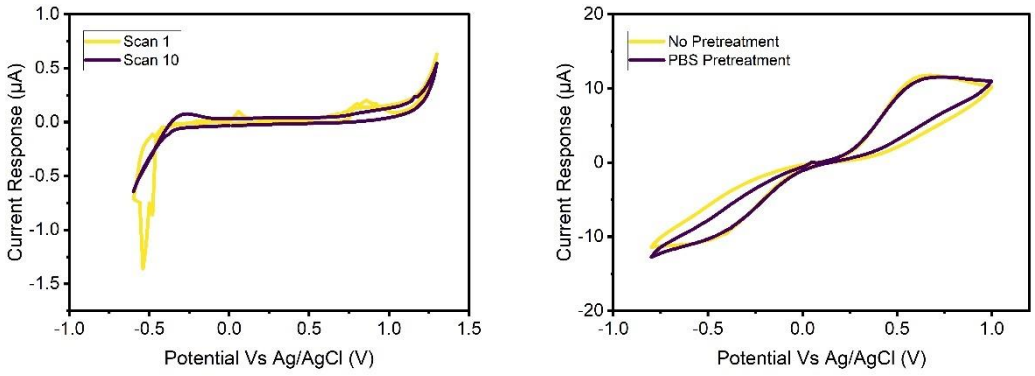

(a) **(b)**

Figure 5.3: Example of a CV pretreatment cycle in 1 x PBS, first and last scan for a single channel of a chip presented**(a)**. Post pretreatment CV plots in 2 mM FF in 1 x PBS for separate chips that have and have not undergone pretreatment **(b)**.

To provide an initial comparison with PBS results (Figure 5.3), a sodium hydroxide pretreatment was performed using 0.5 M sodium hydroxide and a total time of 20 s (10 s per step) as shown in literature[87]. The results of this pretreatment, as well as its characterisation using 2 mM FF in 1 x PBS are shown below (Figure 5.4). Although the single scan nature of pretreatment made it difficult to gauge efficacy during pretreatment, FF CV plots showed more conclusive results. When compared to both PBS and no pretreatment (Figure 5.4b), chips showed more equivalent oxidative and reductive peaks (Table 5.3: The effect of pretreatment approaches on FF peak heights and position.), indicating improved reversibility. More interestingly, a widening of the gap between forward and reverse scans is seen at 0 V vs Ag/AgCl, indicating greater capacitance in the system[231]. A large contributor to this is greater double layer capacitance being generated by more FF adsorbing to the electrodes surface on more oxidative groups.

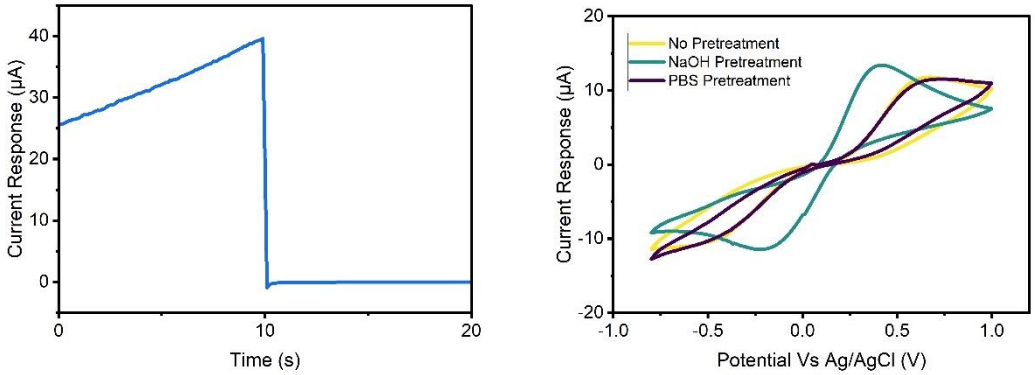

(a) **(b)**

Figure 5.4**a)**: Multi step amperometry pretreatment scan of a single channel in 10 mM sodium hydroxide **(a)** and example post pretreatment scans in 2 mM FF in 1 x PBS of three separate electrode chips pretreated with sodium hydroxide, 1 x PBS and without pretreatment **(b)**. Although full chips were pretreated and characterised (n = 8), single channels are shown for clarity.

Table 5.3: The effect of pretreatment approaches on FF peak heights and position.

Pretreatment Type	**Oxidative Peak current (µA)**	**Reductive Peak current (µA)**	**ΔE_p (mV)**
No Pretreatment	3.84 (±1.04)	-1.76 (± 0.66)	1126 (±60)
NaOH Pretreatment	11.09 (± 1.46)	-9.27 (± 2.28)	650 (±59)
PBS Pretreatment	12.30 (±6.35)	-3.14 (±2.12)	1162 (±94)

Initial comparisons showed that sodium hydroxide pretreatment could increase reductive peak currents and ΔEp (highlighted in Table 5.3: The effect of pretreatment approaches on FF peak heights and position.). This pretreatment was therefore optimised for use with the carbon paste chips, beginning with the timings of amperometric steps. Chips were pretreated over a range of timings (chosen over a similar range as source material[87]) using 0.5 M sodium hydroxide solution in 1 x PBS and characterised via CV in 2 mM FF in 1 x PBS. Resulting ΔEp and oxidative peak currents are plotted for comparison.

Looking at oxidative peak currents (Figure 5.5b), differences between pretreatment timings were visually difficult to discern and when grouped via statistical methods this was confirmed, where all timings shared the same group. Grouping did however highlight the ability of any pretreatment to cause significant changes in the peak currents the carbon paste could produce. Peak separation (shown in Figure 5.5a) showed much larger differences between timings. Improvements versus both PBS cycling and no pretreatment were both visually and statistically apparent and increasing pretreatment time did significantly decrease ΔEp. Although ΔEp never reached ideal separation of 59 mV (lowest ΔEp was 200s hydroxide @ 234 mV), given the expected resistivity of the carbon paste higher ΔEp was expected (as seen in literature where plasma treatment could produce peak separations of between 219 and 105 mV[232]).

Although the reduction in peak separation was significant as pretreatment time increased, due to lack of improvements in peak currents 10 second pretreatments were taken forward to reduce pretreatment times.

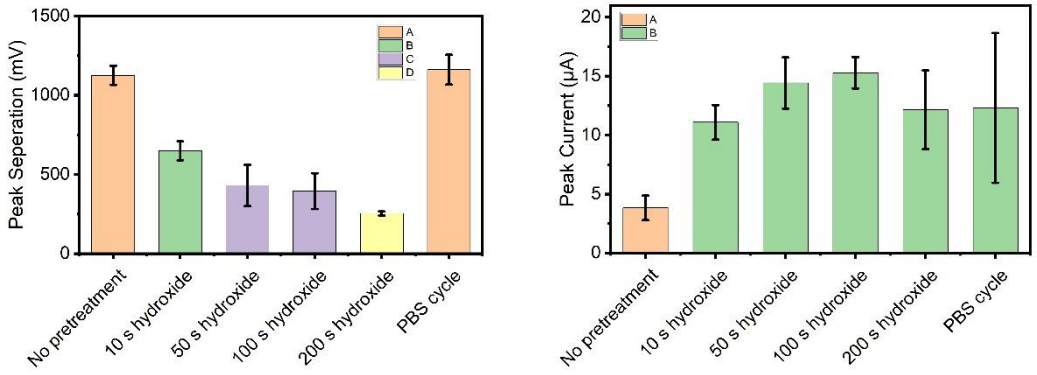

(a) **(b)**

Figure 5.5: Peak characteristics of chips characterised using 2 mM FF in 1 x PBS solution on electrodes pretreated for different lengths of time in 0.5 M sodium hydroxide vs a PBS pretreatment control (times shown are for a single step). ΔEp **(a)** and oxidative peak current **(b)** are plotted as an average of values taken for each channel on a chip (n = 8) and plotted +/- one sample standard deviation. One way Anova was performed on origin software with a significance level of 0.05, grouping of results was performed with Tukey post hoc testing at 0.05 significance level. Resulting groups are highlighted by bar colour.

The next logical step was to investigate the effect of concentration on chip performance. Concentrations from 0.5 M seen commonly in literature[228,87] to 0.0625 M via serial dilutions were used with 10 s of pretreatment and characterised in 2 mM FF; results are shown below (Figure 5.6).

Again, differences in peak current of these results were difficult to discern. Peak separations were also high and similarly grouped. Interestingly statistical grouping did not show any clear trend (i.e. data was not grouped by lowering/higher concentrations), and so differences were likely random and stemmed from chip variation rather than any effect of concentration. The lack of differences between concentrations indicated that chips are 'saturated' with pretreatment agent at quite a low concentration level that was not reached.

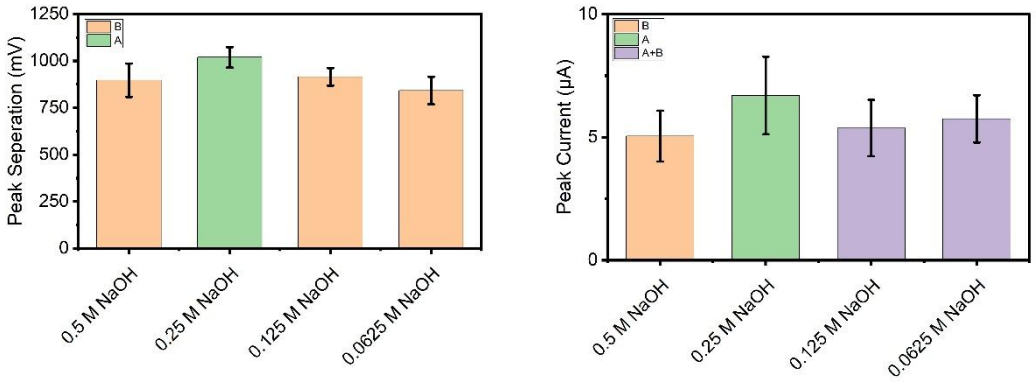

(a) **(b)**

Figure 5.6 CV measurements of 2 mM FF in 1 x PBS on electrodes pretreated in different concentrations of sodium hydroxide for a total time of 20 s. ΔEp **(a)** and oxidative peak currents **(b)** are plotted as an average of values taken for each channel on a chip (n = 8) and plotted +/- one sample standard deviation. One way Anova was performed on origin software with a significance level of 0.05, grouping of results was performed with Tukey post hoc testing at 0.05 significance level. Resulting groups are highlighted by bar colour.

After the promising improvements that sodium hydroxide was able to provide for the detection of the inner sphere redox mediator FF (Figure 5.5), an attempt was made to gauge if this pretreatment would produce any impact on real world detection via the detection of ELISA products. A duoset PSA ELISA was performed as instructed by the kit and incubated with a substrate solution containing H_2O_2 and TMB in order to produce TMB^+ and, after the addition of 0.1 M H_2SO_4, TMB^{2+}. TMB^{2+} product was then measured both by absorbance at 450 nm and by pipetting well contents onto pretreated electrodes and performing chronoamperometry at 0.2 V vs Ag/AgCl.

A single carbon paste chip was used for this electrochemical measurement, with rinses being performed with deionised water between measurements. Absorbance measurements (Figure 5.7:a) were as expected, producing an exponential curve with an LoD of 1.875 ng/ml.

Electrochemical results (Figure 5.7:b/c) produced an S – shaped sigmoidal curve typical of immunoassay results[51], with higher standard deviations at lower and

higher ends of the concentration range tested. Despite the presence of this expected shape, control measurements taken to generate a 'zero line' yielded much greater currents with a large standard deviation. As these were the first measurements taken, this indicated that pretreatment had poor stability and could 'wear off' over time, hinting that the pretreatment worked by the creation of oxide groups on already exposed graphite edges rather than the creation of new edge defects via intercalation.

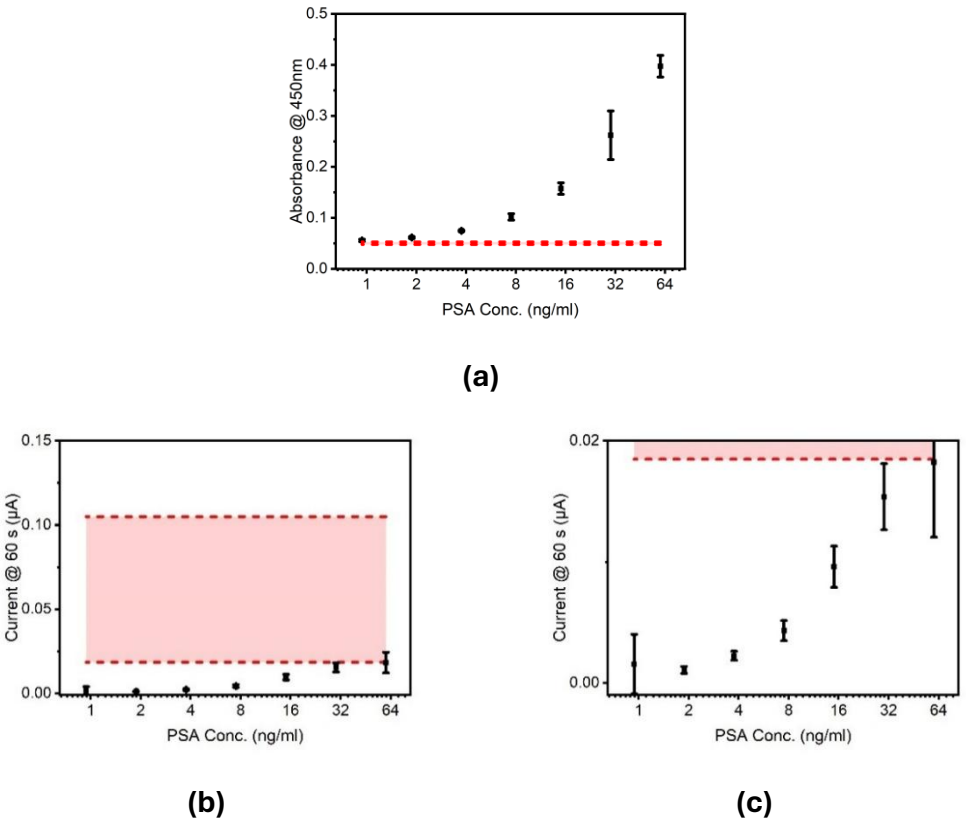

Figure 5.7: Absorbance of PSA sandwich ELISA performed with 60, 30, 15, 7.5, 3.75, 1.88 and 0.94 ng/ml standards of PSA diluted with 1 % BSA in 1 x PBS**(a)**. Four wells of ELISA were performed for each concentration and plotted with zero line (error bars plotted as +/- one sample standard deviation) (n = 4). Chronoamperometric measurement of well solutions pipetted onto chip, measured at 0.2 V vs Ag/AgCl over 60 s using all 8 electrodes of a single chip (n = 8), compared to PBS baseline measurements (red zone) (n = 8) (error bars plotted as +/- one sample standard deviation)**(b)**. Same dataset zoomed in to allow distinction of sample measurements**(c)**.

5.4.2 Manufacturing

Visually comparing different approaches to manufacturing (Figure 5.8), FDM chips had clearly defined counter and reference tracks, although working tracks were poorly defined and many seemed to short circuit to one another. This short circuiting was most clearly visible at the tip of tracks, where a channel produced by the FDM method could fill with paste material. This effect was much clearer on chips produced by press manufacturing, potentially due to the pressure produced being able to widen these tracks. In contrast, SLA chips were much cleaner, both when filled manually and via pressing, highlighting the ability of the SLA printer to produce smooth surfaces which, unlike FDM chips, had no cavities to fill with paste material. UV treatment had no visual effect on chips. Although shortly after treatment chips had a glossy appearance, this quickly faded, and electrodes became indistinguishable from their non-treated counterparts.

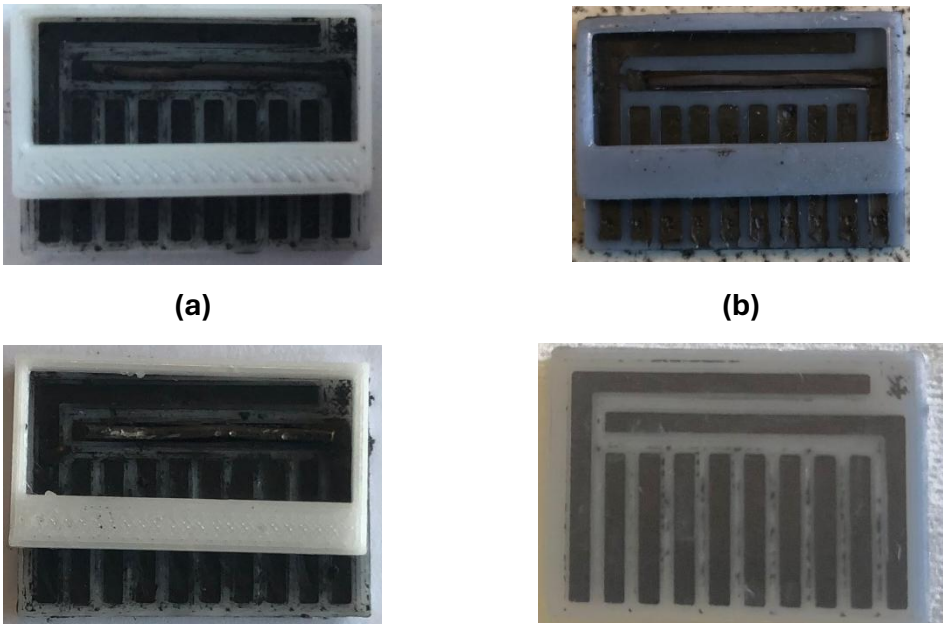

Figure 5.8: Visual comparison of differently manufactured electrodes. Manual FDM **(a)**, Manual SLA **(b)**, Pressed FDM **(c)** and Pressed SLA **(d)**.

Chips were also characterised electrochemically via CV using FF in 1 x PBS (Figure 5.9a)and Ruhex in 1 x PBS(Figure 5.9b) and via SWV using Ruhex in 1 x PBS (Figure 5.10). CV measurements showed the ability of press filling chips to increase peak heights, both in Ruhex and FF as well as visually reducing ΔEp in FF measurements indicating changes to the surface of the paste.

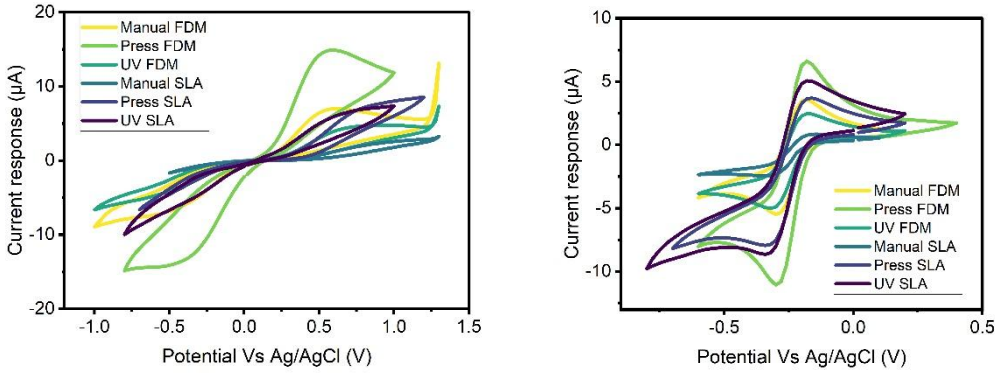

(a) **(b)**

Figure 5.9: CV characterisation of chips manufactured using different methods in 2 mM FF in 1 x PBS **(a)** and 1 mM Ruhex in 1 x PBS **(b)**. Redox mediator was pipetted onto chip surfaces and CV cycling was performed at a rate of 100 mV/s between solution limits. Although every electrode on each chip was measured (n = 8), only one is shown for clarity.

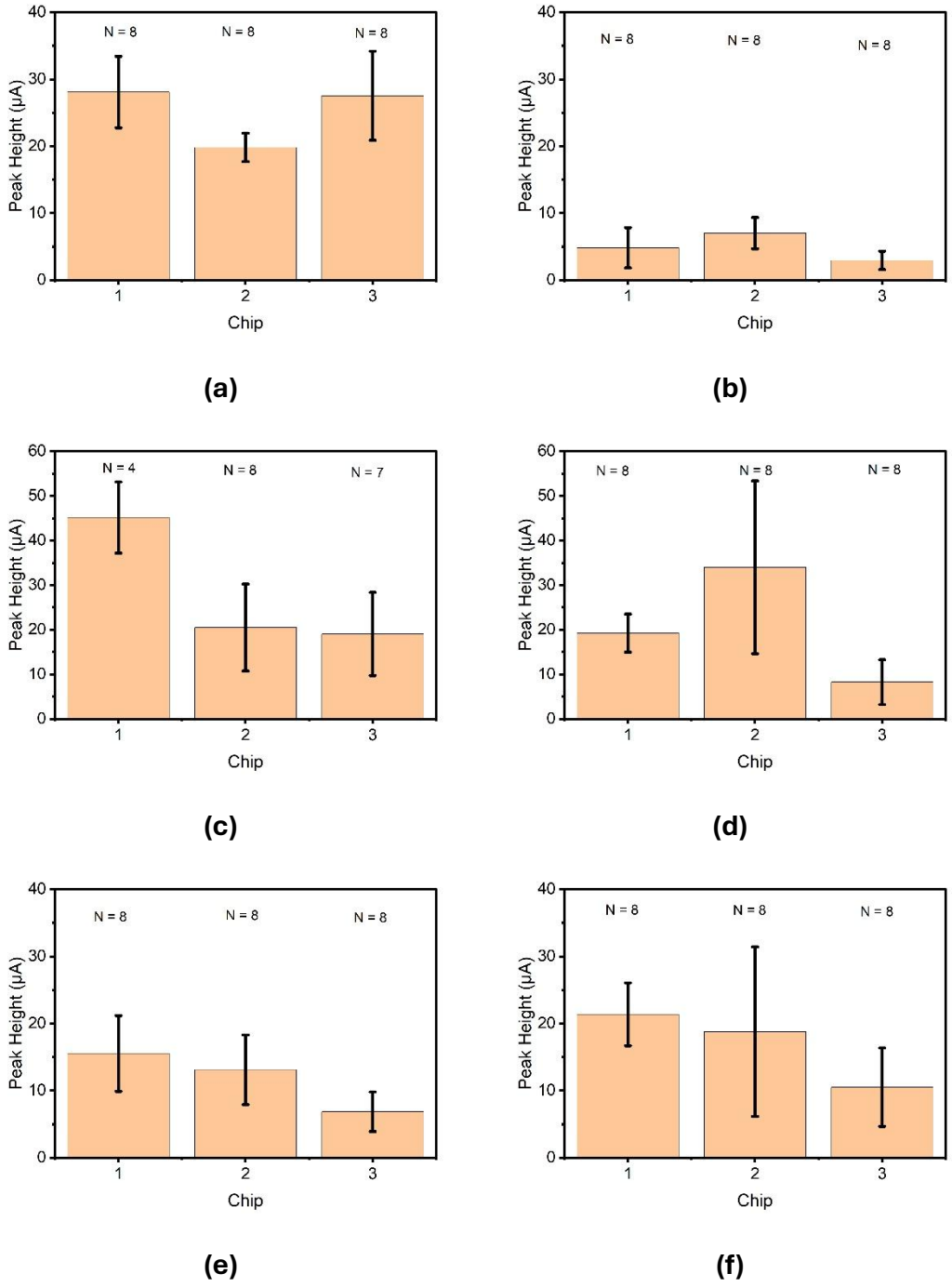

Figure 5.10: SWV characterisation of manufactured chips. After manufacturing, chips were characerised via SWV in 1 mM Ruhex solution and peak heights found. Each subfigure displays data gathered from three separate chips as averages ± one standard deviation (The number of working/measured channels are shown above each chips data). Characterisation was performed for manual FDM chips **(a)**, manual SLA chips **(b)**, pressed FDM chips **(c)**, pressed SLA chip **(d)**, UV treated manual FDM chips **(e)**, UV treated manual SLA chip **(f)**.

Unfortunately, both in CV and SWV results UV pretreatment performed poorly, although SLA chips were able to generate larger peak currents after treatment, large standard deviations remained when compared to non-UV-treated counterparts. SWV results also showed the ability of press filling chips to increase peak current of measurements, especially in SLA based chips. One explanation for this is the possible compression of paste material, which not only increased the number of conductive tracks in the bulk material, but also the density of functional groups on the surface. However again here, during measurement some FDM pressed electrodes failed. Interestingly, results also showed that when bases are manually filled, higher peak currents are produced from FDM moulds. This may show an increase in electrode surface area from the rough and difficult to clean FDM chips. Whereas on SLA chips paste is limited to the channels.

During measurements issues were seen in FDM chips filled with paste via pressing. Many of the channels in these chips produced flat plots indicating that working and counter electrodes were being short-circuited. On visual inspection of chips, no short circuits were apparent on the surface of chips however the process of forcing paste into channels may have separated FDM layers and allowed this to take place deeper in the chip.

The coefficients of variation of measured peak heights were also calculated (see Table 5.4) to gauge which method of manufacturing was able of producing reproducible chips. Interestingly the manufacturing approach that produced the lowest variation was Manual FDM manufacturing, potentially due to the operators experience with this approach which was performed throughout the thesis. It should be noted however that high variation of over 10% was seen in all methods and so none can produce chips with repeatable performance.

Table 5.4: Coefficients of variation calculated from SWV characterisation of differently manufactured chips (shown in Figure 5.10)

Manufacturing Approach	**Coefficient of Variation**		
	Chip 1	Chip 2	Chip 3
Manual FDM	0.19	0.11	0.24
Manual SLA	0.62	0.33	0.47
Pressed FDM	0.18	0.48	0.49
Pressed SLA	0.22	0.57	0.61
UV treated manual SLA	0.22	0.67	0.56
UV treated manual FDM	0.36	0.40	0.43

While results showed that pressing was potentially able to improve peak currents of responses, overall chip variability was poor regardless of manufacturing approach. This indicates that variation may stem from the paste material rather than manufacturing processes and so manufacturing should be selected for other reasons (e.g. cost, practicality, scalability.)

Given the primary objective of cost, this is unsurprising, the lubricant grade of graphite powder has a large range of particle sizes. These large, variable particles in the powder may lead to a resulting chip surface that is both rough and inconsistent.

5.4.3 Paste Modification

Chips were also produced from an additional paste mixture based on carbon black, a material with much smaller particle size compared to graphite that has been shown in literature to be capable of producing improved signal to noise ratios in electrochemical measurements when compared to graphite[219].

Initially, it was intended that this paste would be produced in the same 1:1 ratio as graphite paste. However, during initial mixing, it was discovered that this weight ratio produced a dusty mixture unsuitable for use. A 1:2 ratio of carbon black: paraffin wax was required and used to fill chip tracks.

Visually, Figure 5.11 shows that completed chips look alike those produced from graphite paste via pressing (Figure 5.8) where paste material fills small channels produced during the FDM printing process. Here again, material fills tracks without causing short circuit (as measured via a multimeter), although it is caused by the smaller particle size of the carbon black enabling track filling rather than any bulk paste being forced into tracks.

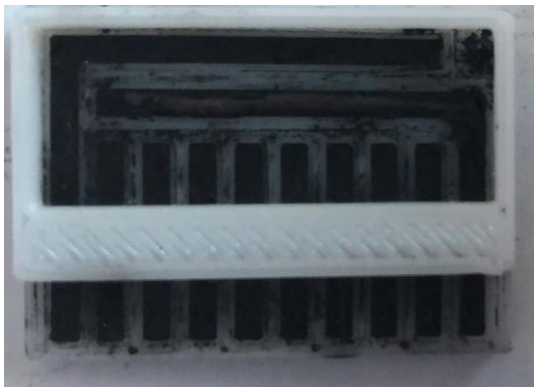

Figure 5.11: Chips produced from filling of channels printed out of PETG with a 2:1 carbon black: paraffin wax paste mixture.

When carbon black chips are interrogated via CV cycling in FF in 1 x PBS (Figure 5.12a) and Ruhex in 1 x PBS (Figure 5.12b) they produce poor results: FF responses fail to show any expected oxidation or reduction peaks and although

Ruhex plots show peaks, they are both inconsistent between channels on the chip and indicate poor reversibility (shown by uneven peak current). SWV results in Ruhex shown in Figure 5.13 are also poor, showing both poor reproducibility in chips and also the lowest magnitude of response when compared to those produced from the graphite mix (Figure 5.10). These poor results in both redox mediators suggest that the carbon black paste not only has variable surface characteristics (through poor surface sensitive FF measurements), but also variable electronic structure (through Ruhex which is affected by the electronic structure rather than surface characteristics[233]) as well as the lower conductivity in carbon black comparatively to graphite[234]. Lower particle sizes have also been shown to reduce peak currents in literature, done with sizes of glassy carbon spherical microparticles[235]. Variability in carbon black results may indicate that non-conductive binder element matters more than hypothesised, both in carbon black results as well as those seen from graphite mixes. The potential of binder-free electrodes (shown to be possible via thermally oxidising carbon black[236]) should therefore be explored.

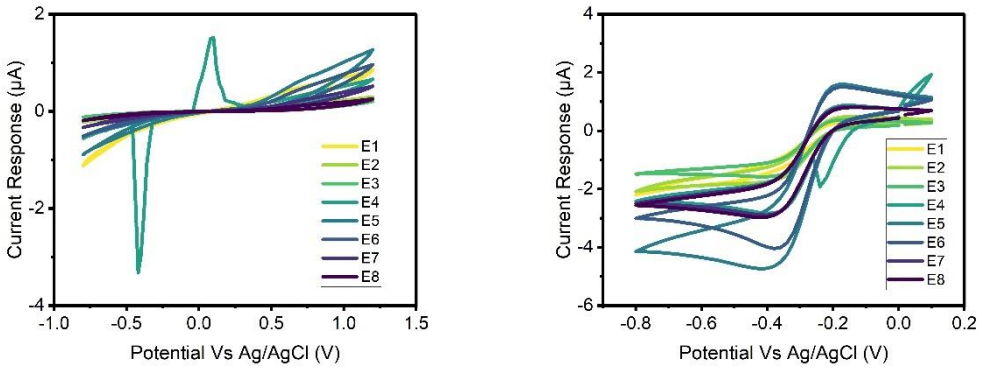

Figure 5.12: CV characterisation of a chip produced using the carbon black/paraffin mixture, all 8 channels of a single chip are shown (n = 8). Performed in 2 mM FF in 1 x PBS **(a)** and 1 mM Ruhex in 1 x PBS **(b)**.

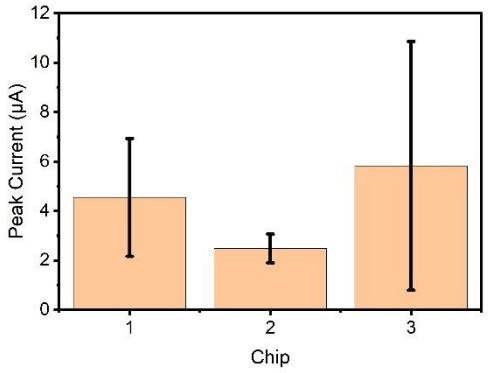

Figure 5.13: SWV peak currents of chips manufactured using carbon black/paraffin mixture. Plotted for three separate chips as means of all chips +/- one standard deviation (n = 8).

5.5 Conclusions

Throughout this thesis issues arose from the inter and intra variability of carbon paste chip. In literature, these issues are often addressed via pretreatment, however given the homemade nature of the paste chips, manufacturing techniques and the paste components themselves may also have been a major source of variability. Improvements were seen in chips when pretreated with sodium hydroxide and multi-step amperometry. This pretreatment was able to both increase peak currents and reduce ΔEp in ferri-ferrocyanide CVs. Despite this promising start, when ELISA products were measured this pretreatment appeared to wear off over time.

Use of different manufacturing techniques was also unable to produce appreciable improvements in chip performance. Although pressing paste into moulds could improve paste performance, due to the compression of the paste material however this did not lead to improvements in variability.

Finally, an attempt was made to improve the performance of the chips via replacement of their graphite component with carbon black, a carbon material

with smaller particle sizes. Again, this was unsuccessful and resulting CVs were poor.

Future work should focus on the stabilisation of this pretreatment for employment on single use sensors, through improved storage of pretreated chips and the investigation of hydrogen terminated surfaces.

6 Conclusions and Future work

6.1 Conclusions

The goal of this thesis was to detect key cancer biomarkers in blood using electrochemical immunoassay on carbon paste electrodes. It contains two major themes:

1. The development of carbon paste electrodes.
2. The detection of cancer related biomarkers via sandwich immunoassays.

Chapters two, three and five were primarily focused on the development and characterisation of a carbon paste electrode to function as a base for measurements. Work in chapter two focused on the manufacturing and pretreatment of simple, planar graphite paste electrodes. These electrodes were manually made and were based on a 50:50 mix of graphite powder and paraffin wax. A range of physical and chemical pretreatment methods were performed on electrodes however none were able to significantly improve the performance of electrodes in comparison to those that were not treated. This lack of improvement in electrodes stemmed from large initial errors in chips which itself stemmed from inconsistencies in their manufacturing.

Chapter three aimed to address this inconsistency through the use of the paste in a multiplexed chip format which included a more uniform shape with integrated reference and counter electrodes. While these chips were both more consistent and convenient to use, when used in the detection of key biomarkers such as dopamine and Interleukin-6 large errors in results made the quantitative measurement of biomarkers challenging above an initially good LoD.

After attempts to detect prostate specific antigen in chapter four (which again suffered from poor resolution), chapter five attempted to improve paste performance and consistency through further investigation of chemical and UV pretreatments and changes in manufacturing methods. Although initially

electrochemical pretreatment using sodium hydroxide seemed promising, being able to improve chip performance in the measurement of inner sphere redox mediators, when used in the measurement of immunoassays this pretreatment appeared to wear off over time. Investigation of manufacturing techniques and UV pretreatments also yielded poor results, through the analysis of coefficients of variation, it was seen that the most consistent electrode chips were those produced throughout the rest of the thesis, potentially due to the practice users had making them. It should be noted however that consistency was still poor and at the end of this thesis, carbon paste chips may be more suited to qualitative rather than quantitative measurement.

Cancer related biomarkers were detected primarily in chapters three and four, although throughout the thesis they were used to assess the utility of paste electrodes for 'real world' measurement. In chapter three the target of these assays was interleukin-6, an inflammatory biomarker that is raised in cancer patients. This measurement was performed using a sandwich ELISA assay kit tipped with a HRP enzyme tag which performed well when measured colourimetrically, however when measured electrochemically results were more suited for qualitative detection rather than quantitative.

Chapter four targeted a biomarker which is more closely linked to cancer diagnoses, prostate specific antigen. It was again detected using a sandwich ELISA kit and again produced suitable results when measured colourimetrically, and poorer results when measured electrochemically. Attempts were therefore made to improve its electrochemical performance via the immobilisation of the sandwich onto the surface of electrodes and although this binding was possible (most effectively using a protein intermediate), this binding reduced assay performance.

Overall, this thesis focused on the combination of carbon paste electrodes and standard sandwich ELISA techniques to detect key cancer biomarkers. Overall key findings were:

- Carbon paste electrodes can be produced simply in the lab at a low cost.
- These electrodes are suitable for the measurement of analytes both directly and indirectly, although large standard deviations in results indicate that this measurement is at best semi-quantitative.
- Binding of ELISA components to the surfaces of these electrodes leads to a reduction in their performance.

6.2 Limitations and future work

The work presented has limitations which leave the potential for future work. One of the principal limitations is the limited characterisation of the carbon paste material. Although characterisation was performed through electrochemical analysis, SEM and FTIR, further characterisation would provide greater insight into the materials performance. This work could be performed through a range of methods including:

- The measurement of surface roughness and topography using atomic force microscopy.
- The measurement of surface conductivity using conductive atomic force microscopy.
- The visualisation of surface conductivity through scanning electron microscopy after the deposition of metallic nanoparticles.
- The visualisation of antibody binding using fluorescent antibodies.

Limitations can also be seen in the lack of investigation of paste constituents. Although basic work was performed on the substitution of graphite in the paste with carbon black, work could easily be progressed using other carbon materials (e.g. Carbon nanotubes or graphene). Work could also be expanded through investigation of the binder materials, potentially through the use of conductive polymers such as Poly(3,4-ethylenedioxythiophene) (PEDOT).

There is also a lack of investigation into the automated manufacturing of electrodes which may have helped address issues arising from their homemade nature. Although requiring changes in the paste formation this could be achieved simply using screen printing or 3D printing.

There were also limitations in the immunoassays used. The targets used in immunoassay measurements were general and do not provide a large amount of prognostic value alone. This could be remedied through the quantification of key biomarkers in specified cancers to produce a biomarker panel. This panel could

potentially be produced through a literature review, or through the quantification of biomarkers in clinical samples through methods such as Liquid Chromatography-Tandem Mass Spectrometry (LCMS).

The tags used during immunoassays was also not explored and the HRP tag used is primarily used in colourimetric measurement. Further exploration of electrochemically active tags (such as metal nanoparticles or redox tags) could improve results.

In summary, future work that would build on this thesis and help address limitations found therein could include:

- More detailed characterisation of carbon paste materials.
- Further development of paste constituents.
- Use of automated manufacturing methods with carbon pastes.
- Development of a multiplex assay to enable specific cancer identification.
- Investigation of electrochemically relevant assay tags.

7 References

1 C. A. . Almeida and S. A. . Barry, in *Cancer : basic science and clinical aspects*, Blackwell Publishing, Chichester, 1st edn., 2010.

2 S. I. Hajdu, *Cancer*, 2011, **117**, 1097–1102.

3 R. Harker, *Cancer: Summary of Statistics (England)*, London, 2024.

4 T. Dyba, G. Randi, F. Bray, C. Martos, F. Giusti, N. Nicholson, A. Gavin, M. Flego, L. Neamtiu, N. Dimitrova, R. Negrão Carvalho, J. Ferlay and M. Bettio, *Eur. J. Cancer*, 2021, **157**, 308–347.

5 F. Bray, M. Laversanne, H. Sung, J. Ferlay, R. L. Siegel, I. Soerjomataram and A. Jemal, *CA Cancer J. Clin.*, 2024, **74**, 229–263.

6 R. A. Weinberg, *Sci. Am.*, 1996, **275**, 62–70.

7 S. Hodgson, *J. Zhejiang Univ. Sci. B*, 2008, **9**, 1–4.

8 K. F. Brown, H. Rumgay, C. Dunlop, M. Ryan, F. Quartly, A. Cox, A. Deas, L. Elliss-Brookes, A. Gavin, L. Hounsome, D. Huws, N. Ormiston-Smith, J. Shelton, C. White and D. M. Parkin, *Br. J. Cancer*, 2018, **118**, 1130–1141.

9 A. Jones, *J. Med. Surg. Pathol.*, 2023, **8**, 1000267.

10 N. M. Anderson and M. C. Simon, *Current Biology*, 2020, **30**, R921–R925.

11 E. Gonzalez-Gugel, M. Saxena and N. Bhardwaj, *Cancer Immunology, Immunotherapy*, 2016, **65**, 1261–1268.

12 S. Terry, S. Buart and S. Chouaib, *Front. Immunol.*, 2017, **8**, 1625.

13 W. Luo and Y. Wang, in *Hypoxia and Cancer Metastasis*, Springer, Cham, 1st edn., 2019, vol. 1136, pp. 1–18.

14 W. Hamilton, *Nat. Rev. Clin. Oncol.*, 2012, **9**, 251–252.

15 I. N. Olver, in *The MASCC Textbook of Cancer Supportive Care and Survivorship*, Springer, New York, 2010, pp. 3–7.

16 R. Nair, R. Nair and S. T. Sonis, in *Orofacial Supportive Care in Cancer: A Contemporary Oral Oncology Perspective*, Springer, New York, 2022.

17 NHS England, Breast screening pathway requirements, https://www.gov.uk/government/publications/breast-screening-programme-, (accessed 16 February 2026).

18 P. R. Eby, S. Ghate and R. Hooley, *J. Breast Imaging*, 2022, **4**, 346–356.

19 NHS England, Bowel cancer screening: programme overview, https://www.gov.uk/government/collections/nhs-population-screening-access-for-all, (accessed 16 February 2026).

20 J. S. John and P. Grogan, *Asia. Pac. J. Clin. Oncol.*, 2016, **12**, 7–9.

21 NHS England, Cervical Screening: programme overview, https://www.gov.uk/guidance/cervical-screening-programme-overview, (accessed 16 February 2026).

22 S. L. Bedell, L. S. Goldstein, A. R. Goldstein and A. T. Goldstein, *Sex. Med. Rev.*, 2020, **8**, 28–37.

23 R. B. Perkins, N. Wentzensen, R. S. Guido and M. Schiffman, *JAMA*, 2023, **330**, 547–558.

24 Department of Health and Social Care, New lung cancer screening roll out to detect cancer sooner, https://www.gov.uk/government/news/new-lung-cancer-screening-roll-out-to-detect-cancer-sooner, (accessed 16 February 2026).

25 UK National Screening Committee, Adult screening programme: Prostate cancer, https://view-health-screening-recommendations.service.gov.uk/prostate-cancer/, (accessed 16 February 2026).

26 I. Damjanov, *Cancer Grading Manual*, Springer, New York, 1st edn., 2006, vol. 1.

27 A. Andreou, D. A. Barocas, A. B. Benson, K. Bilimoria, E. Blackstone, G. J. Chang, S. S. Chang, B. D. Cheson, P. Goldstraw, J. M. Jessup, J. M. McKiernan, R. Pollock, Th. W. Rice, V. W. Rusch, J. P. Shah, M. T. Tetzlaff and J. N. Vauthey, *Cancer Staging Atlas*, Springer, London, 2nd edn., 2012, vol. 1.

28 I. D. L. Cavalcanti and J. C. S. Soares, *Advances in cancer treatment*, Springer, Cham, 1st edn., 2021, vol. 1.

29 M. Castiglia, L. Incorvaia, V. Gristina, U. Malapelle, V. Bazan, C. Rolfo and A. Russo, in *Practical Medical Oncology Textbook*, Springer, Heidelberg, 1st edn., 2021, vol. 1, pp. 99–122.

30 P. Mondelo-Macía, J. García-González, L. León-Mateos, A. Castillo-García, R. López-López, L. Muinelo-Romay and R. Díaz-Peña, *Biomedicines*, 2021, **9**, 1–22.

31 S. Das, M. K. Dey, R. Devireddy and M. R. Gartia, *Sensors*, 2024, **24**, 37.

32 E. Geeurickx and A. Hendrix, *Mol. Aspects Med.*, 2020, **72**, 100828.

33 W. Arancio, B. Belmonte, M. Castiglia, A. Di Napoli and C. Tripodo, in *Liquid Biopsy in Cancer Patients, Current Clinical Pathology*, Springer, London, 1st edn., 2017, vol. 1, pp. 41–49.

34 D. Wild, in *The Immunoassay Handbook: Theory and Applications of Ligand Binding, ELISA and Related Techniques*, Elsevier, Amsterdam, 2013, pp. 7–10.

35 C. P. Price and D. J. Newman, in *Principles and Practice of Immunoassay*, Macmillan Publishers, London, 1st edn., 1991, vol. 1, pp. 246–264.

36 L. Stryer, in *Biochemistry*, W.H.Freeman & Co, New York, 2nd edn., 1981, vol. 1, pp. 789–813.

37 T. Y. Sam-Yellowe, in *Immunology: Overview and Laboratory Manual*, Springer International Publishing, Cham, 2021, pp. 65–72.

38 R. Burns, in *The Protein Protocols Handbook*, ed. J. M. Walker, Humana Press, Totowa, 3rd edn., 2009, pp. 1679–1686.

39 B. J. Mills, E. M. Moussa and F. Jameel, in *AAPS Advances in the Pharmaceutical Sciences Series*, Springer, New York, 2020, vol. 35, pp. 3–26.

40 W. Wang, S. Singh, D. L. Zeng, K. King and S. Nema, *J. Pharm. Sci.*, 2007, **96**, 1–26.

41 B. J. Sutton, A. M. Davies, H. J. Bax and S. N. Karagiannis, *Antibodies*, 2019, **8**, 19.

42 J. Hunt, A. H. Keeble, R. E. Dale, M. K. Corbett, R. L. Beavil, J. Levitt, M. J. Swann, K. Suhling, S. Ameer-Beg, B. J. Sutton and A. J. Beavil, *Journal of Biological Chemistry*, 2012, **287**, 17459–17470.

43 B. J. Sutton and H. J. Gould, *Nature*, 1993, **366**, 421–428.

44 S. C. Parija, *Textbook of Microbiology and Immunology*, Springer, Singapore, 4th edn., 2023.

45 K. Chen and A. Cerutti, *Curr. Opin. Immunol.*, 2011, **23**, 345–352.

46 E. S. Edholm, E. Bengten and M. Wilson, *Dev. Comp. Immunol.*, 2011, **35**, 1309–1316.

47 P. de Sousa-Pereira and J. M. Woof, *Antibodies*, 2019, **8**, 57.

48 I. S. Hansen, D. L. P. Baeten and J. den Dunnen, *Cellular and Molecular Life Sciences*, 2019, **76**, 1041–1055.

49 B. Alberts, A. Johnson, J. Lewis, D. Morgan, M. Raff, K. Roberts and P. Walter, in *Molecular Biology of the Cell*, Taylor & Francis Group, New York, 6th edn., 2014, vol. 1, pp. 1297–1342.

50 T. Y. Sam-Yellowe, in *Immunology: Overview and Laboratory Manual*, Springer, Cham, 2021, pp. 349–360.

51 M. S. Tabatabaei and M. Ahmed, in *Methods in Molecular Biology*, Humana Press, Totowa, 2022, vol. 1, pp. 115–134.

52 J. Moore and R. Langley, in *Biochemistry For Dummies*, John Wiley & Sons, Hoboken, 2nd edn., 2008, vol. 1, pp. 85–107.

53 G. H. Bell, J. N. Davidson and H. Scarborough, in *Textbook of Physiology and Biochemistry*, E. & S. Livingstone, Edinburgh, 4th edn., 1963, vol. 1, pp. 70–79.

54 S. Kostadinova and M. Marhova, *Biotechnology and Biotechnological Equipment*, 2010, **24**, 602–606.

55 K. Sun, N. Ramgir and S. Bhansali, *Sens. Actuators B Chem.*, 2008, **133**, 533.

56 K. Gjesing Welinder, *FEBS Lett.*, 1976, **72**, 19–23.

57 S. Gu, S. Risse, Y. Lu and M. Ballauff, *ChemPhysChem*, 2020, **21**, 450–458.

58 S. Pluschkell, K. Hellmuth and U. Rinas, *Biotechnol. Bioeng.*, 1996, **51**, 215–220.

59 A. Deisseroth and A. L. Dounce, *Physiol. Rev.*, 1970, **50**, 319–375.

60 M. M. Goyal and A. Basak, *Protein Cell*, 2010, **1**, 888–897.

61 P. A. Prakash, U. Yogeswaran and S. M. Chen, *Sensors*, 2009, **9**, 1821–1844.

62 N. M. Bakhori, N. A. Yusof, J. Abdullah, H. Wasoh, S. K. A. Rahman and S. F. A. Rahman, *Materials*, 2020, **13**, 149.

63 P. H. Rieger, in *Electrochemistry* , Chapman & Hall, New York, 2nd edn., 1987.

64 C. H. Hamann, A. Hamnett and W. Vielstich, in *Electrochemistry*, Wiley-VCH, Weinheim, 2nd edn., 2007, vol. 2, pp. 115–133.

65 D. Pletcher, in *A first course in electrode processes*, Royal Society of Chemistry, Cambridge, 2nd edn., 2009, vol. 1, pp. 17–28.

66 P. T. Kissinger and W. R. Heineman, *J. Chem. Educ.*, 1983, **60**, 702–706.

67 N. Elgrishi, K. J. Rountree, B. D. McCarthy, E. S. Rountree, T. T. Eisenhart and J. L. Dempsey, *J. Chem. Educ.*, 2018, **95**, 197–206.

68 E. P. Randviir, *Electrochim. Acta*, 2018, **286**, 179–186.

69 J. Wang, in *Analytical Electrochemistry*, Wiley, Weinheim, 3rd edn., 2006, pp. 34–35.

70 G. C. Barker and I. L. Jenkins, *Analyst*, 1952, **77**, 685–696.

71 V. Mirceski, S. Skrzypek and L. Stojanov, *ChemTexts*, 2018, **4**, 17.

72 G. Inzelt, in *Encyclopedia of Applied Electrochemistry*, Springer, New York, 2014, pp. 207–213.

73 P. Chandrasekhar, in *Conducting Polymers, Fundamentals and Applications*, Springer International Publishing, Cham, 2nd edn., 2018, pp. 283–309.

74 H. A. Abdulbari and E. A. M. Basheer, *ChemBioEng Reviews*, 2017, **4**, 92–105.

75 S. Zhang, G. Wright and Y. Yang, *Biosens. Bioelectron.*, 2000, **15**, 273–282.

76 P. S. Shlepakov, I. V. Uvarov, V. V. Naumov and V. B. Svetovoy, *J. Phys. Conf. Ser.*, 2020, **1695**, 012155.

77 R. Antiochia, I. Lavagnini, F. Magno, F. Valentini and G. Palleschi, *Electroanalysis*, 2004, **16**, 1451–1458.

78 A. Morrin, A. J. Killard and M. R. Smyth, *Anal. Lett.*, 2003, **36**, 2021–2039.

79 V. Naresh and N. Lee, *Sensors*, 2021, **21**, 1109.

80 C. D. Bain, E. B. Troughton, Y. T. Tao, J. Evall, G. M. Whitesides and R. G. Nuzzo, *J. Am. Chem. Soc.*, 1989, **111**, 321–335.

81 Z. Taleat, A. Khoshroo and M. Mazloum-Ardakani, *Microchimica Acta*, 2014, **181**, 865–891.

82 R. N. Adams, *Scientific communications*, 1958, **30**, 1576.

83 S. A. Wring and J. P. Hart, *ANALYST*, 1992, **117**, 1215.

84 D. Bellido-Milla, L. M. Cubillana-Aguilera, M. El Kaoutit, M. P. Hernández-Artiga, J. L. Hidalgo-Hidalgo De Cisneros, I. Naranjo-Rodríguez and J. M. Palacios-Santander, *Anal. Bioanal. Chem.*, 2013, **405**, 3525–3539.

85 L. Zhao, G. Rosati, A. Piper, C. de Carvalho Castro e Silva, L. Hu, Q. Yang, F. Della Pelle, R. R. Alvarez-Diduk and A. Merkoçi, *ACS Appl. Mater. Interfaces*, 2023, **7**, 9024–9033.

86 T. Shamspur, Z. Biniaz, A. Mostafavi, M. Torkzadeh-Mahani and M. Mohamadi, *IEEE Sens. J.*, 2018, **18**, 4861–4868.

87 Z. Xue, K. Patel, P. Bhatia, C. L. Miller, R. S. Shergill and B. A. Patel, *Anal. Chem.*, 2024, **96**, 12701–12709.

88 A. Rahman, R. K. Pal, N. Islam, R. Freeman, F. Berthiaume, A. Mazzeo and A. Ashraf, *Sensors*, 2023, **23**, 8115.

89 S. R. Nxele and T. Nyokong, *J. Inorg. Biochem.*, 2021, **221**, 111462.

90 A. Wang, Y. Ding, L. Li, D. Duan, Q. Mei, Q. Zhuang, S. Cui and X. He, *Talanta*, 2019, **192**, 478–485.

91 D. Thorat, S. Tripathy and N. G. Shimpi, in *Graphene-Based Photocatalysts*, Springer, Cham, 2024, vol. 217, pp. 3–23.

92 S. Hasoň, A. Daňhel, K. Schwarzová-Pecková and M. Fojta, in *Nanotechnology and Biosensors*, Elsevier, Amsterdam, 1st edn., 2018, vol. 1, pp. 51–111.

93 V. Uskoković, *Carbon Trends*, 2021, **5**, 100116.

94 A. Klinkova and H. Therien-Aubin, in *Nanochemistry*, Elsevier, Amsterdam, 2024, vol. 7, pp. 111–141.

95 M. D. Obradović, G. D. Vuković, S. I. Stevanović, V. V. Panić, P. S. Uskoković, A. Kowal and S. L. Gojković, *Journal of Electroanalytical Chemistry*, 2009, **634**, 22–30.

96 S. J. Cobb, Z. J. Ayres and J. V Macpherson, *Annual Review of Analytical Chemistry*, 2026, **11**, 463–484.

97 R. Arrigo, M. Hävecker, R. Schlögl and D. S. Su, *Chemical Communications*, 2008, **1**, 4891–4893.

98 D. A. Armbruster and T. Pry, *Clin. Biochem. Rev.*, 2008, **29**, 49–52.

99 C. Davies, in *The Immunoassay Handbook: Theory and Applications of Ligand Binding, ELISA and Related Techniques*, Elsevier, Amsterdam, 4th edn., 2013, pp. 11–26.

100 S. K. Vashist and J. H. T. Luong, in *Handbook of Immunoassay Technologies: Approaches, Performances, and Applications*, Elsevier, Amsterdam, 2018, pp. 81–95.

101 P. Kartikay, A. Yella and S. Mallick, *Mater. Chem. Phys.*, 2020, **256**, 123594.

102 H. Wheetal, L. Bowers, J. Kulys, H. Hansen, A. Amine, J. M. Kauffmann, A. Zaks and A. M. Klibanov, *Anal. Chem.*, 1997, **69**, 3124–3127.

103 S. J. Malode, P. Sharma, M. R. Hasan, N. P. Shetti and R. J. Mascarenhas, in *Electrochemical Sensors: From Working Electrodes to Functionalization and Miniaturized Devices*, Elsevier, Amsterdam, 2022, pp. 79–114.

104 I. Švancara, K. Vytřas, K. Kalcher, A. Walcarius and J. Wang, *Electroanalysis*, 2009, **21**, 7–28.

105 A. Walcarius, P. Mariaulle and L. Lamberts, *Journal of Solid State Electrochemistry*, 2003, **7**, 671–677.

106 R. Domingo-Roca, A. R. Macdonald, S. Hannah and D. K. Corrigan, *Analyst*, 2022, **147**, 4598.

107 J. B. He, F. Qi, Y. Wang and N. Deng, *Sens. Actuators B Chem.*, 2010, **145**, 480–487.

108 S. Moanea, M. R. Smyth and M. O'keeffeb, *Analyst*, 1996, **121**, 779–784.

109 R. Maalouf, A. Soldatkin, O. Vittori, M. Sigaud, Y. Saikali, H. Chebib, A. S. Loir, F. Garrelie, C. Donnet and N. Jaffrezic-Renault, *Materials Science and Engineering C*, 2006, **26**, 564–567.

110 M. I. González-Sánchez, B. Gómez-Monedero, J. Agrisuelas, J. Iniesta and E. Valero, *Electrochem. commun.*, 2018, **91**, 36–40.

111 S. Hannah, M. Al-Hatmi, L. Gray and D. K. Corrigan, *Bioelectrochemistry*, 2020, **133**, 107480.

112 M. C. C. G. Carneiro, F. T. C. Moreira, R. A. F. Dutra, R. Fernandes and M. G. F. Sales, *Microchemical Journal*, 2018, **138**, 35–44.

113 R. J. Forster, *Chem. Soc. Rev.*, 1994, **23**, 289–297.

114 X. Cai, B. Ogorevc and K. Kalcher, *Electroanalysis*, 1995, **7**, 1126–1131.

115 H. Dellweg, J. W. Engels, J. L. Fox, L. M. Gierasch, R. P. Gregson, B. Heinritz, H. G. W. Leuenberger, M. Moo-Young, A. Moser, B. Nagel, L. Nyeste, L. Pénasse, G. B. Petersen, M. Van Montagu and Y. Yamada, *Pure & Applied Chemistry*, 1992, **64**, 143–168.

116 F. Ricci, G. Adornetto and G. Palleschi, *Electrochim. Acta*, 2012, **84**, 74–83.

117 H. Abu-Ali, O. Cansu, F. Davis, N. Walch and A. Nabok, *Chemosensors*, 2020, **8**, 28.

118 Z. Lin, G. Wu, L. Zhao and K. W. C. Lai, *IEEE Nanotechnol. Mag.*, 2019, **13**, 4–14.

119 O. Fernando and E. Magner, *Sensors*, 2020, **20**, 3561.

120 K. Jacobs, S. F. Wolf, L. Haines, J. Fisch, J. N. Kremsky, J. P. Dougherty, R. H. Symons, N. Habili, J. L. Mclnnes, G. Gentilomi, E. Ferri, S. Girotti, Y. W. Kan, F. F. Chehab, J. S. Sevall, H. Prince, G. ; Garratty, W. A. O'brien, J. A. Zack, K. M. Millan, S. R. Mikkelsen, K. Hashimoto, K. Miwa, Y. Ishimori, K. Ito, A. J. Bard and . T Cater, *Anal. Chem.*, 1994, **66**, 3830–3833.

121 L. Fritea, M. Tertis, R. Sandulescu and C. Cristea, *Methods Enzymol.*, 2018, **609**, 293–333.

122 Z. Taleat, A. Khoshroo and M. Mazloum-Ardakani, *Microchimica Acta*, 2014, **181**, 865–891.

123 S. Lee, W. J. Kim and M. Chung, *Analyst*, 2021, **146**, 5236–5244.

124 S. Tajik, H. Beitollahi, F. G. Nejad, M. Safaei, K. Zhang, Q. Van Le, R. S. Varma, H. W. Jang and M. Shokouhimehr, *RSC Adv.*, 2020, **10**, 21561–21581.

125 S. Suresh, A. K. Gupta, V. K. Rao, Om kumar and R. Vijayaraghavan, *Talanta*, 2010, **81**, 703.

126 V. Rajendran, E. Csöregi, Y. Okamoto and L. Gorton, *Anal. Chim. Acta*, 1998, **373**, 241–251.

127 K. Sugawara, T. Takano, H. Fukushi, S. Hoshi, K. Akatsuka, H. Kuramitz and S. Tanaka, *Journal of Electroanalytical Chemistry*, 2000, **482**, 81.

128 S. H. Zuo, L. F. Zhang, H. H. Yuan, M. B. Lan, G. A. Lawrance and G. Wei, *Bioelectrochemistry*, 2009, **74**, 223–226.

129 M. O. Klein, D. S. Battagello, A. R. Cardoso, D. N. Hauser, J. C. Bittencourt and R. G. Correa, *Cell. Mol. Neurobiol.*, 2019, **39**, 31–59.

130 S. J. Li, D. H. Deng, Q. Shi and S. R. Liu, *Microchimica Acta*, 2012, **177**, 325–331.

131 M. Hasanzadeh, N. Shadjou and M. de la Guardia, *Trends in Analytical Chemistry*, 2017, **86**, 107–121.

132 D. J. Wiedemann, K. T. Kawagoe, R. T. Kennedy, E. L. Ciolkowski and R. M. Wightman, *Anal. Chem.*, 1991, **63**, 2965.

133 A. R. Macdonald, F. Charlton and D. K. Corrigan, *Anal. Bioanal. Chem.*, 2023, **415**, 1137.

134 L. Yu, L. Feng, Z. Wei, S. Wang, Y. Feng, Y. Shen, J. Cai, J. Wu and Y. Xiao, *Adv. Funct. Mater.*, 2023, **33**, 2300309.

135 X. Ouyang, Y. Wu, L. Guo, L. Li, M. Zhou, X. Li, T. Liu, Y. Ding, H. Bu, G. Xie, J. Shen, C. Fan and L. Wang, *Angewandte Chemie*, 2023, **62**, e202300893.

136 M. A. Dayton, A. G. Ewing and R. Mark Wightman, *Anal. Chem.*, 1980, **52**, 2392–2396.

137 S. Hosseini, P. V.-V. Marco, R.-P. Sergio and O. Martinez-Chapa, *Enzyme - linked Immunosorbent Assay (ELISA)*, Springer, Singapore, 1st edn., 2018, vol. 1.

138 Z. Yin, Y. Liu, L. P. Jiang and J. J. Zhu, *Biosens. Bioelectron.*, 2011, **26**, 1890–1894.

139 R. R. Mustafa, R. Sukor, S. Eissa, A. N. Shahrom, N. Saari and S. M. Mohd Nor, *Sens. Actuators B Chem.*, 2021, **345**, 130356.

140 M. A. Khan and M. Mujahid, *Sensors*, 2020, **20**, 646.

141 S. Kibe, K. Adams and G. Barlow, *Journal of Antimicrobial Chemotherapy*, 2011, **66**, 33–40.

142 S. Kaur, Y. Bansal, R. Kumar and G. Bansal, *Bioorg. Med. Chem.*, 2020, **28**, 115327.

143 C. Deng, F. Qu, H. Sun and M. Yang, *Sensors and Actuators B*, 2011, **160**, 471–474.

144 G. Wang, X. He, L. Chen, Y. Zhu and X. Zhang, *Colloids Surf. B Biointerfaces*, 2014, **116**, 714–719.

145 R. Kapoor and C. W. Wang, *Biosens. Bioelectron.*, 2009, **24**, 2696–2701.

146 A. E. Ferreira Oliveira, A. C. Pereira, M. A. Campos de Resende and L. F. Ferreira, *Electroanalysis*, 2022, **34**, 809–819.

147 I. Lavagnini, R. Antiochia and F. Magno, *Electroanalysis*, 2004, **16**, 505–506.

148 R. Sánchez-Salcedo, R. Miranda-Castro, N. de-los-Santos-Álvarez, M. J. Lobo-Castañón and D. K. Corrigan, *Anal. Bioanal. Chem.*, 2023, **415**, 7035–7045.

149 R. G. Compton and C. E. Banks, *Understanding Voltammetry*, Imperial College Press, London, 2nd edn., 2011, vol. 1.

150 P. Fanjul-Bolado, D. Hernández-Santos, P. J. Lamas-Ardisana, A. Martín-Pernía and A. Costa-García, *Electrochim. Acta*, 2008, **53**, 3635–3642.

151 J. Wang, □ Ulk□, A. Kirg□ Oz, J.-W. Mo, J. Lu, A. N. Kawde and A. Muck, *Electrochem. commun.*, 2001, **3**, 203–208.

152 G. Cui, Jae Hyun Yoo, Joung Su Lee, J. Yoo, Jung Hee Uhm, Geun Sig Cha and H. Nam, *Analyst*, 2001, **126**, 1399–1403.

153 J. Moldenhauer, M. Meier and D. W. Paul, *J. Electrochem. Soc.*, 2016, **163**, H672–H678.

154 A. C. Lazanas and M. I. Prodromidis, *ACS Measurement Science Au*, 2023, **3**, 162–193.

155 Y. M. Issa, H. M. Abdel-Fattah, O. R. Shehab and N. B. Mohamed, *Electroanalysis*, 2017, **29**, 2541–2550.

156 C. Laghlimi, Y. Ziat, A. Moutcine, M. Hammi, Z. Zarhri, O. Ifguis and A. Chtaini, *Chemical Data Collections*, 2021, **31**, 100595.

157 E. Y. Frag, M. E. B. Mohamed and H. S. Salem, *Journal of the Iranian Chemical Society*, 2017, **14**, 2355–2365.

158 I. Švancara, M. Hvízdalová, K. Vytřas, K. Kalcher and R. Novotný, *Electroanalysis*, 1996, **8**, 61–65.

159 T. Mikysek, I. Švancara, K. Kalcher, M. Bartoš, K. Vytřas and J. Ludvík, *Anal. Chem.*, 2009, **81**, 6327–6333.

160 G. K. R, *Electrochemical Science and Technology*, 1986, **133**, 1375–1379.

161 B. J. Venton and Q. Cao, *Analyst*, 2020, **145**, 1158–1168.

162 S. Schindler and T. Bechtold, *Journal of Electroanalytical Chemistry*, 2019, **836**, 94–101.

163 S. Anantharaj and S. Noda, *J. Mater. Chem. A Mater.*, 2022, **10**, 9348–9353.

164 S. Pruneanu, A. R. Biris, F. Pogacean, C. Socaci, M. Coros, M. C. Rosu, F. Watanabe and A. S. Biris, *Electrochim. Acta*, 2015, **154**, 197–204.

165 M. Kundys-Siedlecka, E. Baczyńska and M. Jönsson-Niedziółka, *Anal. Chem.*, 2019, **91**, 10908–10913.

166 S. Rantataro, L. Ferrer Pascual and T. Laurila, *Sci. Rep.*, 2022, **12**, 20225.

167 Y. Chang and B. J. Venton, *Analytical Methods*, 2020, **12**, 2893–2902.

168 M. Ni, J. Chen, C. Wang, Y. Wang, L. Huang, W. Xiong, P. Zhao, Y. Xie and J. Fei, *Microchemical Journal*, 2022, **178**, 107410.

169 S. E. Elugoke, O. E. Fayemi, A. S. Adekunle, B. B. Mamba, T. T. I. Nkambule and E. E. Ebenso, *FlatChem*, 2022, **33**, 100372.

170 C.-M. José-Luis, *Emerging Sample Treatments In Proteomics*, Springer, Cham, 1st edn., 2019.

171 S. S. Ghoreishizadeh, G. Nanda, S. Carrara and G. De Micheli, *International Workshop on Advances in Sensors and Interface (IWASI)*, 2013, **1**, 36–39.

172 C. Russell, A. C. Ward, V. Vezza, P. Hoskisson, D. Alcorn, D. P. Steenson and D. K. Corrigan, *Biosens. Bioelectron.*, 2019, **126**, 806–814.

173 X. Zhou, P. Li, X. Wu, X. Lin, L. Zhao, H. Huang, J. Wu, H. Cai, M. Xu, H. Zhou and P. Sun, *Biosens. Bioelectron.*, 2022, **210**, 114257.

174 D. Huang, H. Ying, D. Jiang, F. Liu, Y. Tian, C. Du, L. Zhang and X. Pu, *Anal. Biochem.*, 2020, **588**, 113468.

175 V. L. Kumar and P. K. Majumder, *Int. Urol. Nephrol.*, 1995, **27**, 231–243.

176 S. Bracarda, O. De Cobelli, C. Greco, T. Prayer-Galetti, R. Valdagni, G. Gatta, F. De Braud and G. Bartsch, *Crit. Rev. Oncol. Hematol.*, 2005, **56**, 379–396.

177 NHS, NHS Prostate Cancer Diagnosis Page, https://www.nhs.uk/conditions/prostate-cancer/diagnosis/, (accessed 23 March 2025).

178 J. M. Chan, M. J. Stampfer and E. L. Giovannucci, *Cancer Biology*, 1998, **8**, 263–273.

179 T. J. Wang, H. G. Rittenhouse, R. L. Wolfert, C. M. Lynne and N. L. Brackett, *Clin. Chem.*, 1997, **44**, 895–896.

180 J. Malm and H. Lilja, *Scand. J. Clin. Lab. Invest.*, 1995, **55**, 15–22.

181 U.-H. Stenman, J. Leinonen, W.-M. Zhang and P. Finne, *Cancer Biology*, 1999, **9**, 83–93.

182 V. M. Sundaresan, S. Smani, P. Rajwa, J. Renzulli, P. C. Sprenkle, I. Y. Kim and M. S. Leapman, *Urologic Oncology: Seminars and Original Investigations*, 2025, **43**, 41–48.

183 J. Liang, C. Yao, X. Li, Z. Wu, C. Huang, Q. Fu, C. Lan, D. Cao and Y. Tang, *Biosens. Bioelectron.*, 2015, **69**, 128–134.

184 L. Li, W. Zhang, Y. Wei, L. Yu and D. Feng, *J. Anal. Methods Chem.*, 2022, **2022**, 6209731.

185 L. Zhao, D. Wang, G. Shi and L. Lin, *Luminescence*, 2017, **32**, 1547–1553.

186 Z. Cheng, N. Choi, R. Wang, S. Lee, K. C. Moon, S. Y. Yoon, L. Chen and J. Choo, *ACS Nano*, 2017, **11**, 4926–4933.

187 S. Chen, Z. Wang, X. Cui, L. Jiang, Y. Zhi, X. Ding, Z. Nie, P. Zhou and D. Cui, *Nanoscale Res. Lett.*, 2019, **14**, 71.

188 C. K. Tang, A. Vaze, M. Shen and J. F. Rusling, *ACS Sens.*, 2016, **1**, 1036–1043.

189 X. Liu, D. Wang, J. Chu, Y. Xu and W. Wang, *J. Pharm. Biomed. Anal.*, 2018, **158**, 361–369.

190 S. C. Barman, M. F. Hossain and J. Y. Park, *J. Electrochem. Soc.*, 2017, **164**, B234–B239.

191 N. Sattarahmady, A. Rahi and H. Heli, *Sci. Rep.*, 2017, **7**, 11238.

192 V. Kumar, S. Srivastava, S. Umrao, R. Kumar, G. Nath, G. Sumana, P. S. Saxena and A. Srivastava, *RSC Adv.*, 2014, **4**, 2267–2273.

193 M. Yan, D. Zang, S. Ge, L. Ge and J. Yu, *Biosens. Bioelectron.*, 2012, **38**, 355–361.

194 C. Pezaro, H. H. Woo and I. D. Davis, *Intern. Med. J.*, 2014, **44**, 433–440.

195 P. Rawla, *World J. Oncol.*, 2019, **10**, 63–89.

196 J. R. Prensner, M. A. Rubin, J. T. Wei and A. M. Chinnaiyan, *Sci. Transl. Med.*, 2012, **4**, 127.

197 S. S. Timilsina, P. Jolly, N. Durr, M. Yafia and D. E. Ingber, *Acc. Chem. Res.*, 2021, **54**, 3529–3539.

198 F. Shen, S. Arshi, E. Magner, J. Ulstrup and X. Xiao, *Synth. Met.*, 2022, **291**, 117205.

199 M. Sharafeldin, K. McCaffrey and J. F. Rusling, *Analyst*, 2019, **144**, 5108–5116.

200 O. Laczka, E. Baldrich, F. J. Del Campo and F. X. Muñoz, *Anal. Bioanal. Chem.*, 2008, **391**, 2825–2835.

201 O. Parkash, C. Y. Yean and R. H. Shueb, *Diagnostics*, 2014, **4**, 165–180.

202 B. Attoye, M. J. Baker, F. Thomson, C. Pou and D. K. Corrigan, *Biosensors (Basel).*, 2021, **11**, 42.

203 M. J. Roberts, R. S. Richards, R. A. Gardiner and L. A. Selth, *Biomark. Med.*, 2015, **9**, 77–80.

204 J. M. Guisan, *Immobilization of Enzymes and Cells*, Humana Press, Totowa, 3rd edn., 2013.

205 D. T. Cheung and M. E. Nimni, *Connect. Tissue Res.*, 1982, **10**, 187–199.

206 F. T. Huey, H. Gong, X. D. Dong, X. Zeng, A. L. K. Tan, X. Yang and N. T. Swee, *Anal. Chim. Acta*, 2005, **551**, 23–29.

207 M. Conrad, P. Fechner, G. Proll and G. Gauglitz, *Biosensors (Basel).*, 2023, **13**, 849.

208 N. M. Christopoulou, D. P. Kalogianni and T. K. Christopoulos, *Biosens. Bioelectron.*, 2022, **218**, 114737.

209 R. L. McCreery, *Chem. Rev.*, 2008, **108**, 2646–2687.

210 Z. Su, S. Hu, Y. Zhang, Z. Liang, Y. Peng, Q. Cao, X. Yu, Z. Zhu, P. He and Z. Li, *Analyst*, 2023, **149**, 188–195.

211 R. Domingo-Roca, P. Lasserre, L. Riordan, A. R. Macdonald, A. Dobrea, K. R. Duncan, S. Hannah, M. Murphy, P. A. Hoskisson and D. K. Corrigan, *Biosens. Bioelectron. X*, 2023, **13**, 100308.

212 A. Wong, T. A. Silva and O. Fatibello-Filho, *Electroanalysis*, 2017, **29**, 2491–2497.

213 E. Bahrami, R. Amini and S. Vardak, *J. Alloys Compd.*, 2021, **855**, 157292.

214 K. Miyazaki, A. Iizuka, K. Mikata, T. Fukutsuka and T. Abe, *Chemical Communications*, 2017, **53**, 10034–10037.

215 K. W. Hathcock, J. C. Brumfield, C. A. Goss, E. A. Irene, R. W. Murray and R. L. J Electrochem, *Anal. Chem.*, 1995, **67**, 2201–2206.

216 H. Kim, J. Hong, G. Yoon, H. Kim, K. Y. Park, M. S. Park, W. S. Yoon and K. Kang, *Energy Environ. Sci.*, 2015, **8**, 2963–2969.

217 A. Rana, N. Baig and T. A. Saleh, *Journal of Electroanalytical Chemistry*, 2019, **833**, 313–332.

218 S. I. R. Malha, A. A. Lahcen, F. Arduini, A. Ourari and A. Amine, *Electroanalysis*, 2016, **28**, 1044–1051.

219 X. Zhang, Y. Cui, Z. Lv, M. Li, S. Ma, Z. Cui and Q. Kong, *Int. J. Electrochem. Sci*, 2011, **6**, 6063–6073.

220 J. Liu and P. Wen, *Mater. Des.*, 2022, **215**, 110505.

221 V. G. Surange and P. V. Gharat, *International Research Journal of Engineering and Technology*, 2016, **3**, 1403–1406.

222 V. Katseli, A. Economou and C. Kokkinos, *Anal. Chem.*, 2021, **93**, 3331–3336.

223 S. M. Sibug-Torres, L. P. Go and E. P. Enriquez, *Chemosensors*, 2020, **8**, 130.

224 X. Zhang and F. Liou, in *Additive Manufacturing*, Elsevier, Amsterdam, 1st edn., 2021, vol. 1, pp. 1–31.

225 B. M. Brenda, S. Griveau, F. Bedioui, F. d' Orlye, J. A. F. da Silva and A. Varenne, *Electrochim. Acta*, 2022, **407**, 139888.

226 O. M. Doering, C. Vetter, A. Alhawwash, M. R. Horn and K. Yoshida, *Artif. Organs*, 2022, **46**, 2085–2096.

227 D. Miedzińska, R. Gieleta and A. Popławski, *Materials*, 2020, **13**, 5825.

228 J. R. Camargo, R. D. Crapnell, E. Bernalte, A. J. Cunliffe, J. Redfern, B. C. Janegitz and C. E. Banks, *Appl. Mater. Today*, 2024, **39**, 102285.

229 J. Zhou and D. O. Wipf, *Journal of Electroanalytical Chemistry*, 2001, **499**, 121–128.

230 U. Chadha, P. Bhardwaj, S. Padmanaban, D. Kabra, G. Pareek, S. Naik, M. Singh, M. Banavoth, P. Sonar, S. Singh, S. Latha, A. K. Ray, B. Badoni and N. S. Rao, *J. Electrochem. Soc.*, 2021, **168**, 120555.

231 A. Abdalla, F. Perez, A. T. Cañadas, S. Ray and B. A. Patel, *Journal of Electroanalytical Chemistry*, 2021, **881**, 114937.

232 A. A. Kava and C. S. Henry, *Talanta*, 2021, **221**, 121553.

233 A. G. M. Ferrari, C. W. Foster, P. J. Kelly, D. A. C. Brownson and C. E. Banks, *Biosensors (Basel).*, 2018, **8**, 53.

234 B. Marinho, M. Ghislandi, E. Tkalya, C. E. Koning and G. de With, *Powder Technol.*, 2012, **221**, 351–358.

235 L. Nemcova, J. Barek and J. Zima, *Journal of Electroanalytical Chemistry*, 2012, **675**, 18–24.

236 C. A. Frysz and D. D. L. Chung, *Carbon N. Y.*, 1997, **35**, 1111–1127.